SI - Characterization of Strongly Hyperfine-split Protons by DNP

Gian-Marco Camenisch, Nino Wili, Gunnar Jeschke, Matthias Ernst

Contents

A. Initial EPR Experiments

The reproducibility and reliability of the measurements across different measurement sessions were thoroughly ensured by measuring the sample with 5 mM trityl concentration in the matrix gly-d_8:D_2O:H_2O (6:3:1) before every session. Between the measurement session from 08.01.2025 and 06.10.2025 the digitizer and its sampling rate was changed (from 1.8 GSa/s (SP devices ADQ412) to 10 GSa/s (ADQ7DC) see Section 4.2 in main text. Moreover, the operating system of the computer that controls the EPR spectrometer was updated from Windows 10 to Windows 11. This also required some modifications on the mw bridge of the spectrometer. All this was accounted for by carefully measuring the sample with 5 mM trityl concentration in the matrix gly-d_8:D_2O:H_2O (6:3:1) and comparing to older data for the same sample.

A.1. Single DNP contact with Hahn Echo detection

The pulse sequence of this experiment can be seen in Fig. S1. A single NOVEL DNP contact is followed by a detection π pulse. A $\frac{\pi}{2}$-pulse of 6 ns resp. π-pulse of 12 ns with a scale of 1 were used and $\tau = 600$ ns. For the amplitude sweep (Fig. S2 and Fig. S3), the spin lock of the NOVEL DNP was 2 μs long and its digital amplitude was incremented between 0 and 1 in linear fashion. For the sweep over t_{SL} the amplitude was kept constant at the minima of Fig. S2 and Fig. S3 and t_{SL} was varied between 0 μs and 8 μs. This experiment was used to determine the NOVEL matching condition $|\nu_{1,S}| = |\nu_{0,I}|$.

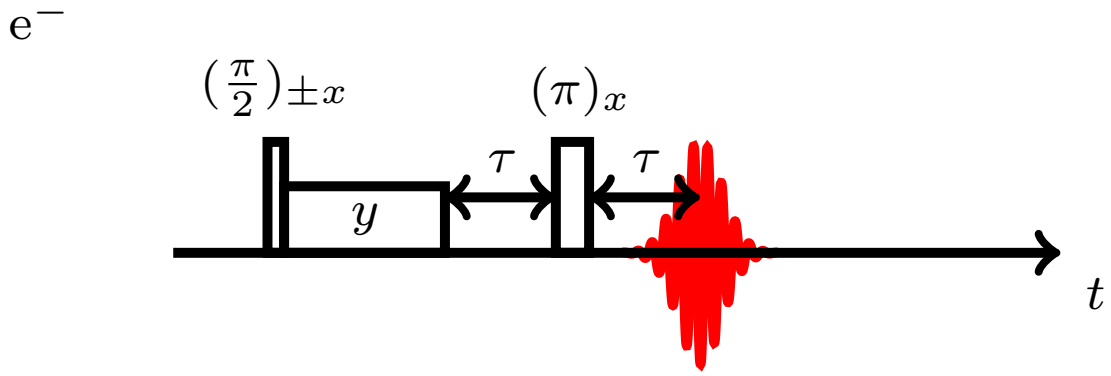

Figure S1: Single DNP contact experiment. The NOVEL DNP sequence was followed a Hahn echo detection with $\tau = 600$ ns. This sequence was used to determine the NOVEL matching condition $|\nu_{1,S}| = |\nu_{0,I}|$.

The experimental data for the amplitude sweep of the spin lock are normalized to EPR Hahn echo intensity of the corresponding sample. The overall agreement between the four different samples is moderate to good. However, at the resonance condition for the proton NOVEL effect (minimum dip) the three samples differ significantly. The sample

with the largest matrix proton concentration (green line) shows the smallest decrease of the integrated echo transient when approaching the resonance condition of NOVEL DNP for proton spins. A reason for this could be that the proton concentration is more prone towards spin diffusion effects considering the rather short DNP contact and the single-shot nature of the experiment. The resonance condition observed for deuterium spins marked with the dotted orange line shows an interesting feature especially in the normalized graph. The dip is smallest for the fully protonated matrix (green line), which makes sense due to the large reduction of deuterium spins in the matrix compared to the other two matrices. The dip is similar for the red and black line corresponding to the matrices gly-d_8:D_2O:H_2O (6:3:1) and gly-d_8:D_2O (6:4). This is expected, as the difference of 1/10 of bulk protons is expected to have a marginal effect.

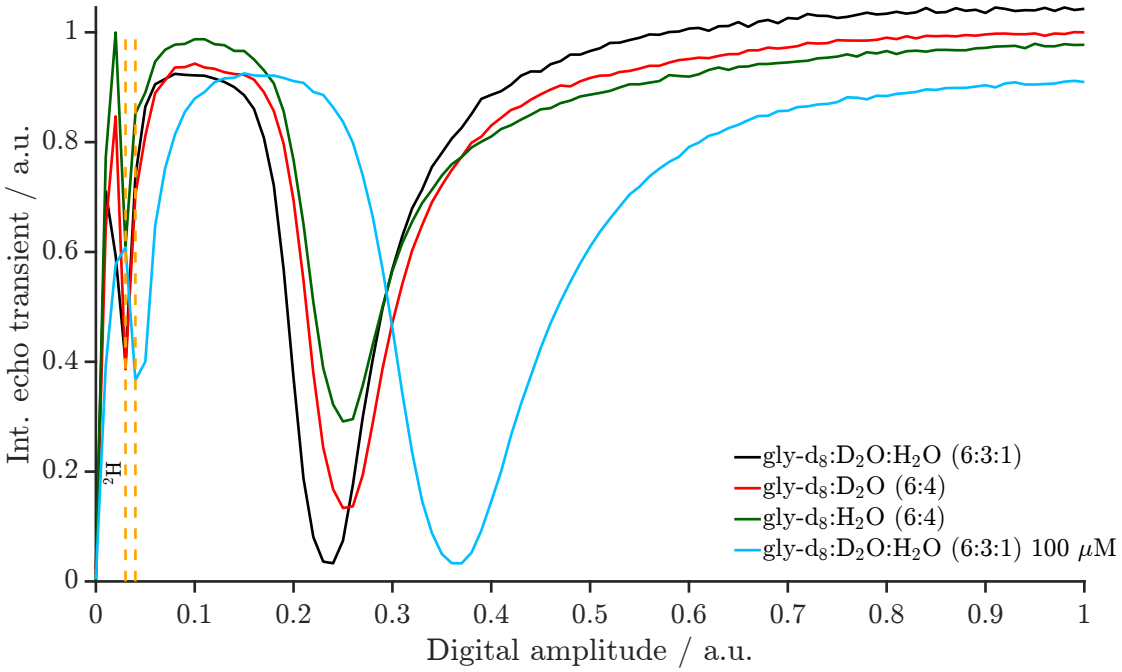

Figure S2: Experimental data for the single DNP contact experiment as shown in Fig. S1. The digital amplitude of the NOVEL DNP contact is linearly swept from 0 to 1 while the length of the spin lock t_{SL} is fixed at 2 μs. The data are normalized to the Hahn echo intensity of the corresponding sample.

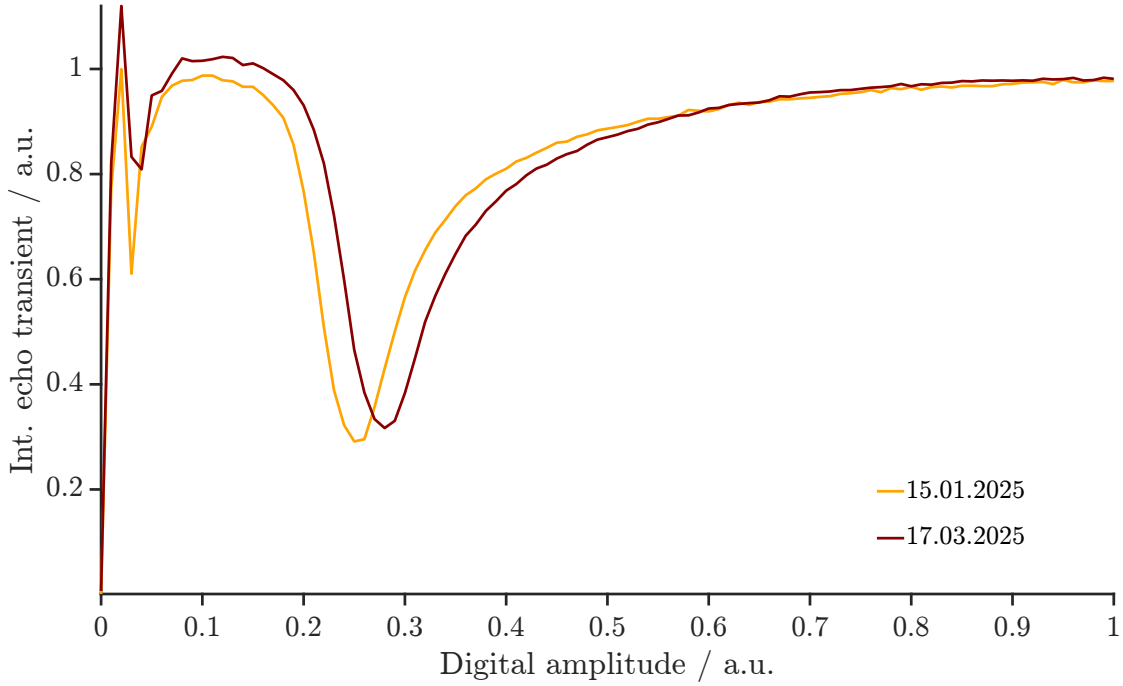

Figure S3: Comparison of experimental data for the single DNP contact experiment as shown in Fig. S1 for different measurement sessions. The digital amplitude of the NOVEL DNP contact is linearly swept from 0 to 1 while the length of the spin lock t_{SL} is fixed at 2 μs. The data are normalized to the Hahn echo intensity of the corresponding sample.

The sweep over the spin lock length (t_{SL}) is shown in Fig. S4. In this experiment the digital amplitude of the spin lock was kept constant to the minimum observed in Fig. S2, while the spin lock length (t_{SL}) was increased linearly from 0 to 8 μs. The overall shape of the four different data sets are identical. However, there is an important difference between the three different matrix compositions gly-d_8:D_2O:H_2O (6:3:1), gly-d_8:D_2O (6:4) and gly-d_8:H_2O (6:4). In the case of the regular DNP juice gly-d_8:D_2O:H_2O (6:3:1) (black line) the echo intensity approaches 0 for $t_{SL} \geq 4$ μs. This is not the case for the other two matrix compositions. A possible explanation for this observation could be the quenched spin diffusion for the matrix gly-d_8:D_2O (6:4). Since the matrix of this sample consists of only deuterium and all the protons are located on the trityl radical (ideal case), spin diffusion to the bulk is quenched. However, this can not serve as an explanation for the sample with the matrix gly-d_8:H_2O (6:4). One would expect that the spin diffusion to the bulk protons is much faster in this matrix and that the echo intensity approaches also 0. That the observed effect is real and not an electronic or experimental error is confirmed by the fact that the sample with the matrix gly-d_8:D_2O:H_2O (6:3:1) and gly-d_8:H_2O (6:4) shows experimental data that are very consistent within different measurement sessions (see Fig. S5 and Fig. S6). Only for the digital amplitude we

observed a change between the different measurement sessions. Once this amplitude was optimized the experimental data are very reproducible as seen on the bottom of Fig. S5 and Fig. S6 for the spin lock length sweep.

In Fig. S7 the sweep over the spin lock length (t_{SL}) for the sample with matrix composition gly-d_8:H_2O (6:4) was measured following a proton saturation train after each shot. As one can see the observed effect of a non-decaying magnetization for this sample does not vanish with post saturation pulses on the proton spin. We conclude that the effect we see is a magnetic resonance effect and not an artifact of the electronic hardware. Our tentative explanation is that in fully protonated matrix the proton spins are so close to each other that they are better described in a triplet and singlet state rather than by two spins 1/2. The singlet state is not accessible and thus the integrated echo transient decays towards a level ~ 0.25.

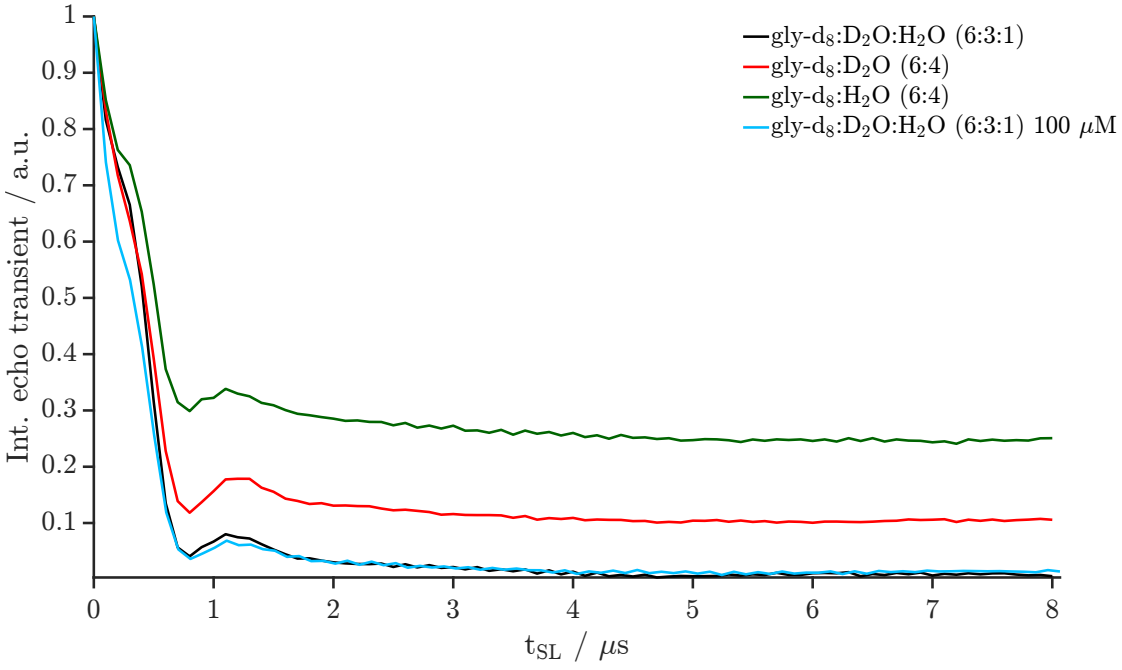

Figure S4: Comparison of experimental data for the single DNP contact for the four different samples. The spin lock length t_{SL} of the NOVEL DNP contact is swept from 0 to 8 μs. The data are normalized to the first data point corresponding to $t_{SL} = 0$ μs, e.g. EPR Hahn echo intensity of the corresponding sample.

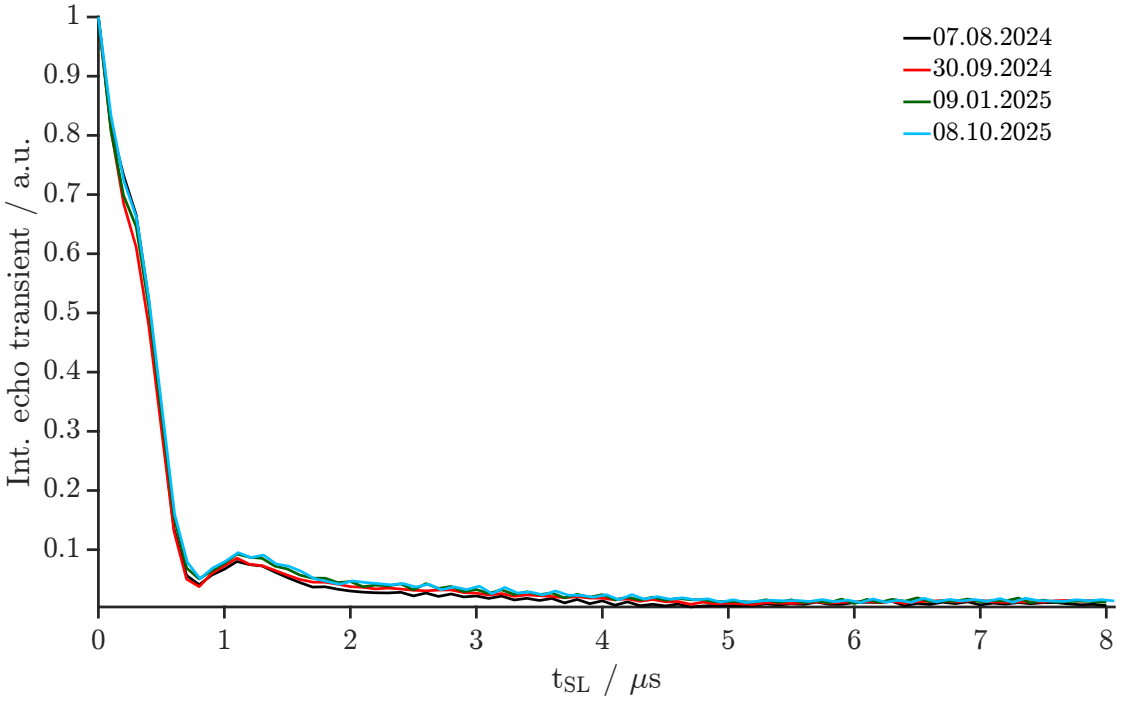

Figure S5: Comparison of experimental data for the single DNP contact for the four different samples. The spin lock length t_{SL} of the NOVEL DNP contact is swept from 0 to 8 μs. The data are normalized to the first data point corresponding to $t_{SL} = 0$ μs, e.g. EPR Hahn echo intensity of the corresponding sample.

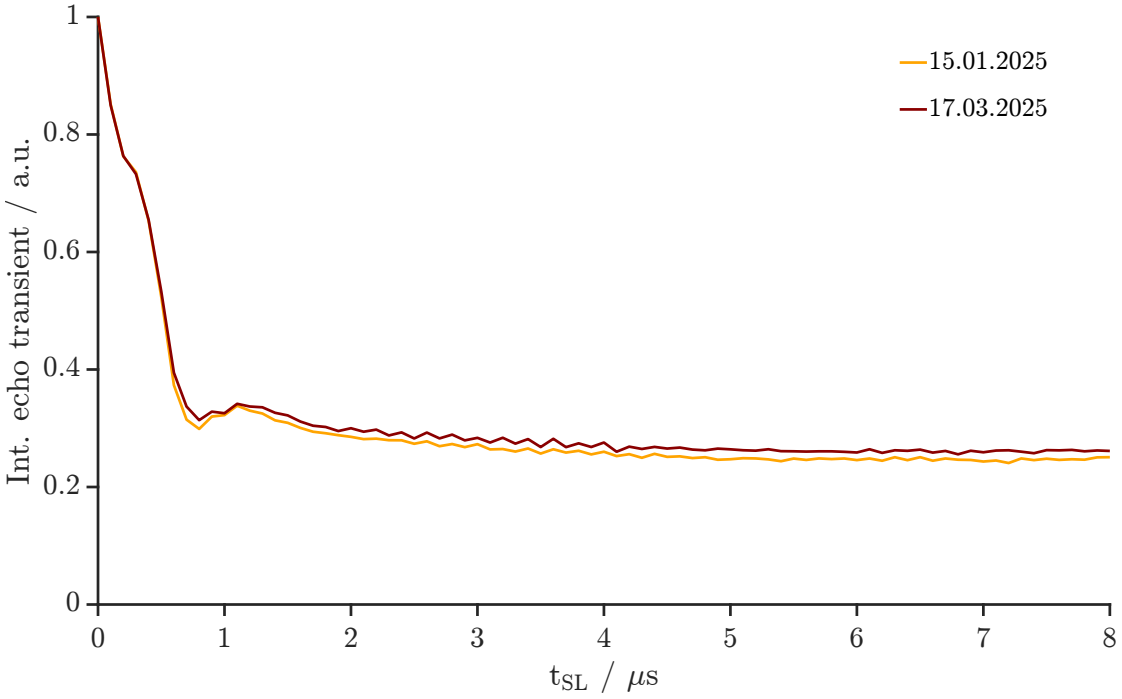

Figure S6: Comparison of experimental data for the single DNP contact for the four different samples. The spin lock length t_{SL} of the NOVEL DNP contact is swept from 0 to 8 μs. The data are normalized to the first data point corresponding to $t_{SL} = 0$ μs, e.g. EPR Hahn echo intensity of the corresponding sample.

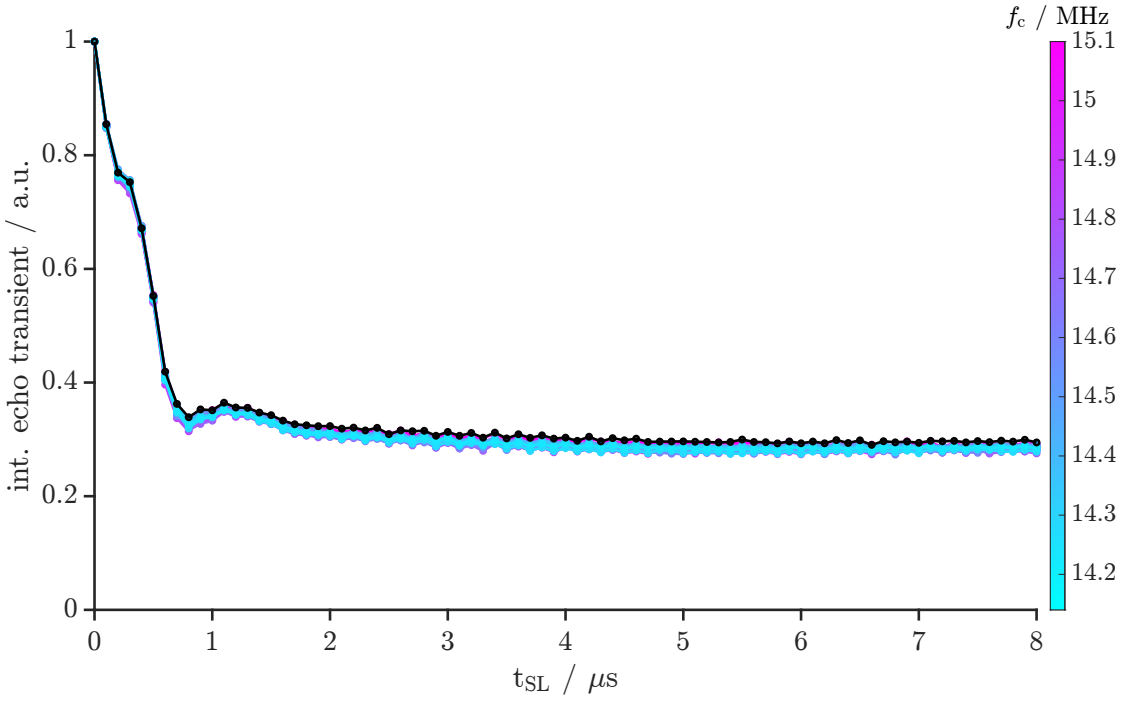

Figure S7: Comparison of experimental data for the single DNP contact for the four different samples. The spin lock length t_{SL} of the NOVEL DNP contact is swept from 0 to 8 μs. The data are normalized to the first data point corresponding to $t_{SL} = 0$ μs, e.g. EPR Hahn echo intensity of the corresponding sample.

A.2. Double DNP contact with subsequent electron detection

In a further step a second DNP contact was added after a delay t_{del} as indicated in Fig. S8. In a first step the digital amplitude of the first contact was swept from 0 to 1 with $t_{del} = 15$ μs. The digital amplitude of the second DNP contact was kept to the optimal value for resonance condition observed in Fig. S2. The spin lock length t_{SL} was set to 4 μs for both DNP contacts. Each shot was followed by a saturation pulse train on the proton spins.

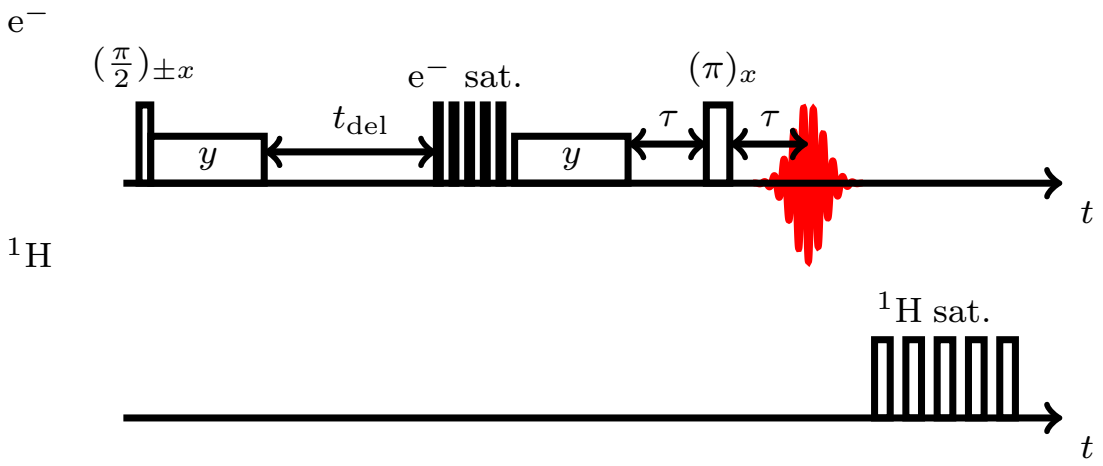

Figure S8: Double DNP contact experiment. After an initial DNP contact the magnetization on the proton spin is evolving for a delay t_{del} with no pulses. After that delay the electron spins are saturated to facilitate the reverse DNP transfer. The magnetization that is transferred back by this step is then measured with a two pulse Hahn echo detection.

Also here the comparison between the four different measurement sessions for the same sample (gly-d_8:D_2O:H_2O (6:3:1)) underline the reproducibility of the measurements within several measurement sessions. The small differences are most likely from hardware changes within the three measurement sessions. There are some difference between the four samples. The sample with the largest proton concentration in the matrix (green line) shows the smallest signal amplitude at exact resonance. This can be explained by an increased spin diffusion towards the bulk protons. This is underlined by the observation that the sample with the smallest matrix proton concentration (red line) has the largest signal amplitude at exact resonance condition.

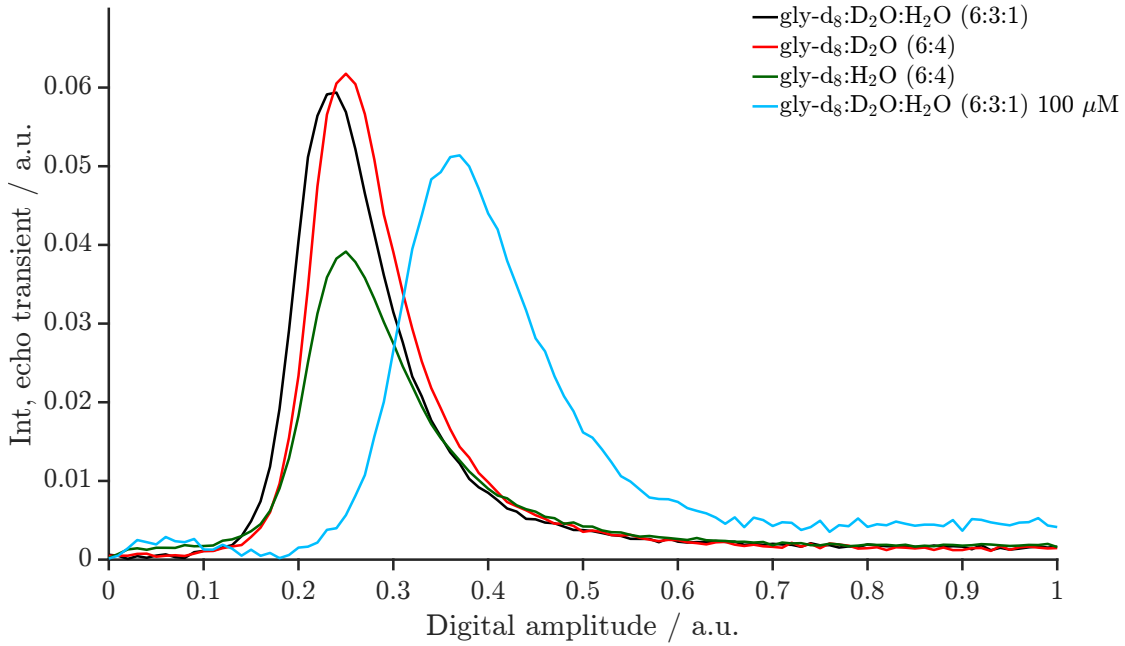

Figure S9: Experimental data for the double DNP contact experiment shown in in Fig. S8. The digital amplitude of the first spin lock was linearly swept from 0 to 1 while the digital amplitude of the second spin lock was kept constant at the value optimal for resonance condition. $t_{\mathrm{del}} = 15$ μs and t_{SL} was set to 4 μs. The experimental data are normalized to EPR Hahn echo intensity of the corresponding sample.

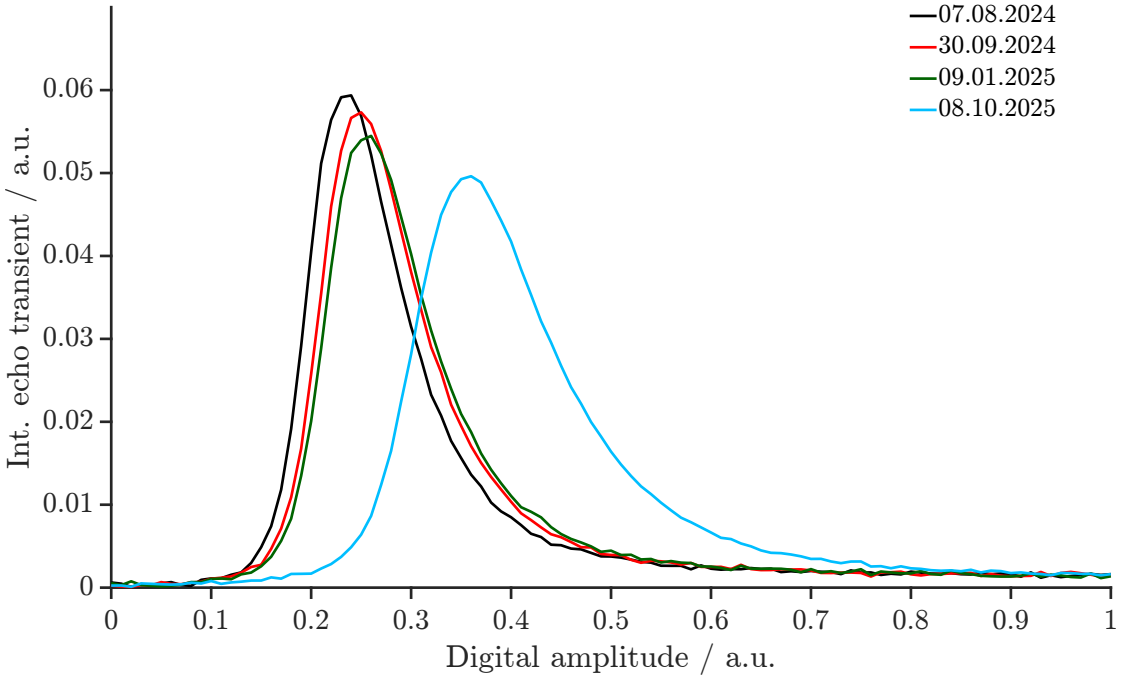

Figure S10: Comparison of experimental data for the double DNP contact experiment as shown in Fig. S8 for different measurement sessions. The digital amplitude of the first NOVEL DNP contact is linearly swept from 0 to 1 while amplitude of the second DNP contact is fixed at the optimum value. The data are normalized to the Hahn echo intensity of the corresponding sample.

Another proof that the measurements are reproducible within several different measurement sessions is shown in Fig. S11. The amplitude sweep of the first spin lock in the double DNP contact experiment for two measurement sessions matches perfectly if one shifts the digital scale axis (see bottom of Fig. S11).

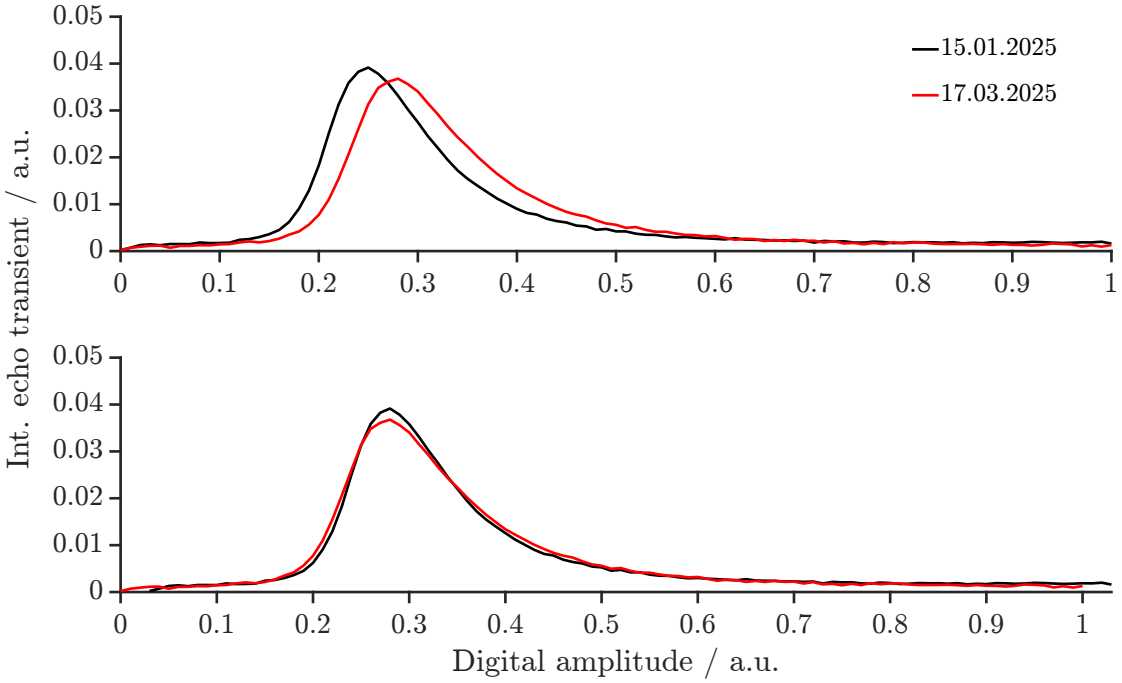

Figure S11: Comparison of the two measurement sessions of the sample with the matrix gly-d_8:H_2O (6:4). Please note that in the plot below the x-axis of the black curve is shifted by +0.03. The experimental data are normalized by the 2 pulse Hahn echo intensity.

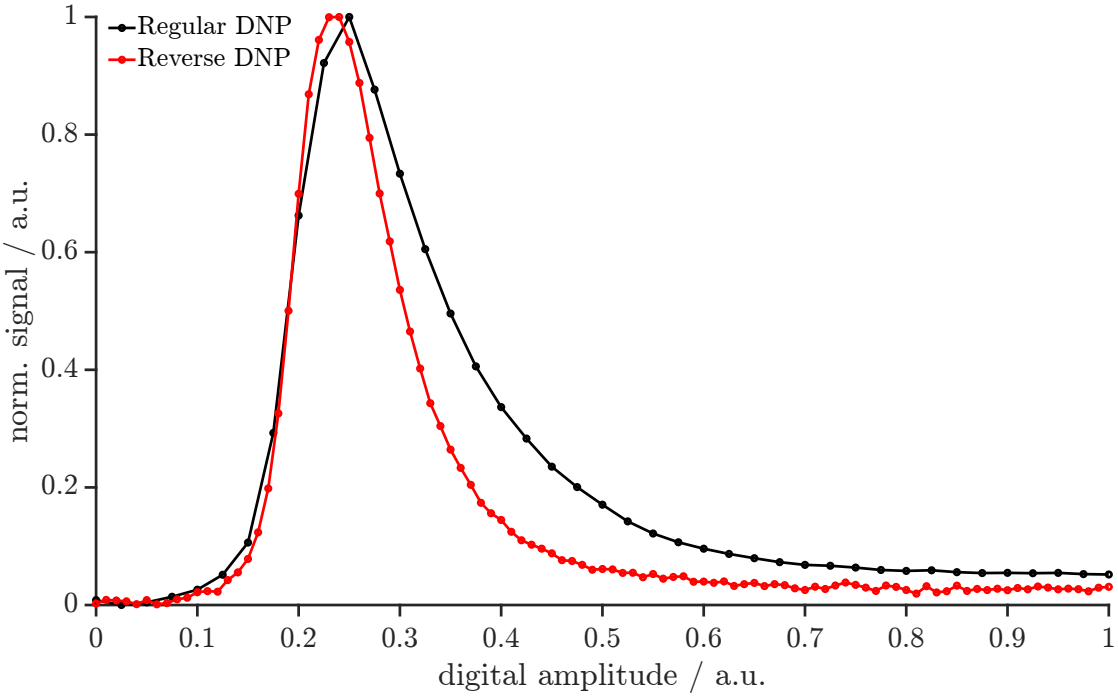

Figure S12: Comparison of the double contact experiment as shown in Fig.A.2 (red) with a regular DNP experiment (black). The NOVEL matching condition can be determined accurately with the double contact experiment.

A.3. Field-swept Echo-detected EPR

Field-swept echo-detected EPR spectrum of the trityl radical in the three different matrices was obtained with a two-pulse sequence $(\frac{\pi}{2}) - \tau - (\pi) - \tau -$ det. with a two- step phase cycle for the first pulse resp. the detection e.g. $(\pm x, x, \pm 1)$ Optimal digital scale of 1 was used for all pulses corresponding to a $(\frac{\pi}{2})$-pulse of 6 ns. τ was set to 600 ns. The number of shots was 100 for the samples with 5 mM trityl concentration and 300 for the sample with 100 μM concentration. The center of the profile was estimated to be $\nu_c = 9.78$ GHz corresponding to $B_0 = 3427.2$ G. The magnetic field was swept in the range $B_0 \pm 40$ G in steps of 0.1 G, while the mw frequency was kept constant at 9.78 GHz. The spectrum of the four different samples are in good agreement with each other. The slightly higher signal at the center of the spectrum for the completely protonated matrix is probably due to a slightly higher electron concentration (forbidden transitions are very similair in intensity).

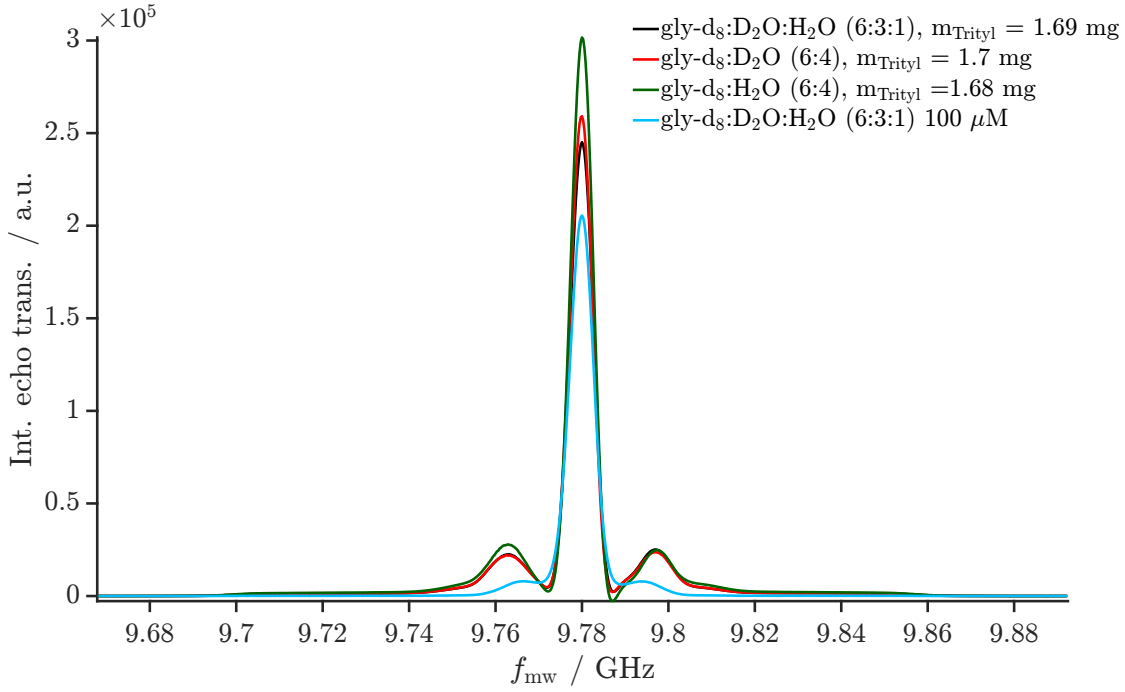

Figure S13: Field-swept echo-detected EPR spectrum for the trityl radical for samples with different matrix composition and electron concentration. A two-pulse sequence $\left(\frac{\pi}{2}\right) - \tau - (\pi) - \tau -$ det. with a two-step phase cycle for the first pulse resp. the detection e.g. $(\pm x, x, \pm 1)$. The optimal scale of 1 was used for all pulses of length 6 ns and $\tau = 600$ ns. The number of shots was 100 for the samples with 5 mM trityl concentration and 300 for the sample with 100 μM trityl concentration. The center of the profile was estimated to be $\nu_c = 9.78$ GHz corresponding to $B_c = 3427.2$ G. The magnetic field was swept in the range $B_c \pm 40$ G in steps of 0.1 G, while the mw frequency was kept constant at 9.78 GHz.

The comparison of the field sweep of the sample with 5mM trityl in the matrix gly-d_8:D_2O:H_2O (6:3:1) across the different measurement sessions is shown in Fig. S14 and in Fig. S15 for the sample with 5mM trityl in the matrix gly-d_8:H_2O (6:4).

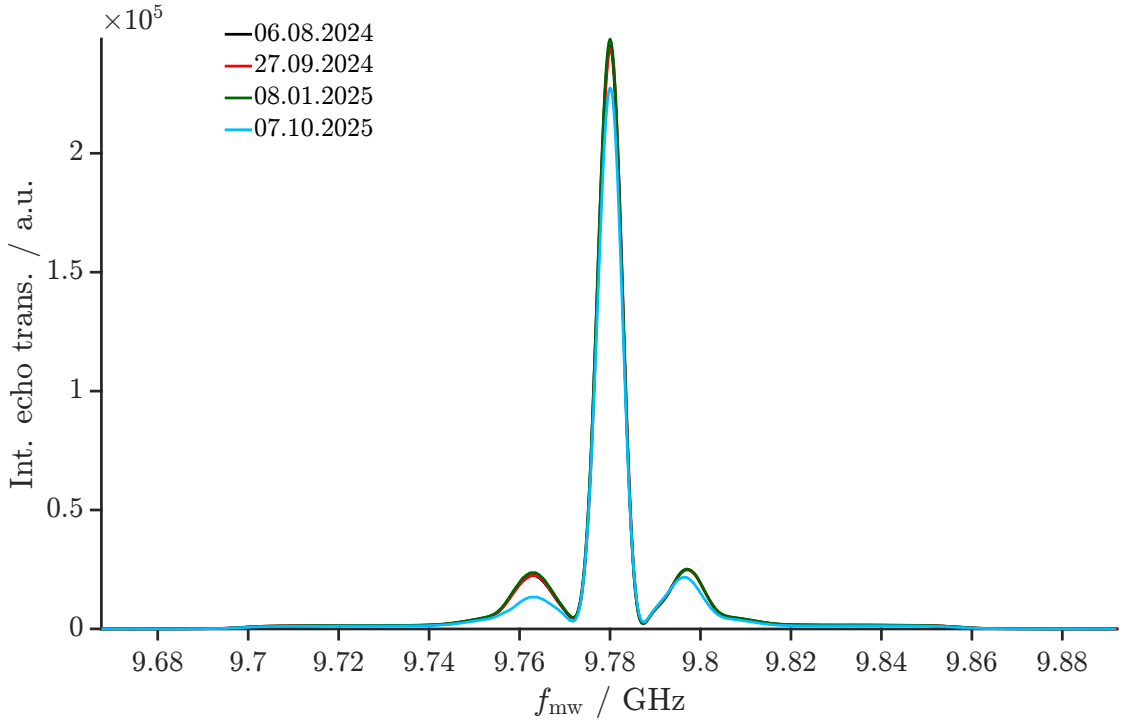

Figure S14: Comparison of field-swept echo-detected EPR spectrum of 5mM trityl in the matrix gly-d_8:D_2O:H_2O (6:3:1) across different measurement sessions. A two-pulse sequence $(\frac{\pi}{2}) - \tau - (\pi) - \tau -$ det. with a two-step phase cycle for the first pulse resp. the detection e.g. $(\pm x, x, \pm 1)$. The optimal scale of 1 was used for all pulses of length 6 ns and $\tau = 600$ ns. The number of shots was 100 for the measurement sessions at 06.08.2024, 27.09.2024 and 08.01.2025. For the measurement at 07.10.2025 the number of shots was 40. The center of the profile was estimated to be $\nu_c = 9.78$ GHz corresponding to $B_c = 3427.2$ G. The magnetic field was swept in the range $B_c \pm 40$ G in steps of 0.1 G, while the mw frequency was kept constant at 9.78 GHz.

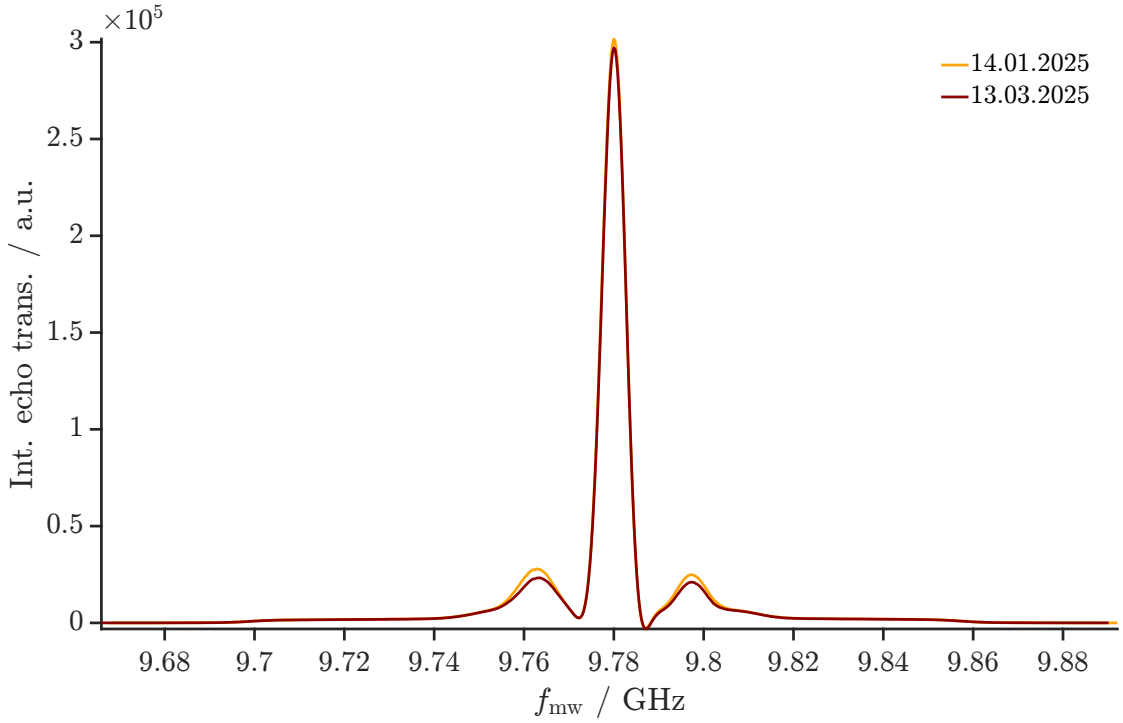

Figure S15: Comparison of field-swept echo-detected EPR spectra of 5 mM trityl in the matrix gly-d_8:H_2O (6:4) across different measurement sessions. A two-pulse sequence $(\frac{\pi}{2}) - \tau - (\pi) - \tau -$ det. with a two-step phase cycle for the first pulse resp. the detection e.g. $(\pm x, x, \pm 1)$. The optimal scale of 1 was used for all pulses of length 6 ns and $\tau = 600$ ns. The number of shots was 100. The center of the profile was estimated to be $\nu_c = 9.78$ GHz corresponding to $B_c = 3427.2$ G. The magnetic field was swept in the range $B_c \pm 40$ G in steps of 0.1 G, while the mw frequency was kept constant at 9.78 GHz.

A.4. Resonator Profile

The resonator profile is measured using a three-pulse experiment. The first pulse serves as a nutation pulse and is incremented from 0 to 128 ns in steps of 2 ns at maximum power (digital scale = 1). Electron spin magnetization after delay T $\sim 5 \cdot T_{2,e}$, is observed with a two-pulse Hahn echo experiment (6 ns $\frac{\pi}{2}$ and 12 ns π pulse at digital scale of 1). The experiment is measured for different offsets $\Omega_{0,S}$ with respect to the center of the resonator.

The four different resonator profiles in Fig. S16 are comparable with each other. The center of the resonator ($f_{mw} = 9.78$ GHz is for all three samples almost identical $\nu_1 \sim 45$ MHz. The reduced maximum in ν_1 for 100 μM trityl in the matrix gly-d_8:D_2O:H_2O (6:3:1) and in measurement the measurements from 13.10.2025 is due to a modification in the mw bridge as outlined at the beginning of this chapter.

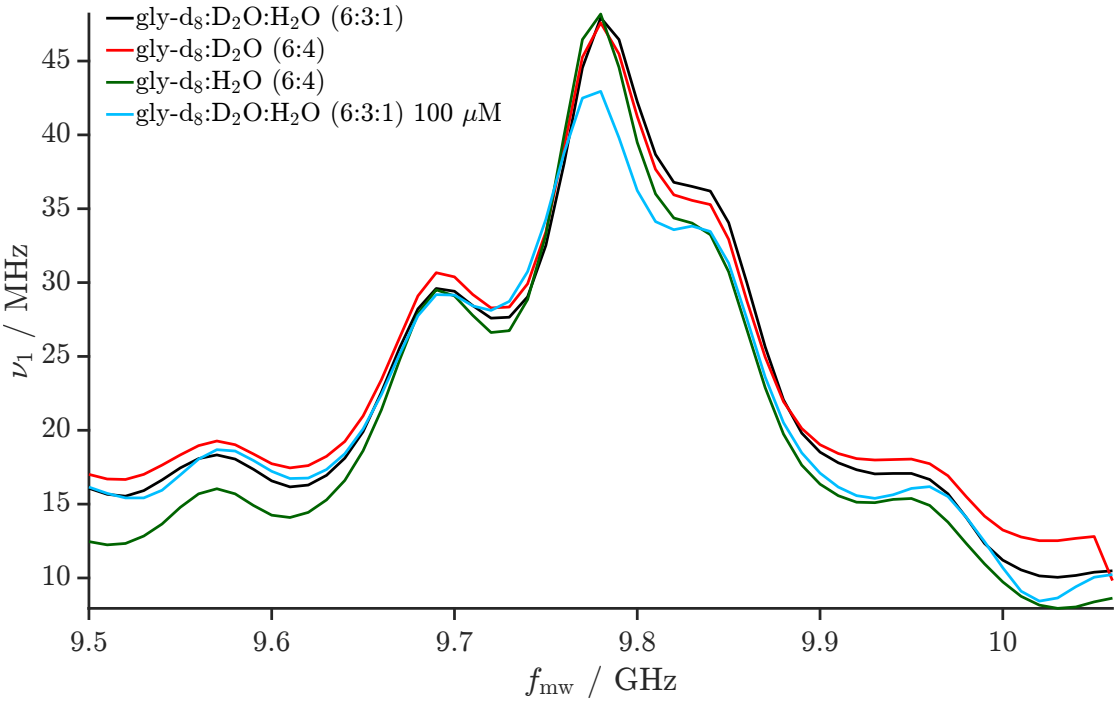

Figure S16: Measured resonator profile for the trityl radical in four samples using an echo-detected nutation pulse sequence $(\beta_{\text{flip}}) - \text{T} - (\frac{\pi}{2}) - \tau - (\pi) - \tau -$ det. with a two-step phase cycle for the second pulse resp. the detection e.g. $(\pm x, x, \pm 1)$. The optimal scale of 1 was used for the second and third pulse. $\tau = 600$ ns and T = 5000 ns were used as delays for the samples with 5 mM trityl concentration. For the sample with 100 μM trityl concentration T = 40 μs was used. The number of shots was 50 for all four samples. The mw frequencies of all pulses are swept from 8.5 to 10.06 GHz in 0.01 GHz steps. The external magnetic field is swept in similar fashion, so that the magnetic field is on-resonance with the mw frequency. The length of the first pulse was increased from 0 to 128 ns in steps of 2 ns at every field/frequency step with a fixed digital scale of 1.

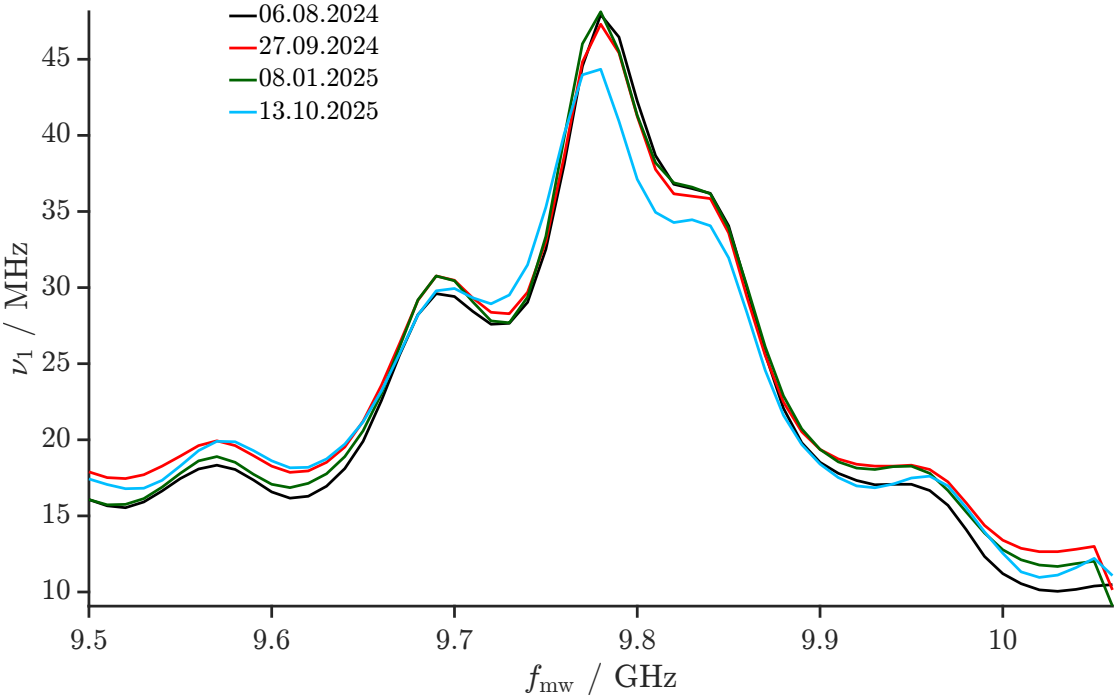

Figure S17: Comparison of resonator profile for the 5 mM sample in the matrix gly-d_8:D_2O:H_2O (6:3:1) using an echo-detected nutation pulse sequence $(\beta_{\mathrm{flip}}) - \mathrm{T} - \left(\frac{\pi}{2}\right) - \tau - (\pi) - \tau -$ det. with a two-step phase cycle for the second pulse resp. the detection e.g. $(\pm x, x, \pm 1)$. The optimal scale of 1 was used for the second and third pulse. τ = 600 ns and T = 5000 ns were used as delays. The number of shots was 50 for all four samples. The mw frequencies of all pulses are swept from 8.5 to 10.06 GHz in 0.01 GHz steps. The external magnetic field is swept in similar fashion, so that the magnetic field is on-resonance with the mw frequency. The length of the first pulse was increased from 0 to 128 ns in steps of 2 ns at every field/frequency step with a fixed digital scale of 1.

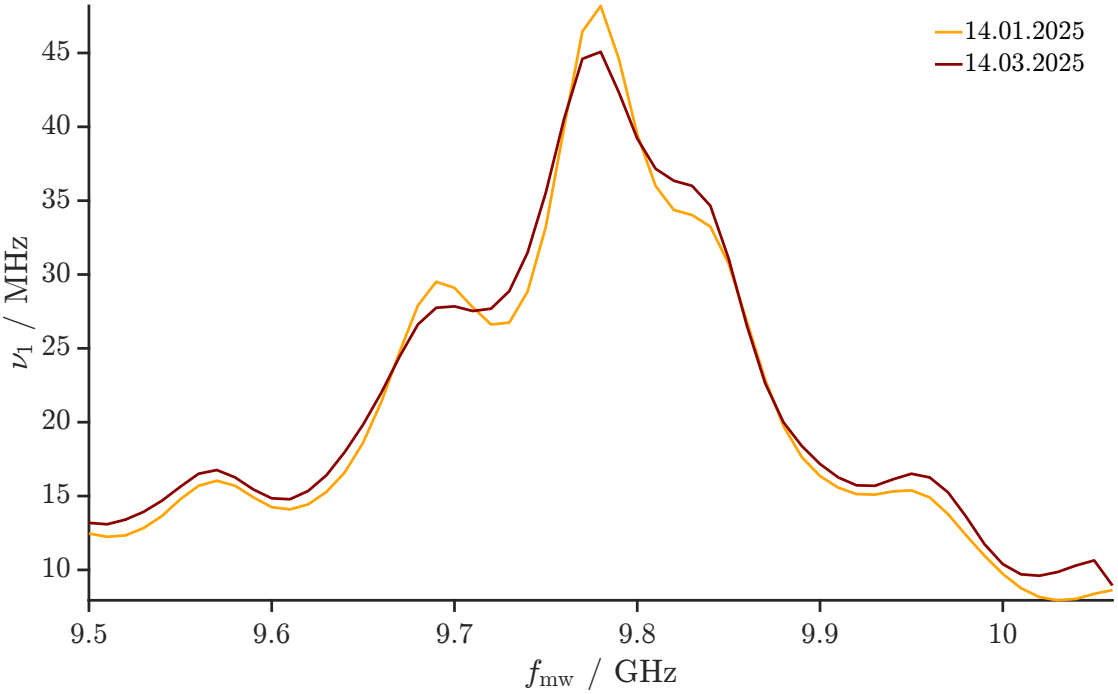

Figure S18: Comparison of resonator profile for 5 mM sample in the matrix gly-d_8:H_2O (6:4) using an echo-detected nutation pulse sequence $(\beta_{\mathrm{flip}}) - \mathrm{T} - \left(\frac{\pi}{2}\right) - \tau - (\pi) - \tau -$ det. with a two-step phase cycle for the second pulse resp. the detection e.g. $(\pm x, x, \pm 1)$. The optimal scale of 1 was used for the second and third pulse. τ = 600 ns and T = 5000 ns were used as delays. The number of shots was 50 for all four samples. The mw frequencies of all pulses are swept from 8.5 to 10.06 GHz in 0.01 GHz steps. The external magnetic field is swept in similar fashion, so that the magnetic field is on-resonance with the mw frequency. The length of the first pulse was increased from 0 to 128 ns in steps of 2 ns at every field/frequency step with a fixed digital scale of 1.

A.5. TWT Non-linearity

The experiment to record the non-linearity of the TWT amplifier is a three-pulse experiment. The first pulse serves as a nutation pulse and is incremented from 0 to 128 ns in steps of 2 ns at various digital scale. Electron spin magnetization after delay $\mathrm{T} \sim 5 \cdot \mathrm{T}_{2,\mathrm{e}}$ is observed with a two-pulse Hahn echo experiment. The experiment is measured at the center of the resonator $\sim$ 9.78 GHz. The three TWT non-linearity curves are in moderate agreement with each other. The TWT non-linearity curve together with the resonator profile was used to compensate the limited width of the microwave resonator mode and differences in non-linearity of the TWT during the acquisition of the experiments. The agreement between the measurements are good. The different shape of the

TWT non-linearity curve for 100 μM trityl in the matrix gly-d_8:D_2O:H_2O (6:3:1) and in the measurements from 07.10.2025 is due to a modification in the mw bridge as outlined at the beginning of this chapter.

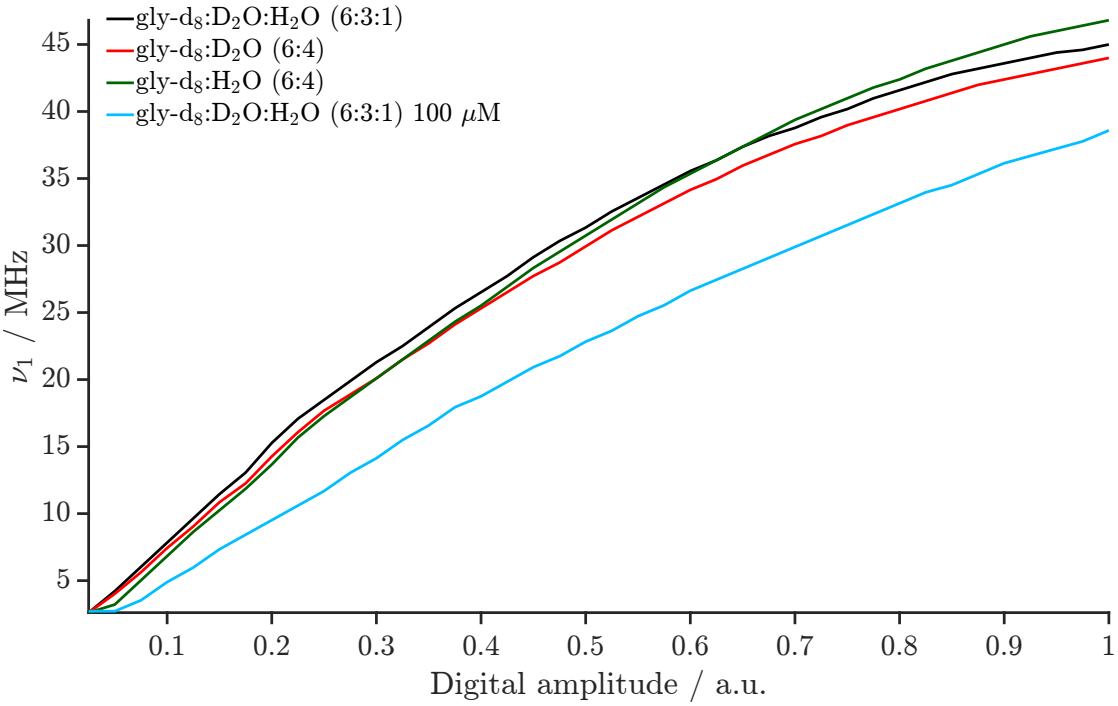

Figure S19: Measured TWT non-linearity curve for the four different samples using an echo-detected nutation pulse sequence $(\beta_{\text{flip}}) - \text{T} - (\frac{\pi}{2}) - \tau - (\pi) - \tau - \text{det.}$ with a two-step phase cycle for the second pulse resp. the detection e.g. $(\pm x, x, \pm 1)$. The optimal scale of 1 was used for the second (6 ns) and third pulse (12 ns). τ = 600 ns and T = 5000 ns were used as delays for the samples with 5 mM trityl concentration. For the sample with 100 μM trityl concentration T = 40 μs was used. The number of shots was 50 for all four samples. The scale of the first pulse was changed from 0 to 1 in 0.02 steps. The length of the first pulse was increased from 0 to 512 ns in steps of 2 ns at every scale. The nutation frequency was determined by taking the maximal frequency of the Fourier transformation of the nutation curve. The experiment was measured at the center of the resonator.

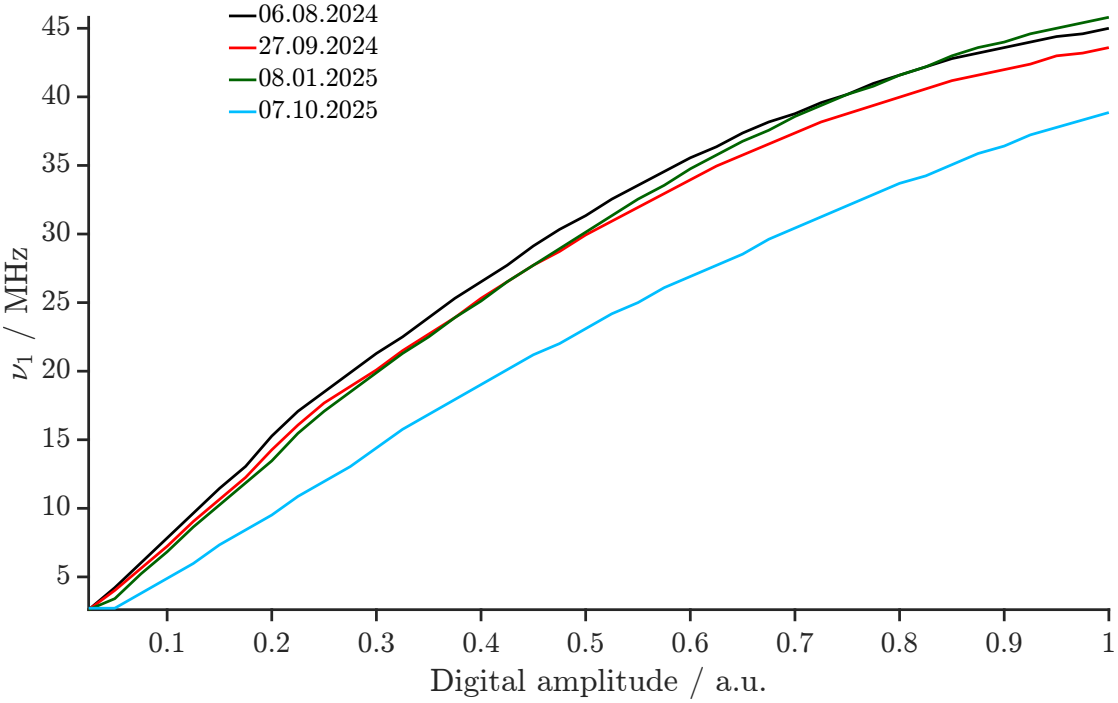

Figure S20: Comparison of the TWT non-linearity curve for the 5 mM sample in the matrix gly-d_8:D_2O:H_2O (6:3:1) using an echo-detected nutation pulse sequence $(\beta_{\text{flip}}) - \text{T} - \left(\frac{\pi}{2}\right) - \tau - (\pi) - \tau -$ det. with a two-step phase cycle for the second pulse resp. the detection e.g. $(\pm x, x, \pm 1)$. The optimal scale of 1 was used for the second (6 ns) and third pulse (12 ns). $\tau = 600$ ns and T = 5000 ns were used as delays for the samples with 5 mM trityl concentration. For the sample with 100 μM trityl concentration T = 40 μs was used. The number of shots was 50 for all four samples. The scale of the first pulse was changed from 0 to 1 in 0.02 steps. The length of the first pulse was increased from 0 to 512 ns in steps of 2 ns at every scale. The nutation frequency was determined by taking the maximal frequency of the Fourier transformation of the nutation curve. The experiment was measured at the center of the resonator.

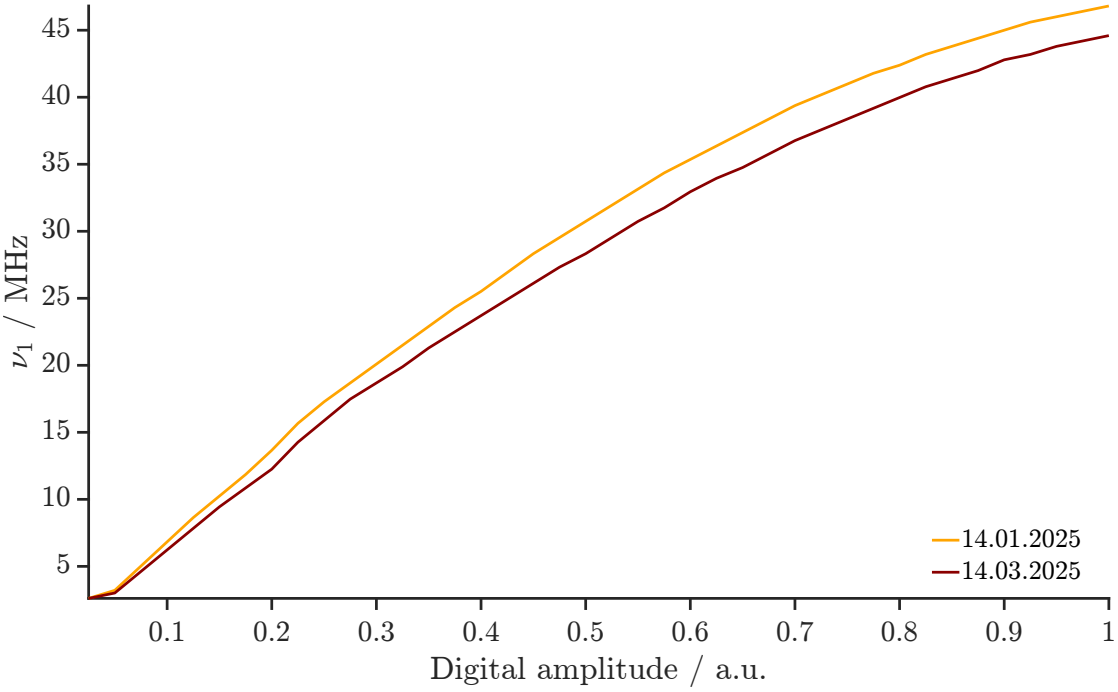

Figure S21: Comparison of the TWT non-linearity curve for the 5 mM sample in the matrix gly-d_8:H_2O (6:4) using an echo-detected nutation pulse sequence $(\beta_{\text{flip}}) - \text{T} - (\frac{\pi}{2}) - \tau - (\pi) - \tau -$ det. with a two-step phase cycle for the second pulse resp. the detection e.g. $(\pm x, x, \pm 1)$. The optimal scale of 1 was used for the second (6 ns) and third pulse (12 ns). $\tau = 600$ ns and T = 5000 ns were used as delays for the samples with 5 mM trityl concentration. For the sample with 100 μM trityl concentration T = 40 μs was used. The number of shots was 50 for all four samples. The scale of the first pulse was changed from 0 to 1 in 0.02 steps. The length of the first pulse was increased from 0 to 512 ns in steps of 2 ns at every scale. The nutation frequency was determined by taking the maximal frequency of the Fourier transformation of the nutation curve. The experiment was measured at the center of the resonator.

A.6. Longitudinal Relaxation time for Electron Spin

The longitudinal relaxation time $\text{T}_{1,\text{e}}$ was measured using a chirp pulse of 400 ns length with digital scale of 1 as inversion pulse followed by a 2 pulse Hahn echo sequence i.e. $(\pi) - \Delta\text{t} - (\frac{\pi}{2}) - \tau - (\pi) - \tau -$ det., where Δt was incremented exponentially between 0.02 and 100 ms. The experimental data are fitted to

$$\text{I} \cdot \left(1 - 2 \cdot \exp\left\{\left(-\frac{\Delta\text{t}}{\text{T}_{1,\text{e}}}\right)\right\}\right) \tag{S.1}$$

The inversion recovery experiment of the four samples are in good agreement with each other resulting in similar $T_{1,e}$ values as shown in Fig. S22.

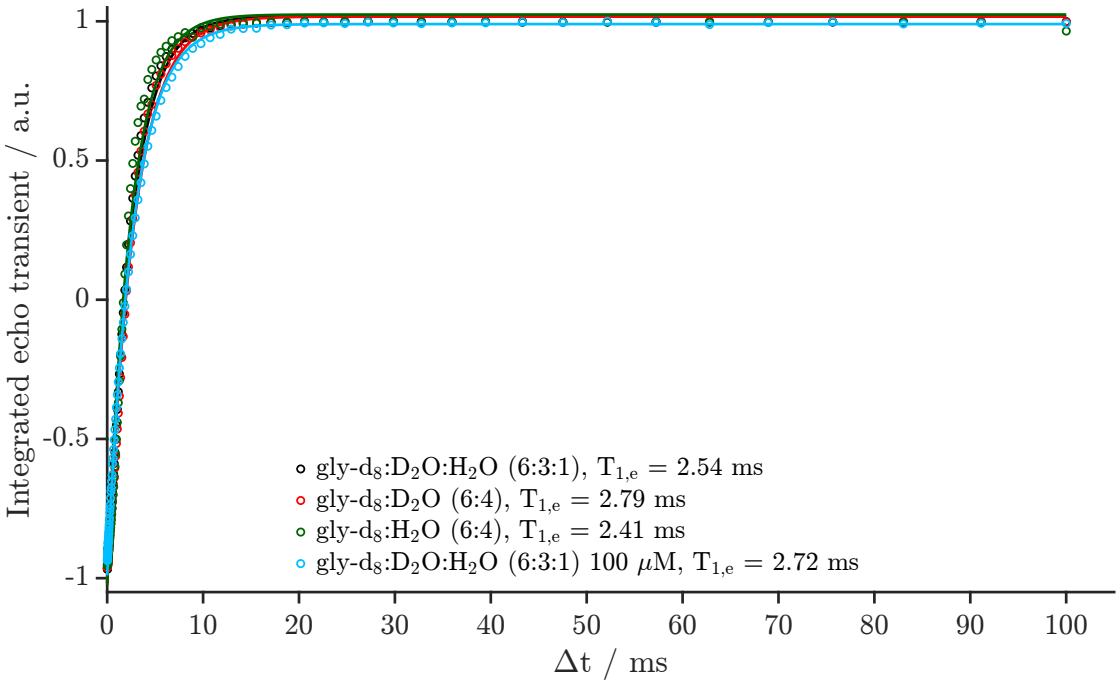

Figure S22: Inversion recovery experiment to determine $T_{1,e}$ for the electron spin (circles) with mono-exponential fit (lines) resulting in $T_{1,e} \sim 2.5$ ms. The π-pulse for inversion was a chirp pulse of 400 ns length with digital scale of 1. 10 shots were used for the samples with a 5 mM trityl concentration and 30 for the sample with 100 μM concentration. The interpulse delay for the Hahn echo was $\tau = 600$ ns. A $\frac{\pi}{2}$-pulse of 6 ns resp. π-pulse of 12 ns with a scale of 1 were used for the Hahn echo pulses.

The comparison of the inversion recovery experiment across the different measurement sessions of the sample with 5mM trityl in the matrix gly-d_8:D_2O:H_2O (6:3:1) is shown in Fig. S23 and in Fig. S24 for the sample with 5mM trityl in the matrix gly-d_8:H_2O (6:4). In both cases the experimental data are highly reproducible.

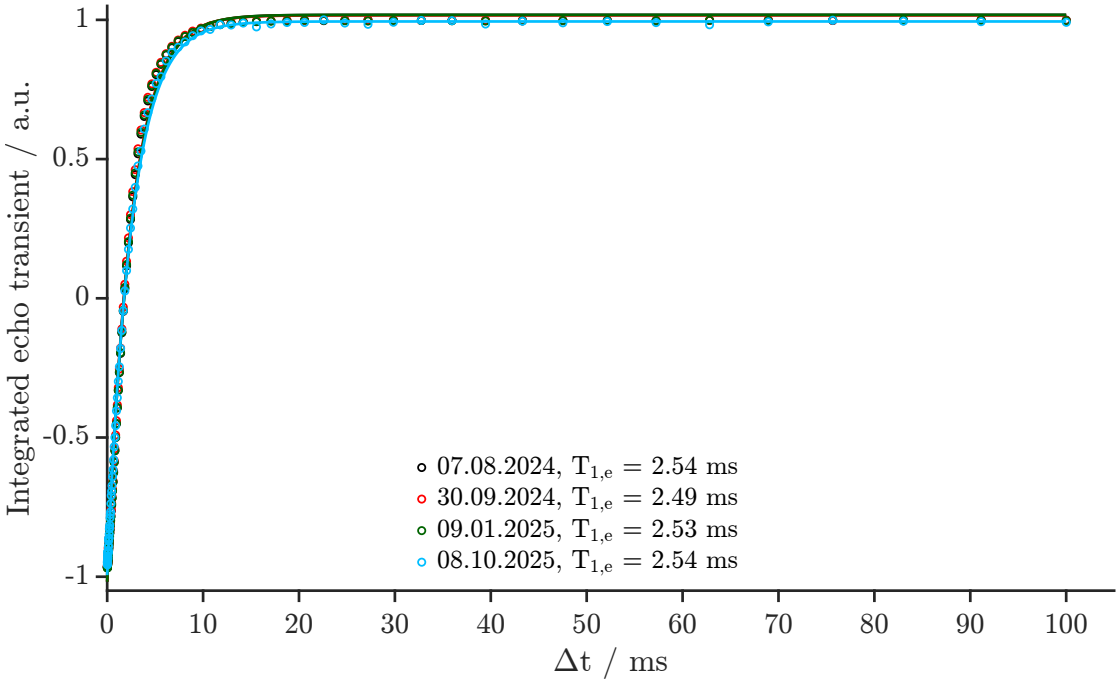

Figure S23: Comparison of the inversion recovery experiment of 5mM trityl in the matrix gly-d_8:D_2O:H_2O (6:3:1) across different measurement sessions. The π-pulse for inversion was a chirp pulse of 400 ns length with digital scale of 1. 10 shots were used and the interpulse delay for the Hahn echo was $\tau = 600$ ns. A $\frac{\pi}{2}$-pulse of 6 ns resp. π-pulse of 12 ns with a scale of 1 were used for the Hahn echo pulses.

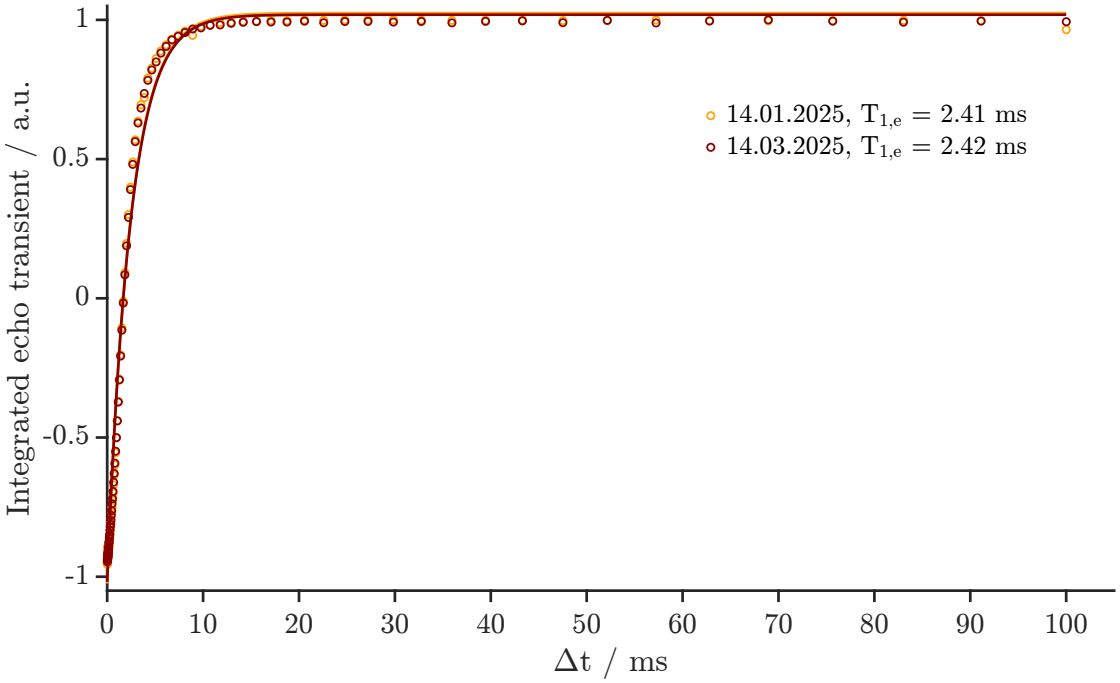

Figure S24: Comparison of the inversion recovery experiment of 5mM trityl in the matrix gly-d_8:H_2O (6:4) across different measurement sessions. The π-pulse for inversion was a chirp pulse of 400 ns length with digital scale of 1. 10 shots were used and the interpulse delay for the Hahn echo was τ = 600 ns. A $\frac{\pi}{2}$-pulse of 6 ns resp. π-pulse of 12 ns with a scale of 1 were used for the Hahn echo pulses.

A.7. Phase Memory time for Electron Spin

The transverse relaxation time or phase memory time T_M was measured using a 2 pulse Hahn echo sequence $\left(\frac{\pi}{2}\right) - \tau - (\pi) - \tau -$ det., where τ was incremented linearly between 400 ns and 8000 ns. The experimental data are fitted to a stretched exponential

$$I \cdot \exp\left\{\left(-\left(\frac{2\tau}{T_M}\right)^{\xi}\right)\right\} \tag{S.2}$$

The experimental data between the 5 mM trityl concentration in gly-d_8:D_2O:H_2O (6:3:1) matrix and gly-d_8:D_2O (6:4) matrix are in very good agreement with each other which is expected due to the marginal change in proton concentration in the matrix (see Fig. S25). Surprisingly the sample with the largest proton concentration in the matrix shows the slowest decay (largest T_M). A possible explanation can be the slightly different electron concentration in that sample. The sample with a 100 μM concentration shows the longest decay due to the reduced electron concentration. One can clearly see the

ESEEM effect for the ^{1}H spin (slow oscillation) and the deuterium (fast oscillation) in the experimental data.

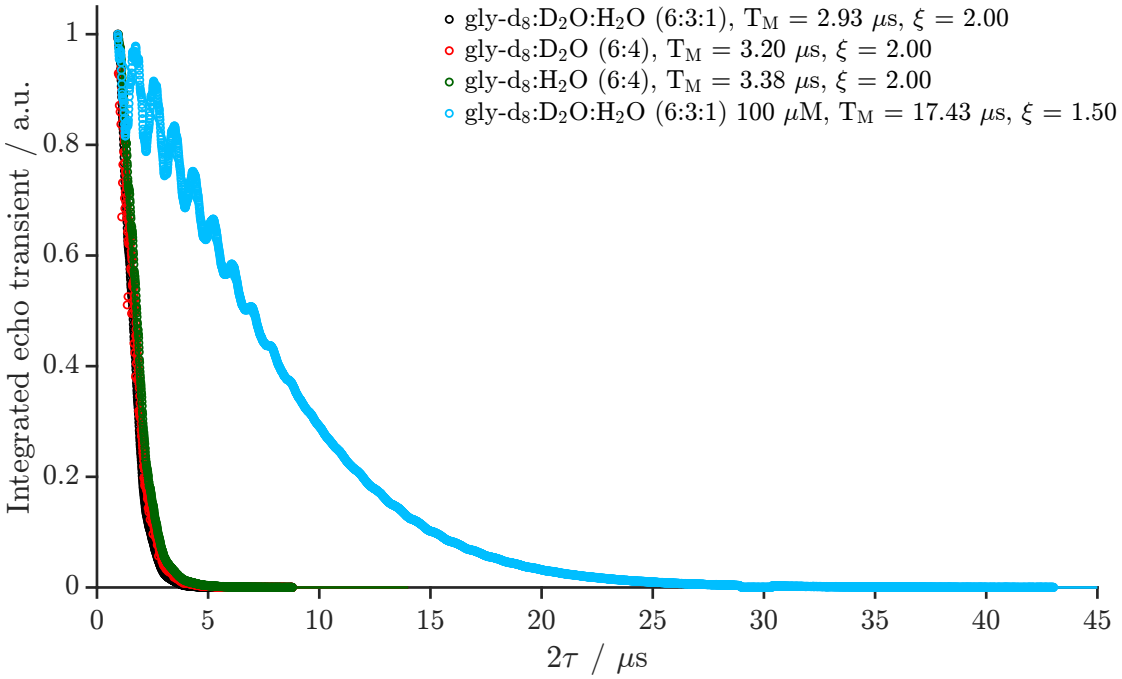

Figure S25: Experiment to determine T_M for the electron spin (circles) with stretched-exponential fit S.2 (lines) resulting in $T_M = 2.93$ μs, $\xi = 2.00$ for the Trityl radical in gly-d$_8$:D$_2$O:H$_2$O (6:3:1) matrix, $T_M = 3.20$ μs, $\xi = 2.00$ in gly-d$_8$:D$_2$O (6:4) matrix and $T_M = 3.38$ μs, $\xi = 2.00$ in gly-d$_8$:H$_2$O (6:4) matrix. For the diluted sample (100 μM trityl concentration) the following parameters were obtained from the fit: $T_M = 17.43$ μs, $\xi = 1.50$. 10 shots were used for the samples with 5 mM trityl concentration and 30 shots for the sample with 100 μM trityl concentration. A $\frac{\pi}{2}$-pulse of 6 ns resp. π-pulse of 12 ns with a scale of 1 were used for the Hahn echo pulses.

The comparison of the two pulse Hahn echo experiments to record T_M across the different measurement sessions of the sample with 5mM trityl in the matrix gly-d$_8$:D$_2$O:H$_2$O (6:3:1) is shown in Fig. S26 and in Fig. S27 for the sample with 5mM trityl in the matrix gly-d$_8$:H$_2$O (6:4). In both cases the experimental data are in good agreement and reproducible across the four measurement sessions.

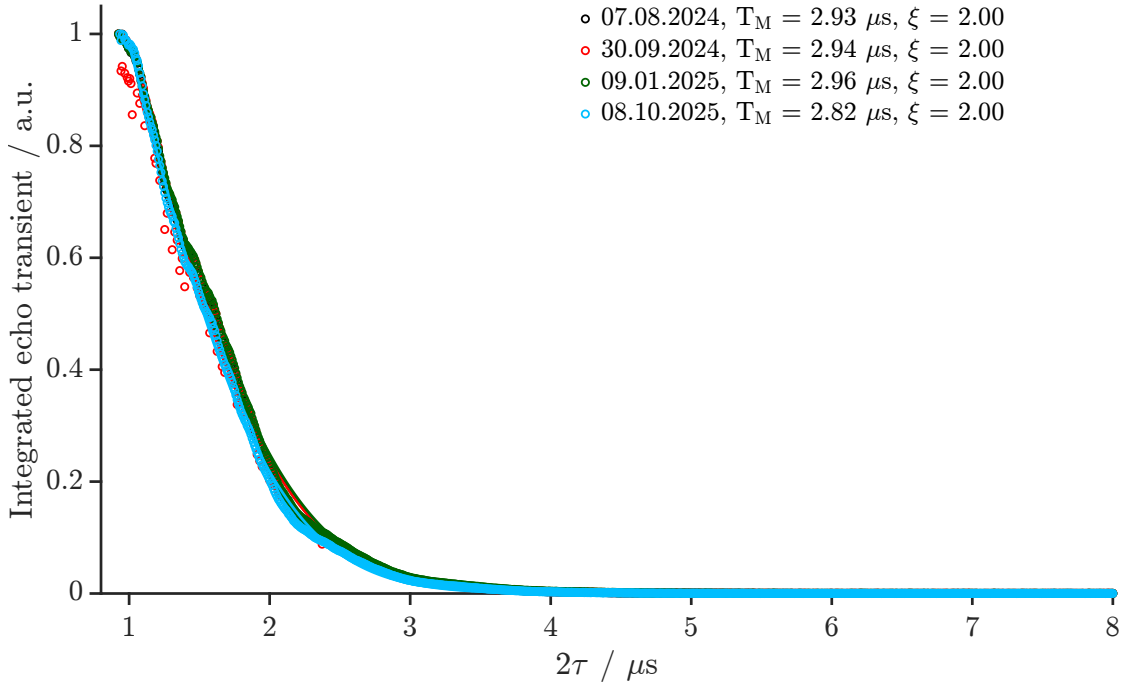

Figure S26: Comparison of T_M for the electron spin (circles) with stretched-exponential fit S.2 (lines) resulting in $T_M \sim 2.9$ μs for 5 mM trityl in the matrix gly-d_8:D_2O:H_2O (6:3:1). 10 shots were used for the samples with 5 mM trityl concentration and $\frac{\pi}{2}$-pulse of 6 ns resp. π-pulse of 12 ns with a scale of 1 for the Hahn echo pulses.

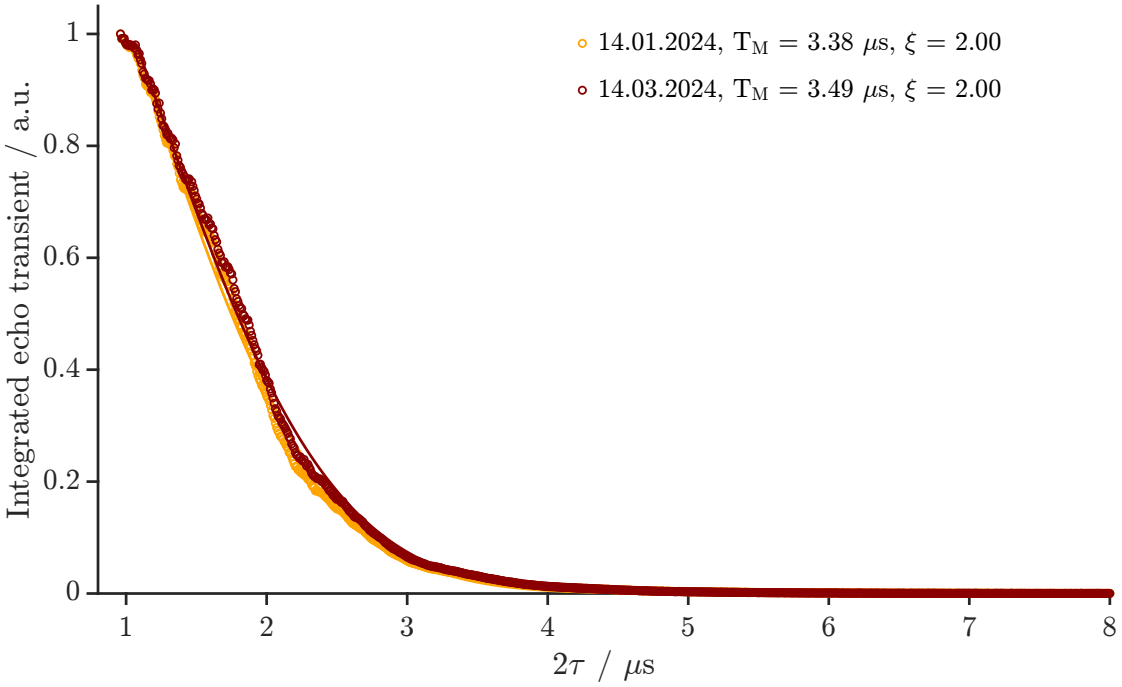

Figure S27: Comparison of T_M for the electron spin (circles) with stretched-exponential fit S.2 (lines) resulting in $T_M \sim 3.4$ μs for 5 mM trityl in the matrix gly-d_8:H_2O (6:4). 10 shots were used for the samples with 5 mM trityl concentration and $\frac{\pi}{2}$-pulse of 6 ns resp. π-pulse of 12 ns with a scale of 1 for the Hahn echo pulses.

B. Electron-detected Proton Spectrum

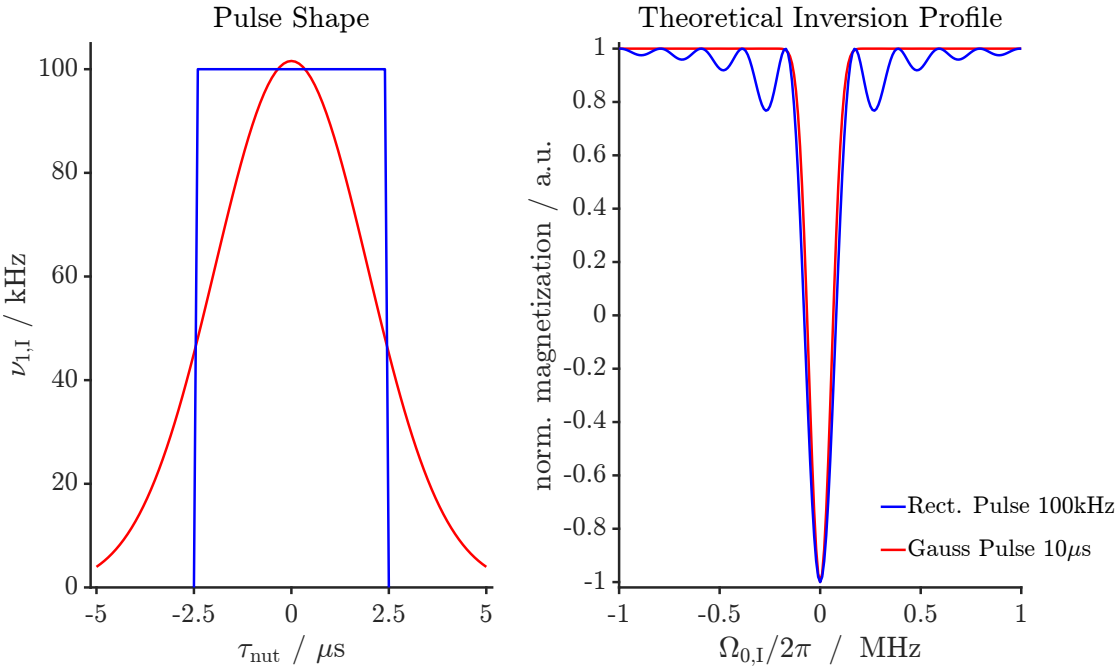

Figure S28: Inversion profiles of a 5 μs rectangular pulse with an amplitude of 100 kHz (blue) and of a Gaussian shaped pulse of 10 μs length with an amplitude at the center of $\sim$ 100 kHz and $\sigma = 1.96$ μs (red). The FWHM of the inversion profiles are $\sim$ 130 kHz for Gauss pulse and $\sim$ 160 kHz for rectangular pulse. The width where the inversion profile has decayed to the baseline of 1 is $\sim$ 360 kHz.

The data points of a nutation trace at offset $\Omega_{0,\mathrm{I}}$ were simulated as the weighted sum of the z-magnetization of each offset after the application of the nutation pulse

$$S_{\mathrm{nut}} = \sum_{i}^{N} 2 \cdot \mathrm{Tr}\left\{ U_{\mathrm{inv},i}^{-1} \hat{S}_{\mathrm{z}} U_{\mathrm{inv},i} \hat{S}_{\mathrm{z}} \right\} \cdot p_i. \tag{S.3}$$

$U_{\mathrm{inv},i}$ is the propagator of the inversion pulse and p_i is the intensity of the theoretical proton spectrum at offset $\Omega_{0,\mathrm{I}}^{(i)}$ (probability to find a spin packet at that offset). N is the number of offsets $\Omega_{0,\mathrm{I}}$ considered, which in our case was 201 over a range -1 MHz to 1 MHz.

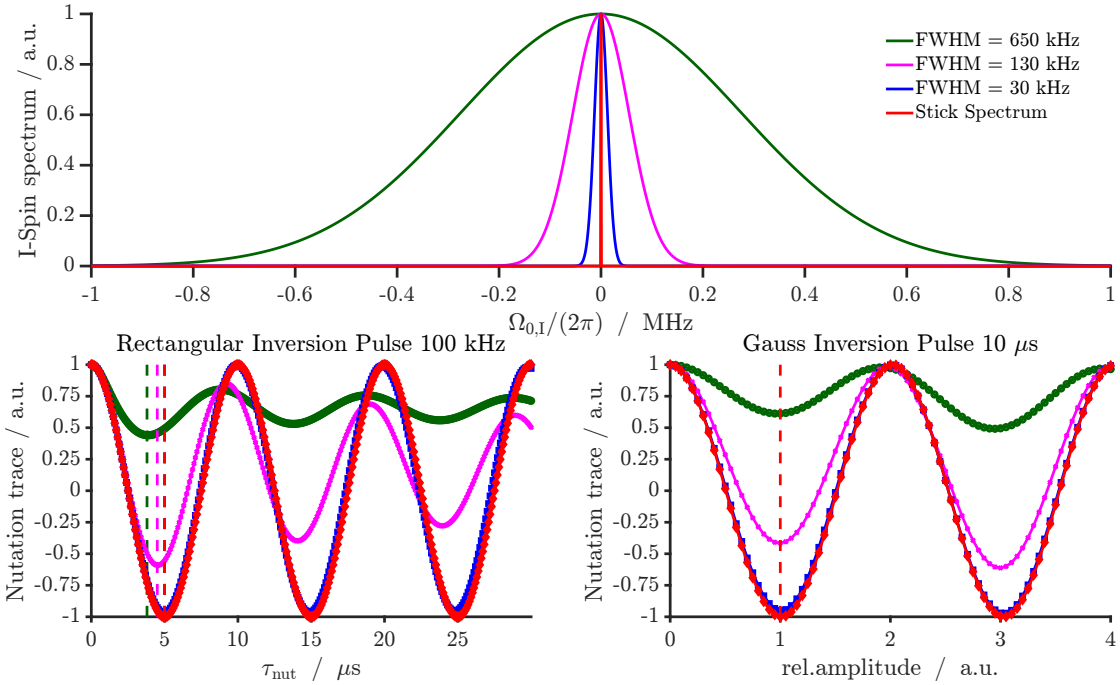

Figure S29: Comparison of simulated nutation traces using a proton spectrum with different FWHM values as indicated in the legend. Nutation traces are shown for a stick spectrum (FWHM = 0 kHz, red), for an FWHM = 30 kHz (blue), for an FWHM = 130 kHz (magenta) and for an FWHM = 650 kHz (dark green). The nutation traces were simulated in the center of the proton line i.e. $\frac{\Omega_{0,I}}{2\pi} = 0$ MHz. The nutation traces for a rectangular inversion pulse with an amplitude of 100 kHz are shown on the left bottom. The first nutation minimum shifts towards lower τ_{nut} for increasing FWHM. This is also observed experimentally when comparing the nutation traces with and without electron decoupling. The nutation traces on the right bottom are simulations using a 10 μs Gauss pulse. A relative amplitude of 1 corresponds to $\sim$ 100 kHz (see Fig. S28). The minima of the nutation traces stay constant at a relative amplitude equal 1, 3, 5, ... An FHWM $\sim$ 650 kHz was found experimentally for the electron-detected proton spectrum without electron decoupling and an FWHM $\sim$ 130 kHz with electron decoupling. The thermal equilibrium proton spectrum has an FWHM of $\sim$ 30 kHz.

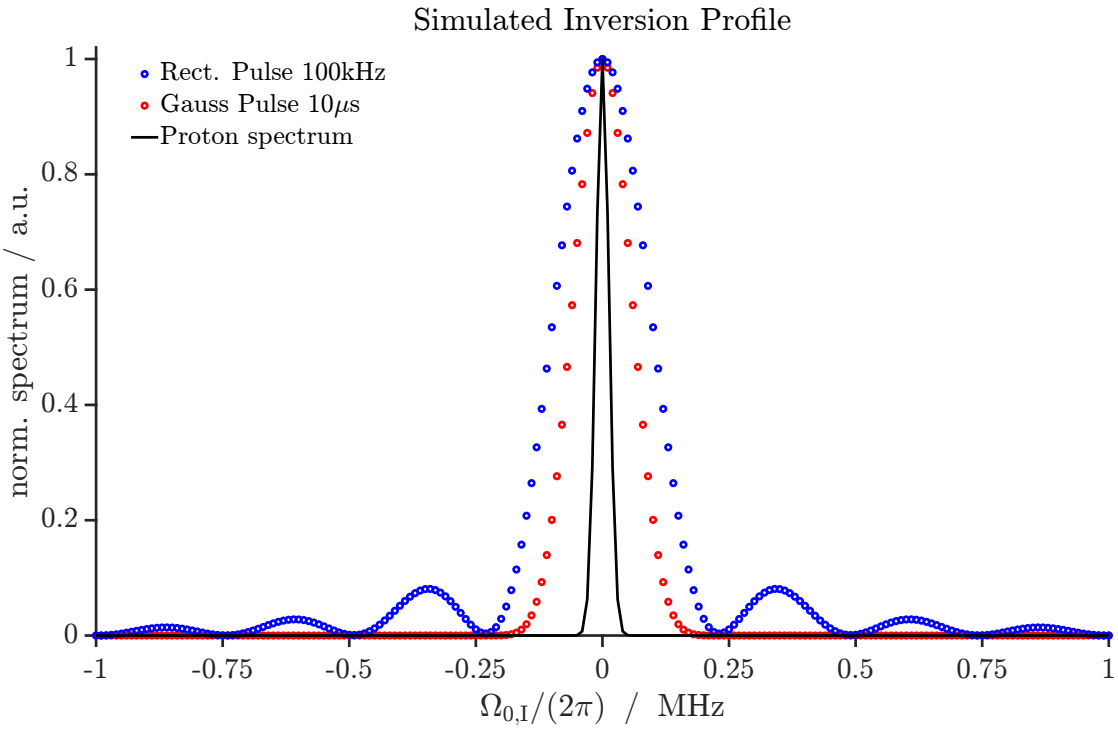

Figure S30: Simulated inversion profile for a proton spectrum with an FWHM = 30 kHz. The blue data points show the simulated inversion profile using a rectangular nutation pulse with a fixed amplitude of 100 kHz and variable pulse length τ_{nut} as shown in Fig. S28. The FWHM of the theoretical inversion profile is $\sim$ 130 kHz for the Gauss pulse and $\sim$ 160 kHz for the rectangular pulse. The red data points show a simulated inversion profile for a Gauss pulse with $\tau_{\mathrm{nut}} = 10$ μs and variable amplitude. A nutation trace for each offset was calculated as shown in Fig. S29 for $\frac{\Omega_{0,\mathrm{I}}}{2\pi} = 0$ MHz. The first minimum of each nutation trace was then extracted and subtracted by the minimum at $\frac{\Omega_{0,\mathrm{I}}}{2\pi} = -1$ MHz. The resulting spectrum was then multiplied by -1 and normalized to the maximum i.e. data point at $\frac{\Omega_{0,\mathrm{I}}}{2\pi} = 0$ MHz. The proton spectrum obtained by using the minima of nutation traces is much broader for both pulse shapes. The reason for this is that the FWHM of the proton spectrum is a factor of $\sim$ 4 smaller than the FWHM of the inversion pulses.

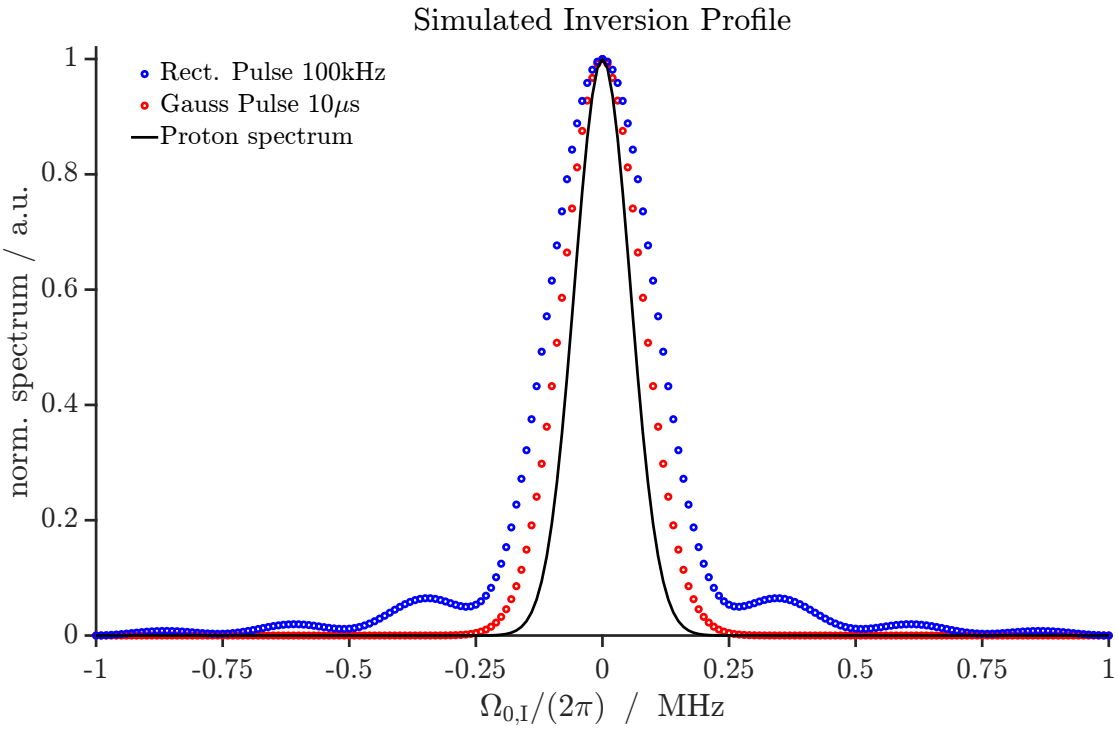

Figure S31: Simulated inversion profile for a proton spectrum with a FWHM = 130 kHz. The blue data points show the simulated inversion profile using a rectangular nutation pulse with a fixed amplitude of 100 kHz and variable pulse length τ_{nut} as shown in Fig. S28. The FWHM of the theoretical inversion profile is $\sim$ 130 kHz for the Gauss pulse and $\sim$ 160 kHz for the rectangular pulse. The red data points show simulated inversion profile for a Gauss pulse with τ_{nut} = 10 μs and variable amplitude. A nutation trace for each offset was calculated as shown in Fig. S29 for $\frac{\Omega_{0,\text{I}}}{2\pi}$ = 0 MHz. The first minimum of each nutation trace was then extracted and subtracted by the minimum at $\frac{\Omega_{0,\text{I}}}{2\pi}$ = -1 MHz. The resulting spectrum was then multiplied by -1 and normalized to the maximum i.e. data point at $\frac{\Omega_{0,\text{I}}}{2\pi}$ = 0 MHz. The proton spectrum obtained by using the minima of nutation traces is much broader spectrum for both pulse shapes. The reason for this is that the FWHM of the proton spectrum is equal to the FWHM of the inversion pulses.

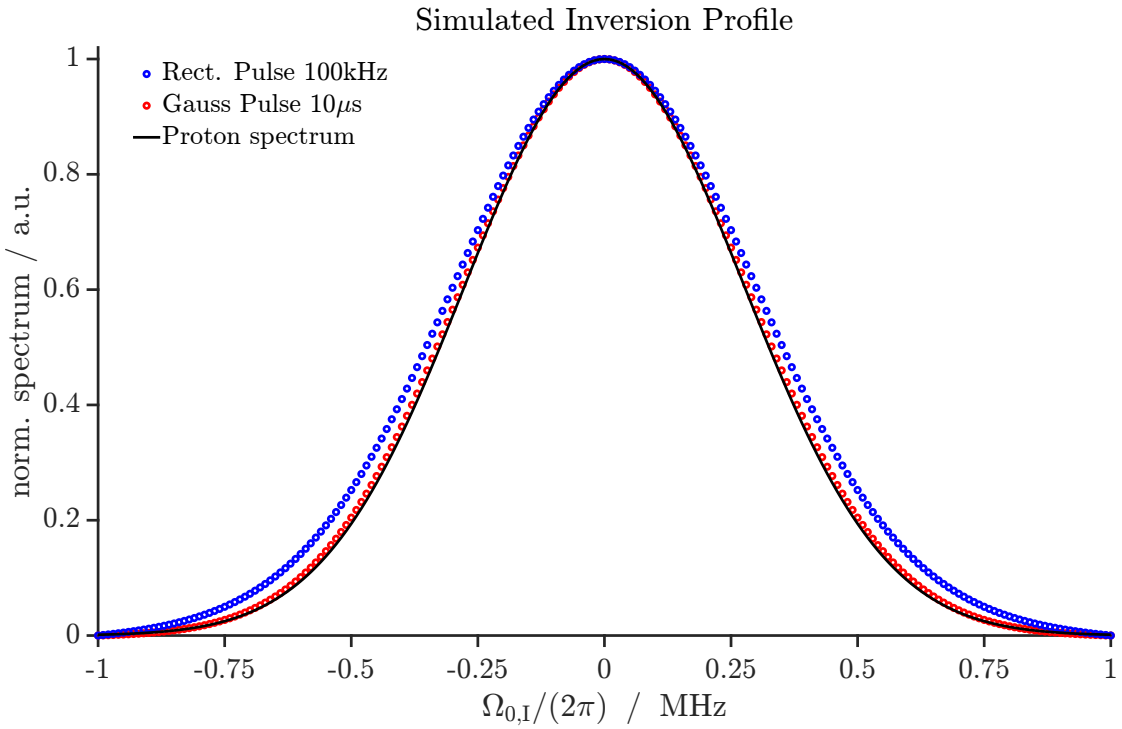

Figure S32: Simulated inversion profile for a proton spectrum with a FWHM = 650 kHz. The blue data points show the simulated inversion profile using a rectangular nutation pulse with a fixed amplitude of 100 kHz and variable pulse length τ_{nut} as shown in Fig. S28. The FWHM of the theoretical inversion profile is $\sim$ 130 kHz for the Gauss pulse and $\sim$ 160 kHz for the rectangular pulse. The red data points show simulated inversion profile for a Gauss pulse with τ_{nut} = 10 μs and variable amplitude. A nutation trace for each offset was calculated as shown in Fig. S29 for $\frac{\Omega_{0,\mathrm{I}}}{2\pi} = 0$ MHz. The first minimum of each nutation trace was then extracted and subtracted by the minimum at $\frac{\Omega_{0,\mathrm{I}}}{2\pi} = -1$ MHz. The resulting spectrum was then multiplied by -1 and normalized to the maximum i.e. data point at $\frac{\Omega_{0,\mathrm{I}}}{2\pi} = 0$ MHz. The proton spectrum obtained by using a Gauss nutation pulse reproduces the theoretical proton spectrum (black) almost perfectly. In case of a rectangular nutation pulse a slightly broader spectrum is obtained compared to the theoretical proton spectrum. The reason for this are the side lobes in the inversion profile of Fig. S28.

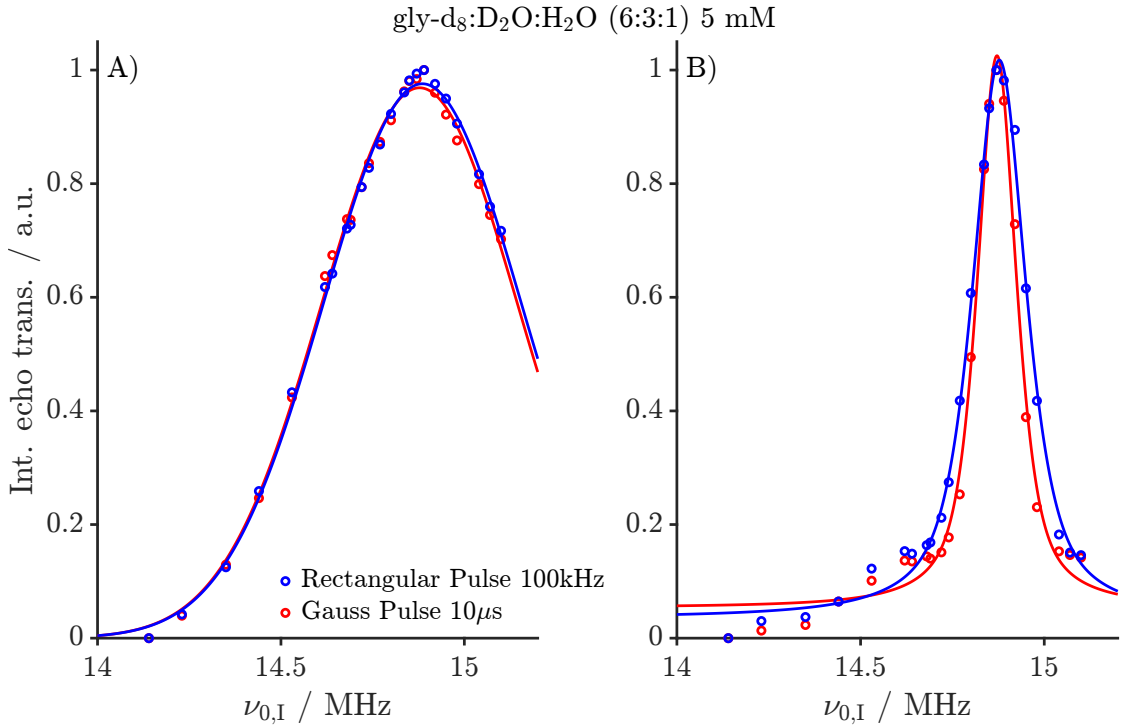

Figure S33: Comparison of electron-detected proton spectra recorded using a rectangular pulse with an Rabi frequency of 100 kHz and a pulse length $\tau_{\mathrm{nut}} \sim 5$ μs and a band-selective Gauss pulse with a Rabi frequency of ~ 100 kHz and a pulse length of 10 μs. In **A)** no electron decoupling was applied during the pulses on the proton channel. In **B)** a π-pulse electron decoupling was applied during the pulses on the proton channel. In **B)** one can nicely observe the effect of the side lobes that are visible in the theoretical inversion profile (Fig. S28).

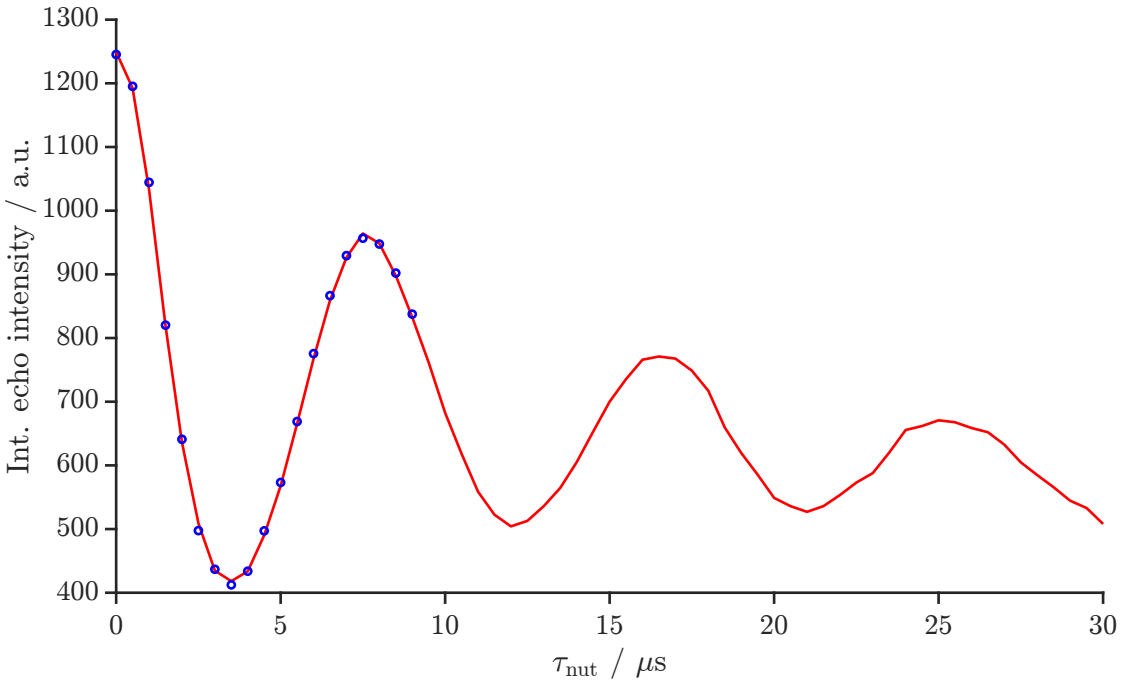

Figure S34: Nutation trace of a rectangular pulse with a fixed amplitude of 100 kHz for 5 mM trityl Ox063 in gly-d_8:D_2O:H_2O (6:3:1) using $\nu_{0,I} = 14.836$ MHz. No electron decoupling was used during the rectangular nutation pulse. The nutation trace in red was recorded for τ_{nut} up to 30 μs and up to 9 μs for the blue dots. For the data presented in this work the nutation traces were measured up to $\tau_{nut} = 9$ μs.

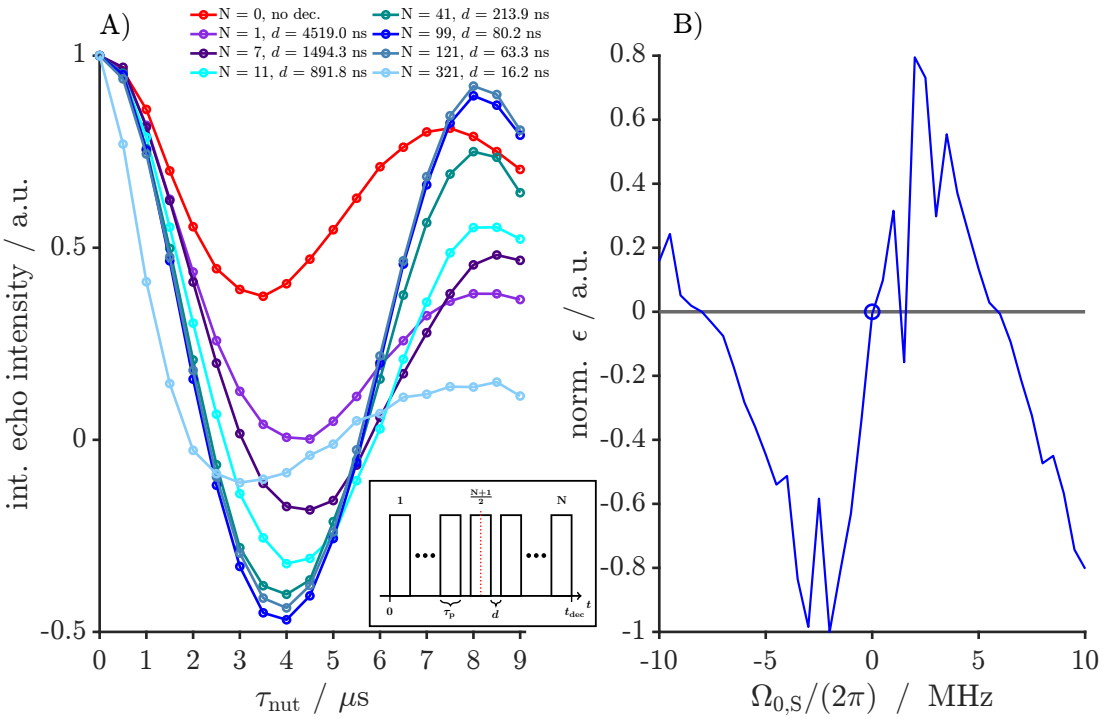

Figure S35: **A)** Comparison of electron decoupling during a rectangular nutation pulse with $\nu_{0,\mathrm{I}} = 14.836$ MHz and an amplitude of 100 kHz. The electron decoupling is a π-pulse train with pulse length $\tau_\mathrm{p} = 12$ ns spaced by a delay d and a total decoupling length $t_\mathrm{dec} = 9.05$ μs. The nutation pulse on the proton channel (not shown) was placed in the center of the decoupling train as indicated by the red dashed line. A π-pulse train with N=99 pulses spaced by $d = 80.2$ ns showed the best decoupling performance (blue data points). **B)** DNP profile using the π-pulse train with N=99 pulses spaced by $d = 80.2$ ns as a DNP contact to check that this pulse train is not a good DNP sequence around $\frac{\Omega_{0,\mathrm{S}}}{2\pi} = 0$ MHz.

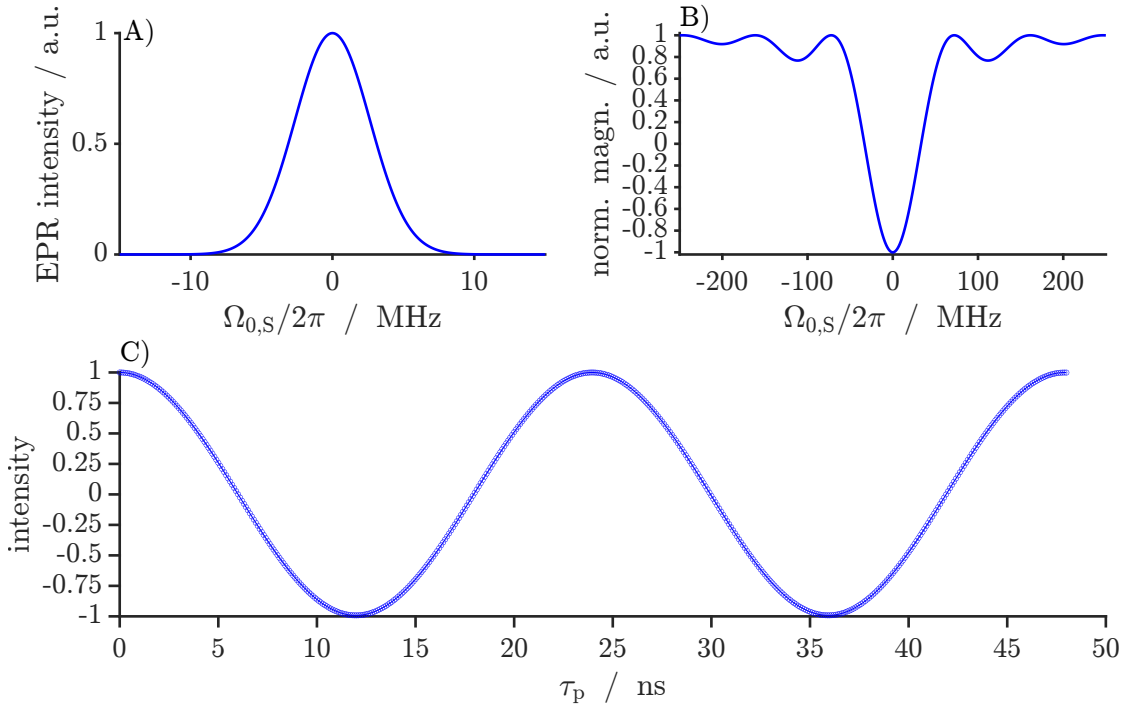

Figure S36: **A)** Theoretical EPR line modelled as a Gaussian line shape with a FWHM of 6.23 MHz. **B)** Inversion profile of a 12 ns rectangular π pulse with an Rabi frequency of $\sim$ 41.667 MHz The FWHM of the inversion profiles is $\sim$ 66.4 MHz. The width where the inversion profile has decayed to the baseline is $\sim$ 144.4 MHz. **C)** Nutation trace calculated for a pulse with varying length and a fixed Rabi frequency $\nu_{1,S} \sim$ 41.667 MHz including the effect of the spectral line with of the EPR line in A). The nutation trace shows a clear minimum at 12 ns.

Sample	$\sum_i (y_{\mathrm{fit},i} - y_{\mathrm{data},i})^2$	y_{off}	w_{G}	I_0	σ_{FWHM} / MHz	$\nu_{0,\mathrm{I}}^{(\mathrm{c})}$ / MHz
gly-d_8:D_2O:H_2O (6:3:1)	0.006	0.000	1.000	0.969	0.629	14.878
gly-d_8:D_2O (6:4)	0.019	0.000	1.000	1.018	0.668	14.883
gly-d_8:H_2O (6:4)	0.008	0.000	0.600	0.987	0.547	14.881
gly-d_8:D_2O:H_2O (6:3:1), 100 μM	0.018	0.000	1.000	1.001	0.655	14.883

Table S1: Fit according to Eq. S.4 of electron-detected proton spectrum using a Gauss nutation pulse of 10 μs and no electron decoupling and $t_{\mathrm{del}} = 15\mu$s

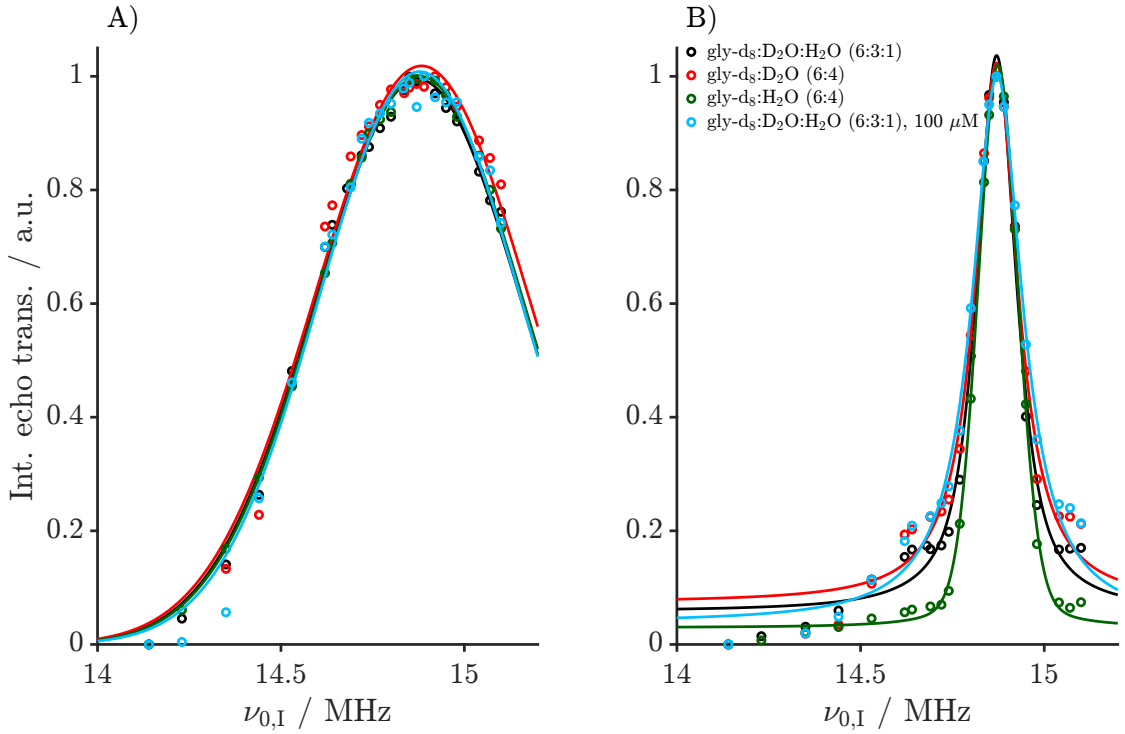

Figure S37: Electron-detected proton spectrum for 5 mM trityl Ox063 in gly-d_8:D_2O:H_2O (6:3:1) black, gly-d_8:D_2O (6:4) red and gly-d_8:H_2O (6:4) green and for 100 μM trityl Ox063 in gly-d_8:D_2O:H_2O (6:3:1). The Gauss nutation pulse was placed in the middle of the delay t_{del} = 800 μs and t_{SL} = 4000 ns. In **A)** the electron-detected proton spectrum without electron decoupling is shown and in **B)** with electron decoupling. Within experimental error between the four different measurement sessions the electron-detected proton spectra are identical.

Sample	$\sum_i (y_{fit,i} - y_{data,i})^2$	y_{off}	w_G	I_0	σ_{FWHM} / MHz	$\nu_{0,I}^{(c)}$ / MHz
gly-d_8:D_2O:H_2O (6:3:1)	0.023	0.053	0.323	0.972	0.127	14.871
gly-d_8:D_2O (6:4)	0.028	0.060	0.085	0.967	0.138	14.871
gly-d_8:H_2O (6:4)	0.006	0.029	0.861	0.991	0.129	14.875
gly-d_8:D_2O:H_2O (6:3:1), 100 μM	0.030	0.051	0.000	0.964	0.168	14.873

Table S2: Fit according to Eq. S.4 of electron-detected proton spectrum using a 10 μs long Gauss nutation pulse, electron decoupling and t_{del} = 15μs

Sample	$\sum_i (y_{\mathrm{fit},i} - y_{\mathrm{data},i})^2$	y_{off}	w_{G}	I_0	σ_{FWHM} / MHz	$\nu_{0,\mathrm{I}}^{(\mathrm{c})}$ / MHz
gly-d_8:D_2O:H_2O (6:3:1)	0.012	0.000	1.000	0.995	0.663	14.875
gly-d_8:D_2O (6:4)	0.029	0.000	1.000	1.018	0.682	14.883
gly-d_8:H_2O (6:4)	0.003	0.000	1.000	1.000	0.661	14.879
gly-d_8:D_2O:H_2O (6:3:1), 100 μM	0.030	0.000	1.000	1.008	0.646	14.878

Table S3: Fit according to Eq. S.4 of electron-detected proton spectrum with a Gauss nutation pulse, no electron decoupling and $t_{\mathrm{del}} = 800\mu$s

Sample	$\sum_i (y_{\mathrm{fit},i} - y_{\mathrm{data},i})^2$	y_{off}	w_{G}	I_0	σ_{FWHM} / MHz	$\nu_{0,\mathrm{I}}^{(\mathrm{c})}$ / MHz
gly-d_8:D_2O:H_2O (6:3:1)	0.030	0.058	0.193	0.979	0.130	14.870
gly-d_8:D_2O (6:4)	0.029	0.073	0.000	0.950	0.140	14.870
gly-d_8:H_2O (6:4)	0.006	0.029	0.788	0.990	0.129	14.874
gly-d_8:D_2O:H_2O (6:3:1), 100 μM	0.029	0.038	0.000	0.963	0.166	14.872

Table S4: Fit according to Eq. S.4 of electron-detected proton spectrum with a Gauss nutation pulse, electron decoupling and $t_{\mathrm{del}} = 800\mu$s

C. Proton NMR experiments without DNP

C.1. Thermal Equilibrium Proton Spectrum

The thermal equilibrium spectrum for the proton spin was recorded using a saturation recovery sequence followed by a solid echo detection i.e. ^{1}H sat. $-\Delta t - (\frac{\pi}{2}) - t_{\mathrm{SE}} - (\pi) - t_{\mathrm{SE}} -$ det. with $\Delta t = 180$ s and $t_{\mathrm{SE}} = 20$ μs. The ^{1}H saturation pulse train consists of eleven 100° pulses spaced by 1 ms to destroy any polarization on the proton spin. The value for Δt was estimated from the $T_{1,\mathrm{H}}$ measurements (see below) for the sample with matrix gly-d_8:D_2O:H_2O (6:3:1), (gly-d_8:H_2O (6:4) and for the diluted sample (gly-d_8:D_2O:H_2O (6:3:1) with 100 μM Ox063 trityl concentration). For the sample with matrix gly-d_8:D_2O (6:4) the value was estimated to be the same as for the other three samples. For the matrices gly-d_8:D_2O:H_2O (6:3:1) and gly-d_8:H_2O (6:4) a number of scans of 424 was used. For the sample (gly-d_8:D_2O (6:4) 384 and for the diluted sample 408. The plotted proton spectra in Fig. S38 are normalized by the number of scans.

The spectra were fitted to a pseudo-Voigt (Gaussian-Lorentzian blend)

$$\mathrm{I}_0 \cdot \left(w_\mathrm{G} \cdot \exp\left\{ \frac{\left(f - \nu_{0,\mathrm{I}}^{(\mathrm{c})}\right)^2}{2 \cdot \left(\frac{\sigma_\mathrm{FWHM}}{2\cdot\sqrt{2\cdot\ln 2}}\right)^2} \right\} + (1 - w_\mathrm{G}) \cdot \frac{(0.5 \cdot \sigma_\mathrm{FWHM})^2}{\left(f - \nu_{0,\mathrm{I}}^{(\mathrm{c})}\right)^2 + (0.5 \cdot \sigma_\mathrm{FWHM})^2} \right) + \mathrm{y}_\mathrm{off}. \quad \text{(S.4)}$$

The fit parameters are given in Tab. S5 for the pseudo-Voigt fit. For the sample with matrices gly-d_8:D_2O (6:4) and gly-d_8:D_2O:H_2O (6:3:1) the spectral line shape is almost a perfect Lorentzian line. For the sample with matrix gly-d_8:H_2O (6:4) there is a slight Gaussian part (up to 20%). Despite having the same number of scans the proton signal for the completely deuterated matrix (green line) is much larger than for the matrix gly-d_8:D_2O:H_2O (6:3:1). This is expected since the number of proton spins is much larger in this sample. The integral of the fitted proton spectrum match well with the calculated number of protons in the three samples see Tab. S6. The calculations of the number of protons include also the protons on the Trityl molecule.

Sample	$\sum_i (y_{\mathrm{fit},i} - y_{\mathrm{data},i})^2$	y_off	w_G	I_0	σ_FWHM / MHz	$\nu_{0,\mathrm{I}}^{(\mathrm{c})}$ / MHz
gly-d_8:D_2O:H_2O (6:3:1), 5 mM	0.060	0.014	0.000	0.208	0.033	14.852
gly-d_8:D_2O (6:4), 5 mM	0.032	0.008	0.043	0.052	0.016	14.852
gly-d_8:H_2O (6:4), 5 mM	0.058	0.028	0.186	0.325	0.054	14.853
gly-d_8:D_2O:H_2O (6:3:1), 100 μM	0.061	0.016	0.000	0.200	0.026	14.852

Table S5: Fit parameters from fitting the thermal equilibrium spectra in Fig. S38 using a pseudo-Voigt fit as given in Eq. S.4.

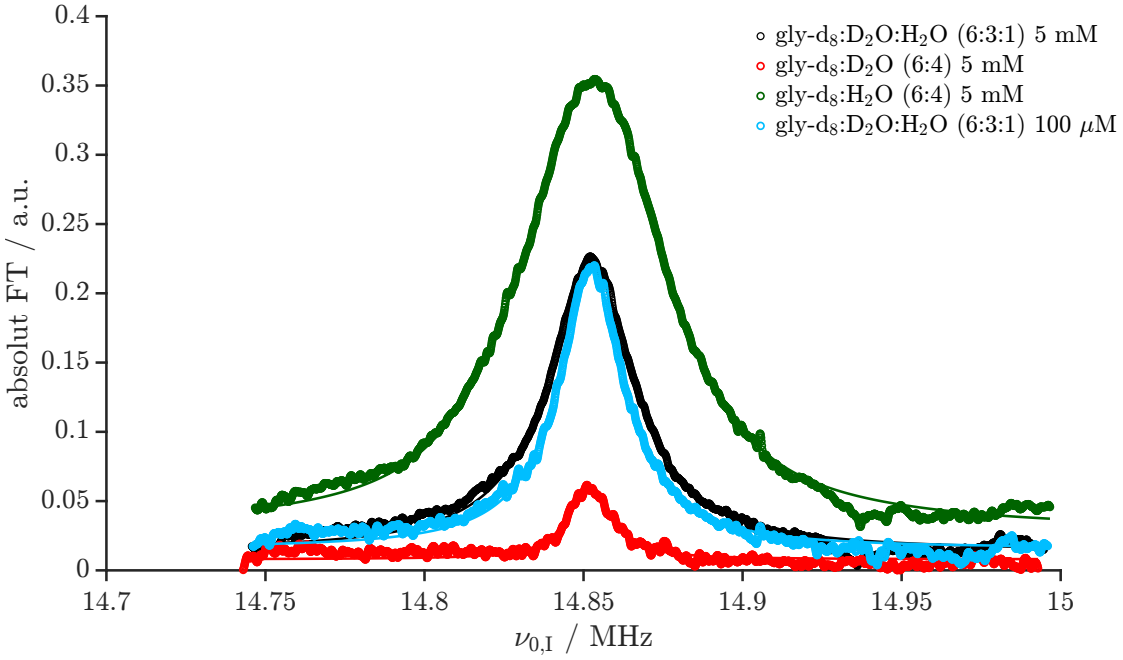

Figure S38: Thermal equilibrium proton spectrum for Trityl Ox063 in three different matrices and with different Trityl concentrations as indicated in the legend of the figure. The data were fitted to a Lorentz-Gauss blend function as given in Eq. S.4.

Sample	Protons in Sample	$\int_A$ Eq. S.4 - y_{off}
gly-d_8:D_2O:H_2O (6:3:1), 5 mM	0.304	0.386
gly-d_8:D_2O (6:4), 5 mM	0.037	0.047
gly-d_8:H_2O (6:4), 5 mM	1.000	1.000
gly-d_8:D_2O:H_2O (6:3:1), 100 μM	0.285	0.293

Table S6: Expected number of protons in the sample compared with the integral of Eq. S.4 minus the offset y_{off}. The integral range was set to $A = (14, 15.7)$ MHz. A possible reason for the difference of $\sim$ 10 % for the matrix gly-d_8:D_2O:H_2O (6:3:1) can be that the used D_2O had exchanged to some extent with atmospheric H_2O during storage.

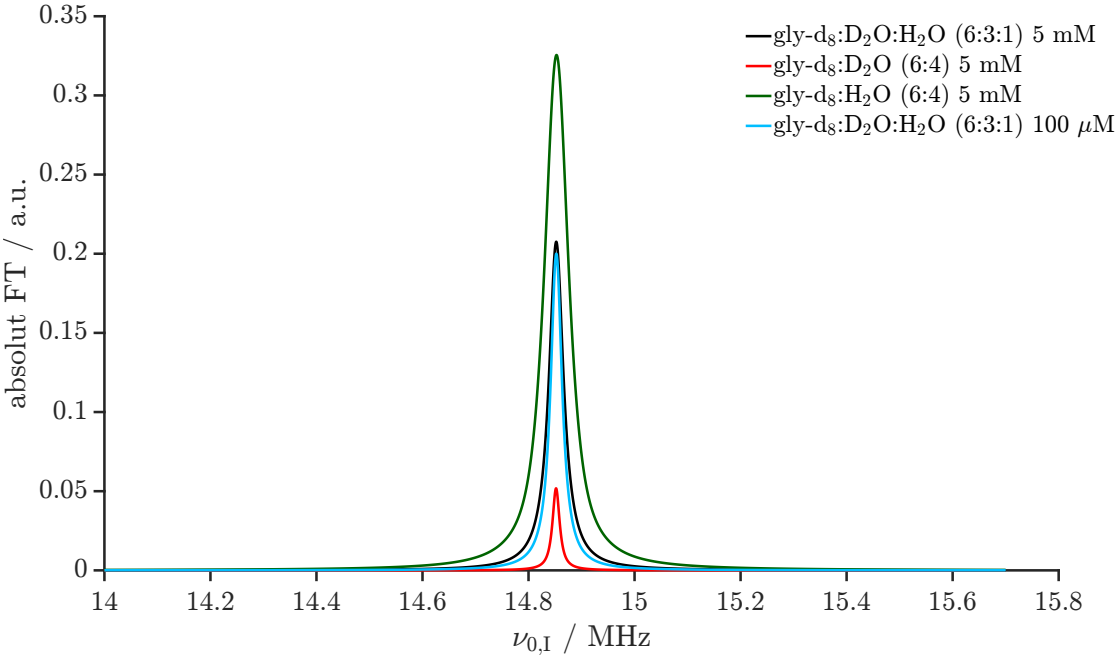

Figure S39: Fitted proton spectra of Fig. S38 used to evaluate the integrals in Tab. S6. The integral range was set to $A = (14, 15.7)$ MHz.

C.2. Longitudinal Relaxation time for Proton Spin

The longitudinal relaxation time for proton spin $T_{1,H}$ was measured using a saturation recovery experiment ^{1}H sat. $-\Delta t-\left(\frac{\pi}{2}\right)-t_{SE}-(\pi)-t_{SE}-$ det. with $t_{SE} = 20$ μs. Δt was varied between 1 s and 180 s. Due to measurement time constraints only the samples with the matrices gly-d_8:D_2O:H_2O (6:3:1) and gly-d_8:H_2O (6:4) were measured. The experimental data are fitted to a mono-exponential function. As expected in the fully protonated matrix the proton spins relaxation is faster ($T_{1,H} = 16.03$ s) compared to the matrix gly-d_8:D_2O:H_2O (6:3:1) $T_{1,H} = 30.04$ s and $T_{1,H} = 38.95$ s. The sample with a 100 μM Trityl concentration in the matrix gly-d_8:D_2O:H_2O (6:3:1) shows a slightly slower decay as the 5 mM sample in the same matrix. Nuclear spins that are hyperfine coupled to an unpaired electron spin relax faster due to the modulation of the magnetic field that the nuclei experiences. But also the coupling network among the ^{1}H spins changes since nuclei close to electron spins are spectrally detuned. Both of this is in agreement with our observation of an increase in $T_{1,H}$ by a decrease of the unpaired electron concentration.

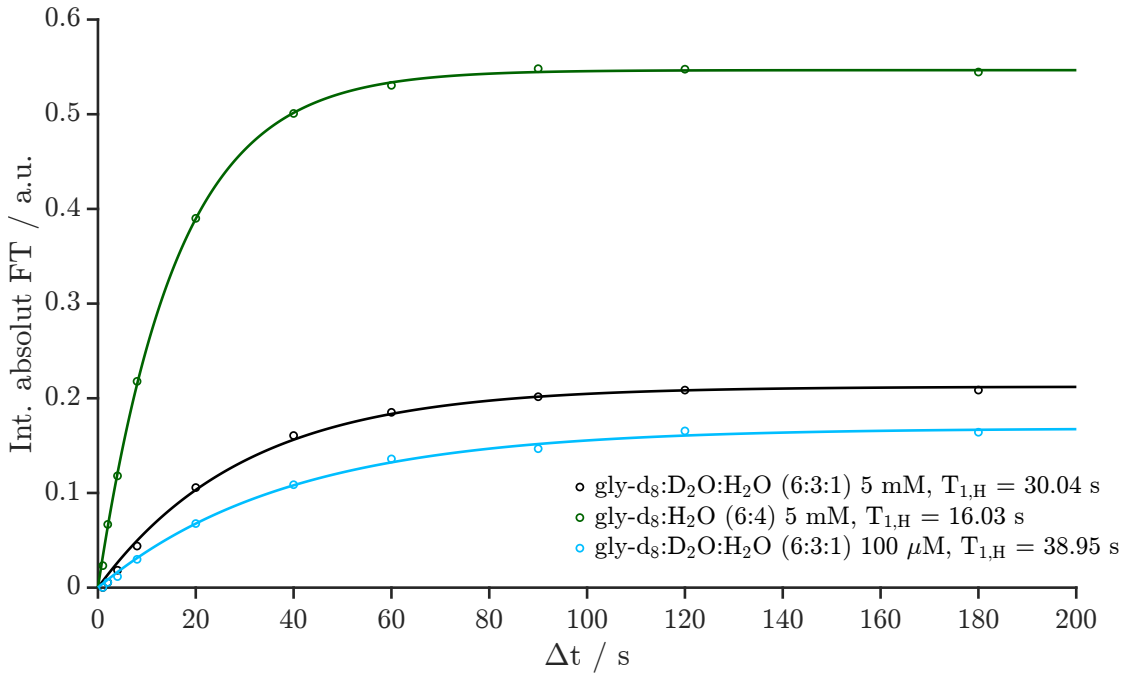

Figure S40: $T_{1,H}$ for the proton spin measurements for the two matrices. The data were fitted to a mono-exponential function.

The relaxation rate constants for the 5 mM sample in in the matrix gly-d_8:D_2O:H_2O (6:3:1) and gly-d_8:H_2O (6:4) were measured over the course of $\sim$ 3 years and $\sim$ 2 months. The extracted $T_{1,H}$ times demonstrate good reproducibility of the measurements.

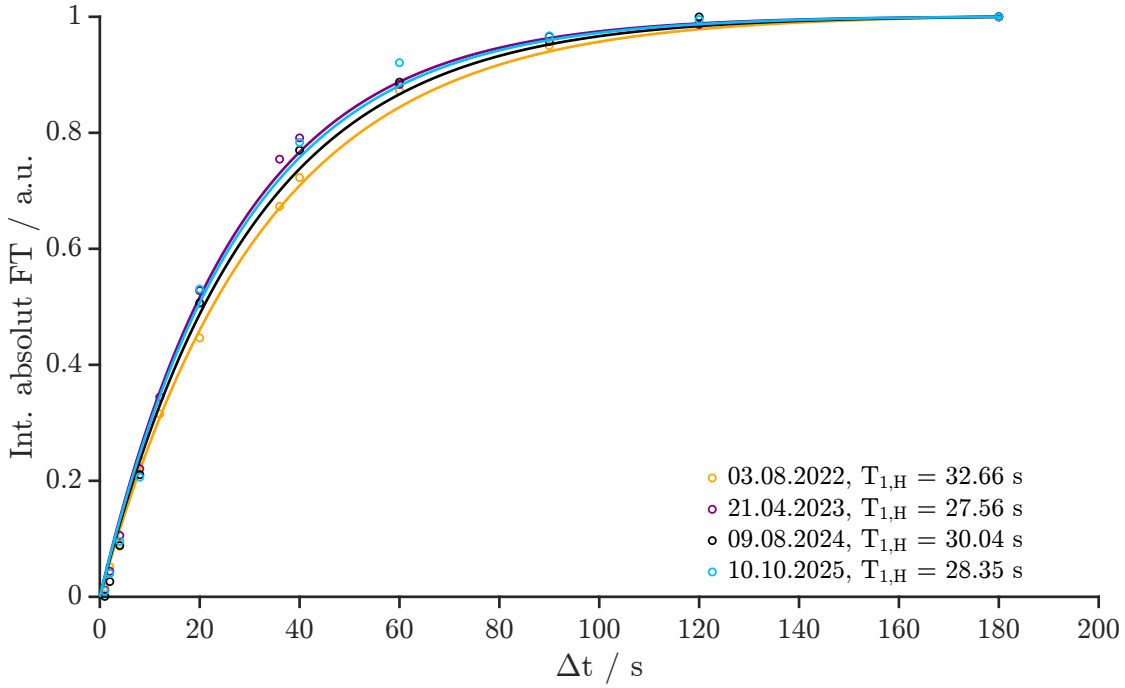

Figure S41: $T_{1,H}$ times for the same 5 mM Ox063 in in the matrix gly-d_8:D_2O:H_2O (6:3:1) measured over the course of $\sim$ 3 years. The data were fitted to a mono-exponential function and normalized towards the data point measured at δt = 180 s.

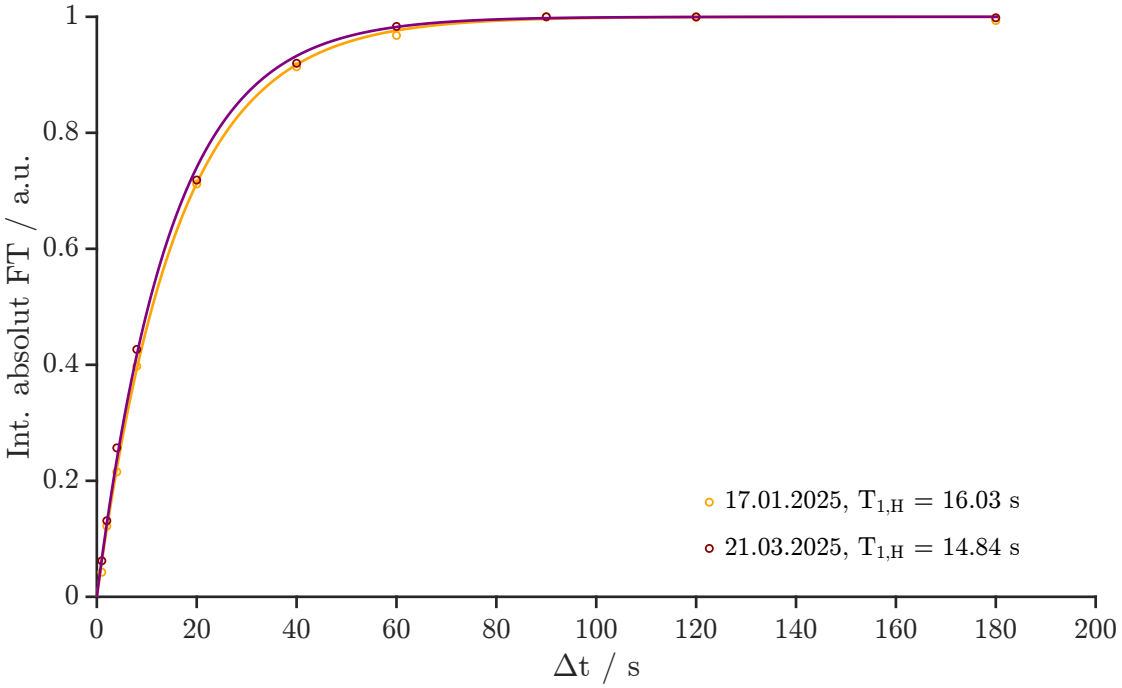

Figure S42: $T_{1,H}$ times for the same 5 mM Ox063 in in the matrix gly-d_8:H_2O (6:4) measured over the course of $\sim$ 2 months. The data were fitted to a mono-exponential function and normalized towards the data point measured at δt = 180 s.

C.3. Proton Pulse Optimization

The pulse amplitudes for bulk proton spins in the DNP sample were optimized by varying the amplitudes of the two pulses of the solid echo simultaneously. The total pulse sequence is shown in Fig. S43. The solid effect at $\frac{\Omega_{0,S}}{2\pi}$ = 14.83 MHz was used as DNP mechanism to optimize the pulse amplitude on the OpenCore spectrometer.

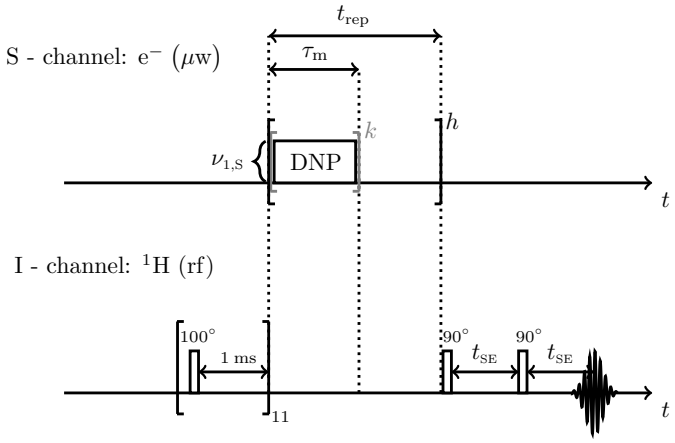

Figure S43: General DNP pulse sequence used in this work. The saturation train on the ^{1}H channel is followed by a repeated DNP cycle (h-loop). The DNP sequence is repeated k-times. The enhanced ^{1}H signal is afterwards recorded with a solid echo with two 90° pulses of 2.5 μs length separated by $t_{\mathrm{SE}} = 20$ μs. A eight-step phase cycle was used for the solid echo with $\{x, x, y, y, -x, -x, -y, -y\}$ for the first pulse and detection and $\{y, -y, x, -x, y, -y, x, -x\}$ for the second pulse.

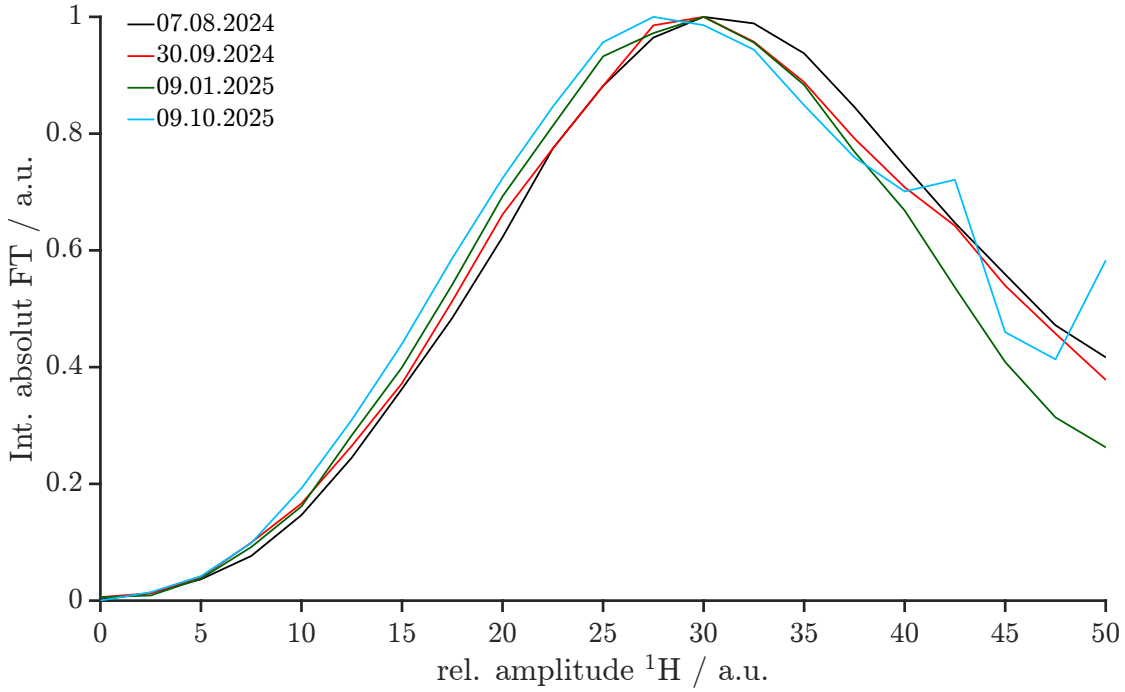

Figure S44: Optimization of a $\frac{\pi}{2}$ pulse on the proton spin for the same 5 mM Ox063 in in the matrix gly-d_8:D_2O:H_2O (6:3:1) measured over the course of $\sim$ 3 years.

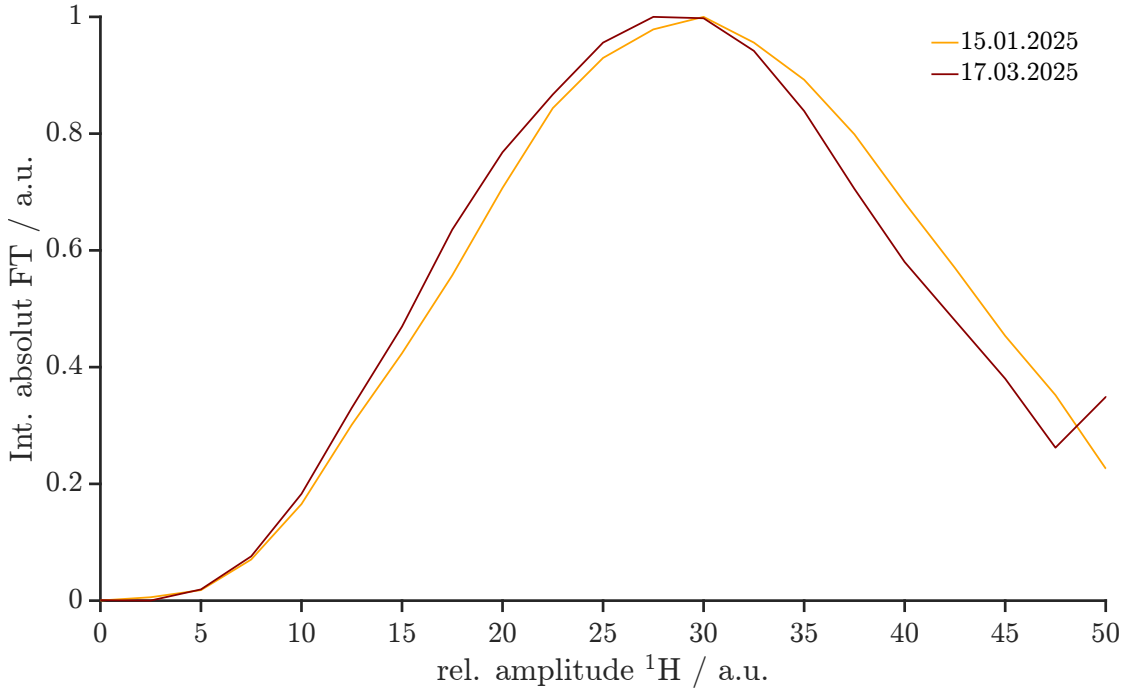

Figure S45: Optimization of a $\frac{\pi}{2}$ pulse on the proton spin for the same 5 mM Ox063 in in the matrix gly-d_8:H_2O (6:4) measured over the course of $\sim$ 2 months.

C.4. Tuning and Matching

At each measurement frequency, the NMR coil in the Bruker EN4118X-MD4 resonator was tuned and impedance matched to optimize signal transmission and reception. An example of a tuning and matching dip for a frequency $f = 14.89$ MHz is shown in Fig. S46. The FWHM of the dip is $\sim$ 270 MHz. A comparison of the tuning and matching behavior for the frequencies measured over the different measurement sessions is plotted in Fig. S47. The largest difference within those four measurement sessions is $\sim$ 2 dB corresponding to an amplitude ratio of $\sim$ 1.259.

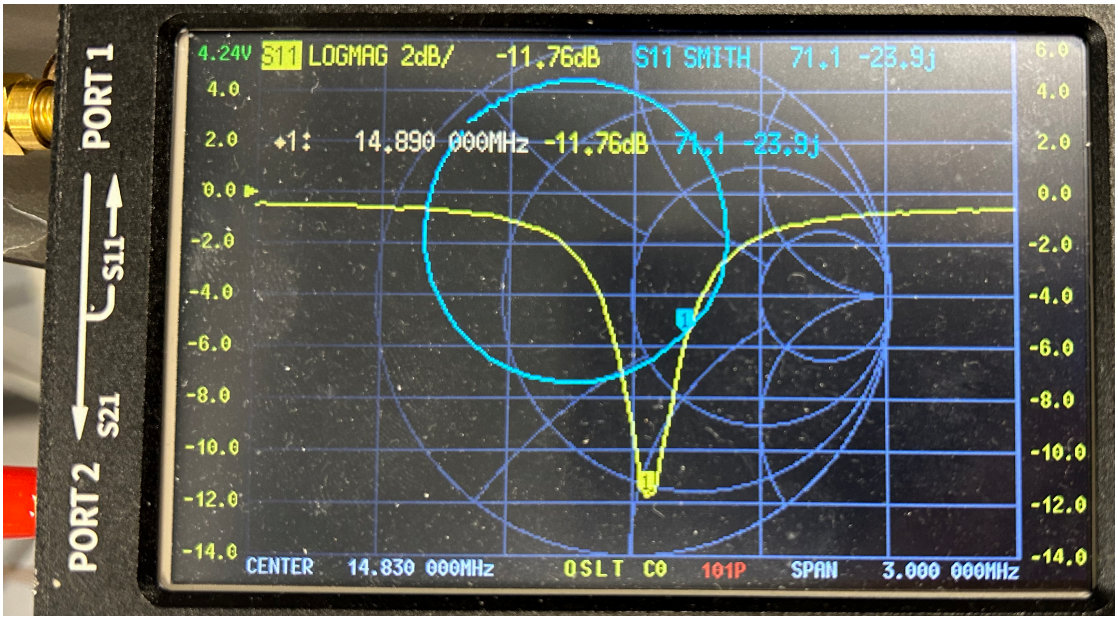

Figure S46: Tuning and matching dip for a frequency of $f = 14.89$ MHz. The minimum of the dip is -11.76 dB. The FWHM of the dip is $\sim$ 270 kHz. The tuning and matching of the NMR coils was done with a NanoVNA V2 (S-A-A-2) vector network analyzer (max. frequency 4 GHz).

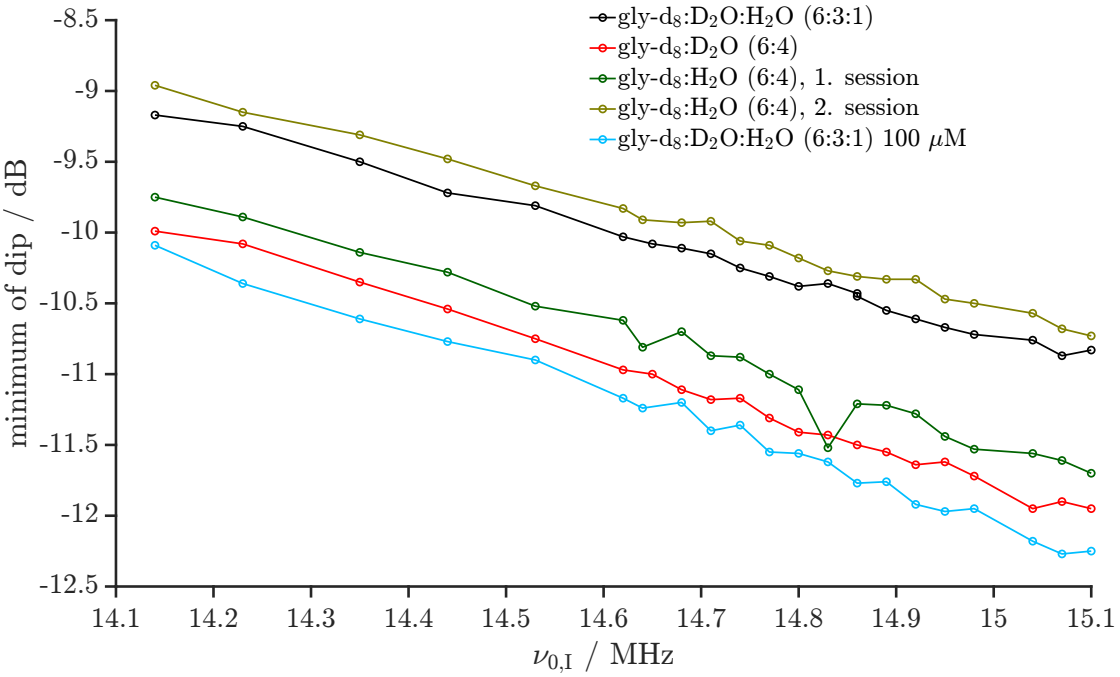

Figure S47: Comparison of the minimum of the tuning and matching dip for each frequency over the different measurement sessions. The largest difference within those four measurement sessions is $\sim$ 2 dB corresponding to an amplitude ratio of $\sim$ 1.259.

D. One Gauss Pulse at the End

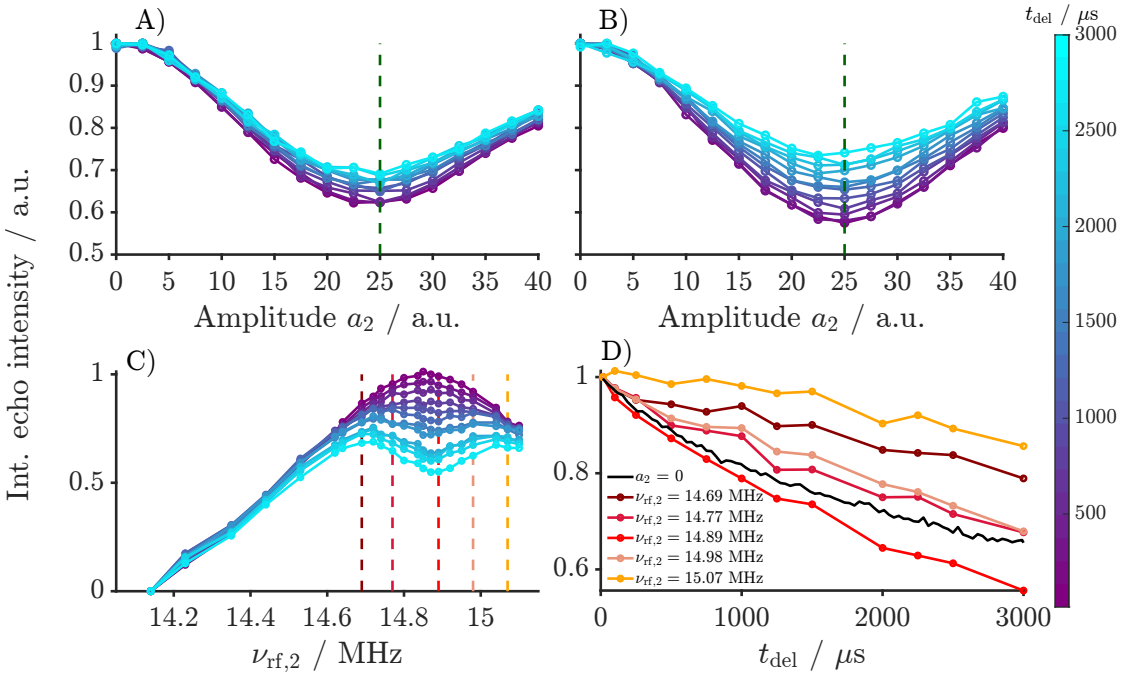

Figure S48: Measurement of spin diffusion from protons nearby an electron spin to bulk protons. **A)** and **B)** Recorded nutation traces for t_{del} ranging from 15 μs to 3000 μs by by varying the amplitude a_2 of the Gauss pulse. The sample was 5 mM trityl in gly-d_8:H_2O (6:4) and t_{SL} = 800 ns. In **A)** the carrier frequency of the Gauss pulse was $\nu_{rf,2}$ = 14.77 MHz and in **B)** 14.89 MHz corresponding to the center of the proton spectrum. The data points to plot the proton spectra were extracted along the green dashed line. **C)** Proton spectra for different delays t_{del}. The spin diffusion towards the bulk is more pronounced in the center of the spectrum. The reddish dashed lines indicate the spectral position where the data points for the traces in **D)** were extracted. **D)** Diffusion traces extracted from **C)** for different frequencies $\nu_{rf,2}$. The diffusion to the bulk is fastest for $\nu_{rf,2}$ = 14.89 MHz corresponding to the center of the spectrum and gets slower moving away from the center. The black solid line indicates a measurement in the absence of any Gauss pulse i.e. $a_2 = 0$.

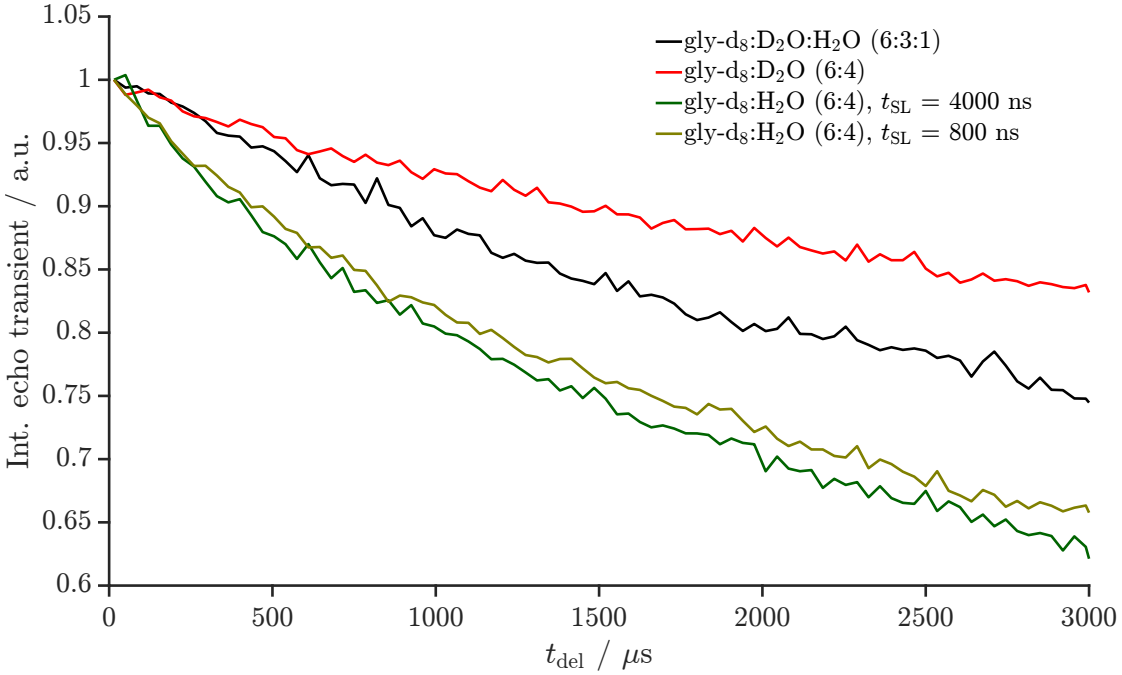

Figure S49: Comparison of the decay of polarization of the proton spins by increasing t_{del} for 5 mM trityl in different matrices. No nutation pulse was applied during t_{del}.The red trace corresponds to the sample with the largest deuteration degree in the matrix (gly-d_8:D_2O (6:4)) and thus shows the slowest decay due to hindered spin diffusion towards the bulk. The sample with the highest protonation degree in the matrix shows the fastest decay (dark green and olive line).

E. Two Gauss Pulse experiment

All the diffusion traces reported in this work are fitted to either

$$I(t) = \Delta I \left(1 - \exp\left(\frac{-t}{\tau}\right)\right) + I_0 \tag{S.5}$$

or

$$I(t) = \Delta I \exp\left(\frac{-t}{\tau}\right) + I_\infty. \tag{S.6}$$

E.1. Comparison across the four different samples

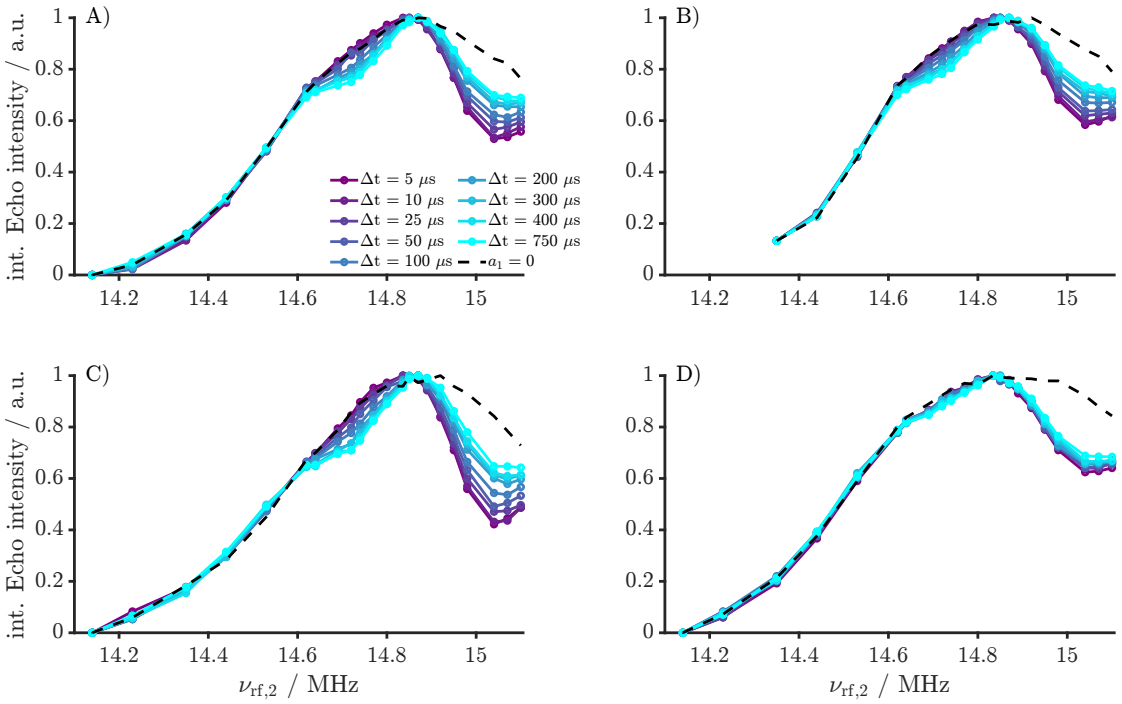

Figure S50: Hole burning spectra for delays Δt between the two Gauss pulses varying from 5 to 750 μs, $t_{del} = 800$ μs and $t_{SL} = 4000$ ns. The hole was burned at $\nu_{rf,1} = 15.04$ MHz. The black dashed lines are obtained by using the data points with $a_1 = 0$ i.e. in the absence of any hole burning pulse. The sample in subplot A) is 5 mM trityl in gly-d_8:D_2O:H_2O (6:3:1), in subplot B) 5 mM trityl in gly-d_8:D_2O (6:4), in subplot C) 5 mM trityl in gly-d_8:H_2O (6:4) and in subplot D) 100 μM trityl in gly-d_8:D_2O:H_2O (6:3:1).

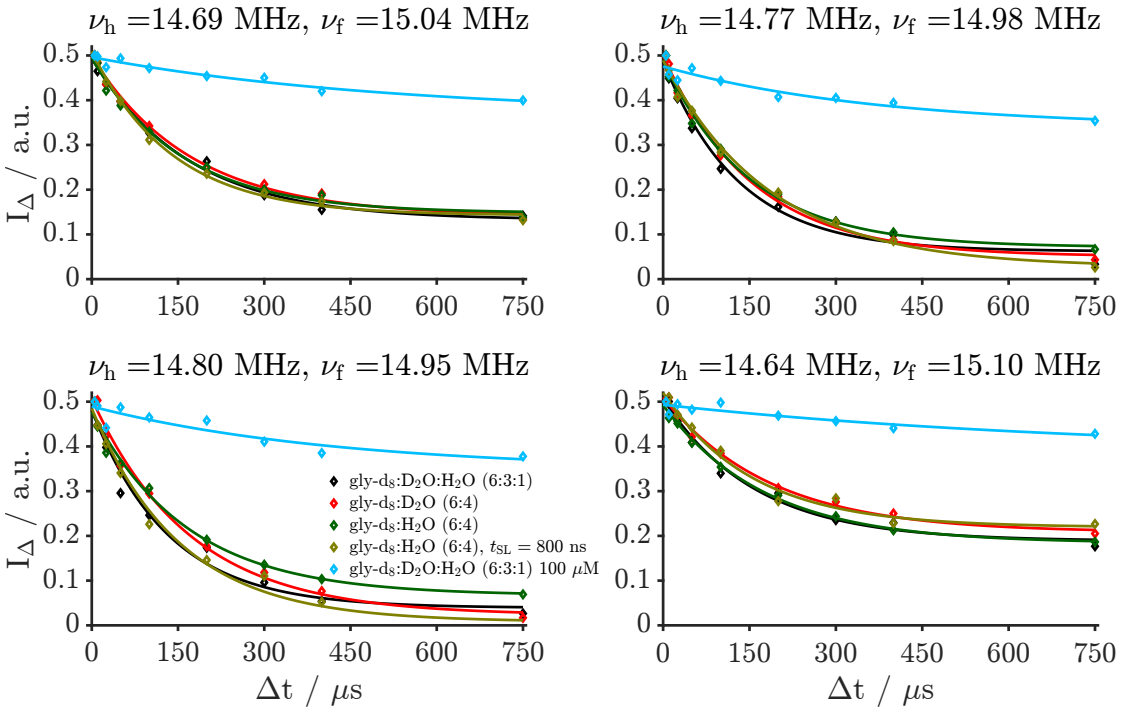

Figure S51: Comparison of the difference magnetization according to Eqs. (2)-(3) in the main text for different combinations of ν_h and ν_f across the four different samples. The hole is burned at $\nu_{rf,1}$ = 14.69 MHz.

Sample	ΔI / a.u.	τ / μs	I_∞ / a.u.
gly-d$_8$:D$_2$O:H$_2$O (6:3:1)	0.361	168.499	0.132
gly-d$_8$:D$_2$O (6:4)	0.356	172.961	0.142
gly-d$_8$:H$_2$O (6:4) / 4000 ns	0.347	155.591	0.148
gly-d$_8$:H$_2$O (6:4) / 800 ns	0.367	140.626	0.142
gly-d$_8$:D$_2$O:H$_2$O (6:3:1) 100 μM	0.129	530.830	0.367

Table S7: Comparison of the fit parameters from a mono-exponential decay as given in Eq. S.6 and shown in Fig. S51 for difference magnetization I_Δ for all four samples. The hole was burned at $\nu_{rf,1}$ = 14.69 MHz and ν_h =14.69 MHz, ν_f =15.04 MHz.

Sample	ΔI / a.u.	τ / μs	I_∞ / a.u.
gly-d_8:D_2O:H_2O (6:3:1)	0.318	158.369	0.189
gly-d_8:D_2O (6:4)	0.302	184.828	0.208
gly-d_8:H_2O (6:4) / 4000 ns	0.308	176.100	0.184
gly-d_8:H_2O (6:4) / 800 ns	0.301	155.195	0.219
gly-d_8:D_2O:H_2O (6:3:1) 100 μM	0.109	773.833	0.384

Table S8: Comparison of the fit parameters from a mono-exponential decay as given in Eq. S.6 and shown in Fig. S51 for difference magnetization I_Δ for all four samples. The hole was burned at $\nu_{rf,1}$ = 14.69 MHz and ν_h =14.64 MHz, ν_f =15.10 MHz.

Sample	ΔI / a.u.	τ / μs	I_∞ / a.u.
gly-d_8:D_2O:H_2O (6:3:1)	0.426	130.713	0.062
gly-d_8:D_2O (6:4)	0.450	154.005	0.051
gly-d_8:H_2O (6:4) / 4000 ns	0.418	149.555	0.071
gly-d_8:H_2O (6:4) / 800 ns	0.462	185.395	0.027
gly-d_8:D_2O:H_2O (6:3:1) 100 μM	0.137	376.367	0.339

Table S9: Comparison of the fit parameters from a mono-exponential decay as given in Eq. S.6 and shown in Fig. S51 for difference magnetization I_Δ for all four samples. The hole was burned at $\nu_{rf,1}$ = 14.69 MHz and ν_h =14.77 MHz, ν_f =14.98 MHz.

Sample	ΔI / a.u.	τ / μs	I_∞ / a.u.
gly-d_8:D_2O:H_2O (6:3:1)	0.443	133.227	0.039
gly-d_8:D_2O (6:4)	0.484	171.248	0.023
gly-d_8:H_2O (6:4) / 4000 ns	0.410	166.270	0.067
gly-d_8:H_2O (6:4) / 800 ns	0.477	153.384	0.008
gly-d_8:D_2O:H_2O (6:3:1) 100 μM	0.143	428.640	0.346

Table S10: Comparison of the fit parameters from a mono-exponential decay as given in Eq. S.6 and shown in Fig. S51 for difference magnetization I_Δ for all four samples. The hole was burned at $\nu_{rf,1}$ = 14.69 MHz and ν_h =14.80 MHz, ν_f =14.95 MHz.

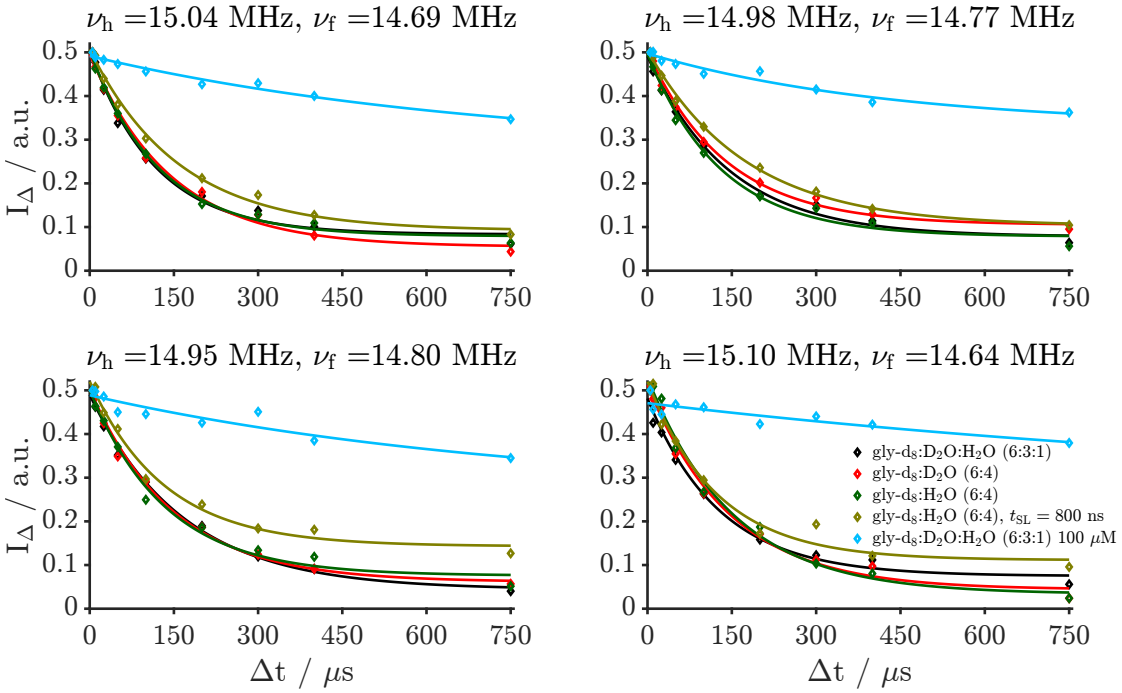

Figure S52: Comparison of the difference magnetization according to Eqs. (2)-(3) in the main text for different combinations of ν_h and ν_f across the four different samples. The hole is burned at $\nu_{rf,1}$ = 15.04 MHz.

Sample	ΔI / a.u.	τ / μs	I_∞ / a.u.
gly-d_8:D_2O:H_2O (6:3:1)	0.421	116.877	0.083
gly-d_8:D_2O (6:4)	0.442	144.066	0.055
gly-d_8:H_2O (6:4) / 4000 ns	0.425	122.797	0.079
gly-d_8:H_2O (6:4) / 800 ns	0.415	158.636	0.092
gly-d_8:D_2O:H_2O (6:3:1) 100 μM	0.219	715.972	0.272

Table S11: Comparison of the fit parameters from a mono-exponential decay as given in Eq. S.6 and shown in Fig. S52 for difference magnetization I_Δ for all four samples. The hole was burned at $\nu_{rf,1}$ = 15.04 MHz and ν_h =15.04 MHz, ν_f =14.69 MHz.

Sample	ΔI / a.u.	τ / μs	I_∞ / a.u.
gly-d_8:D_2O:H_2O (6:3:1)	0.407	128.280	0.075
gly-d_8:D_2O (6:4)	0.469	146.387	0.044
gly-d_8:H_2O (6:4) / 4000 ns	0.495	152.299	0.033
gly-d_8:H_2O (6:4) / 800 ns	0.409	123.983	0.111
gly-d_8:D_2O:H_2O (6:3:1) 100 μM	0.216	1408.415	0.255

Table S12: Comparison of the fit parameters from a mono-exponential decay as given in Eq. S.6 and shown in Fig. S52 for difference magnetization I_Δ for all four samples. The hole was burned at $\nu_{rf,1}$ = 15.04 MHz and ν_h =15.10 MHz, ν_f =14.64 MHz.

Sample	ΔI / a.u.	τ / μs	I_∞ / a.u.
gly-d_8:D_2O:H_2O (6:3:1)	0.413	144.957	0.078
gly-d_8:D_2O (6:4)	0.398	139.507	0.105
gly-d_8:H_2O (6:4) / 4000 ns	0.418	130.949	0.078
gly-d_8:H_2O (6:4) / 800 ns	0.402	174.666	0.103
gly-d_8:D_2O:H_2O (6:3:1) 100 μM	0.167	438.409	0.330

Table S13: Comparison of the fit parameters from a mono-exponential decay as given in Eq. S.6 and shown in Fig. S52 for difference magnetization I_Δ for all four samples. The hole was burned at $\nu_{rf,1}$ = 15.04 MHz and ν_h =14.98 MHz, ν_f =14.77 MHz.

Sample	ΔI / a.u.	τ / μs	I_∞ / a.u.
gly-d_8:D_2O:H_2O (6:3:1)	0.446	166.816	0.044
gly-d_8:D_2O (6:4)	0.442	148.109	0.061
gly-d_8:H_2O (6:4) / 4000 ns	0.426	135.442	0.076
gly-d_8:H_2O (6:4) / 800 ns	0.377	133.333	0.143
gly-d_8:D_2O:H_2O (6:3:1) 100 μM	0.230	781.659	0.259

Table S14: Comparison of the fit parameters from a mono-exponential decay as given in Eq. S.6 and shown in Fig. S52 for difference magnetization I_Δ for all four samples. The hole was burned at $\nu_{rf,1}$ = 15.04 MHz and ν_h =14.95 MHz, ν_f =14.80 MHz.

E.2. 5 mM trityl in gly-d_8:D_2O:H_2O (6:3:1)

$\nu_{rf,1}$ = 14.69 MHz

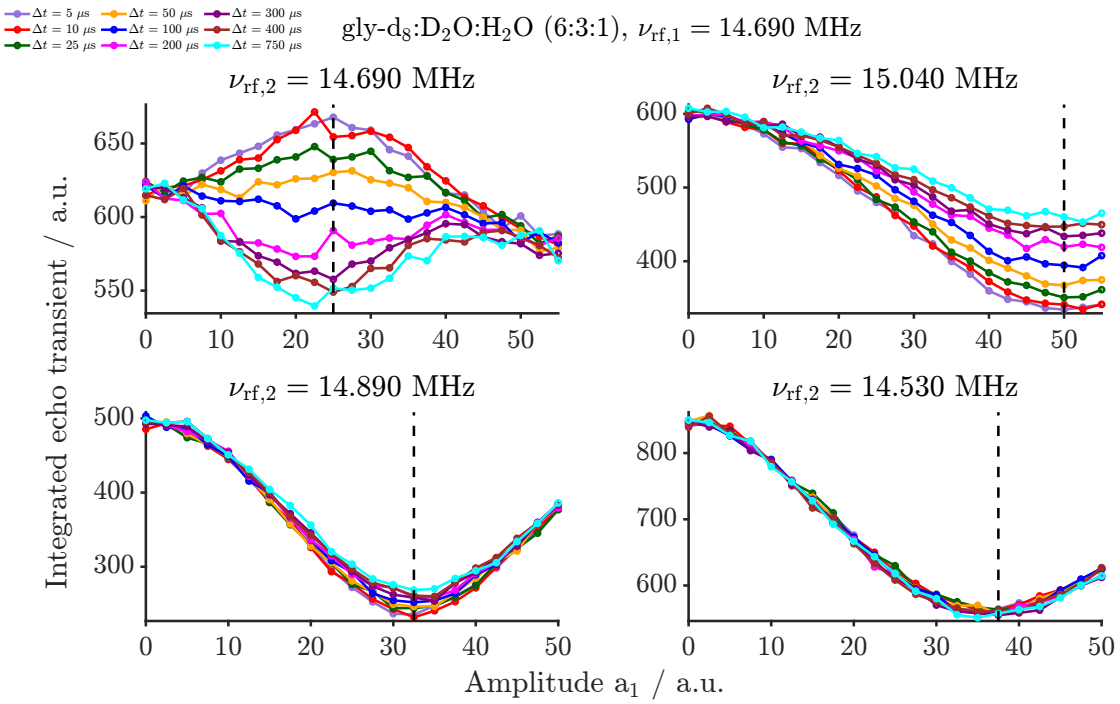

Figure S53: Amplitude traces recorded by sweeping the amplitude a_1 of the first Gauss pulse in steps of 2.5 for $\nu_{rf,1}$ = 14.69 MHz. An amplitude a_1 of 30 corresponds to a Rabi frequency of 100 kHz. The delay Δt between the first and second Gauss pulse was varied from 5 to 750 μs and is indicated in the legend of the figure. Here four different frequencies as examples are shown for the second Gauss pulse $\nu_{rf,2}$ = 14.53, 14.69, 14.89 and 15.04 MHz for the matrix gly-d_8:D_2O:H_2O (6:3:1). 10 shots were used for each individual data point, t_{del} = 800 μs and t_{SL} = 4000 ns.

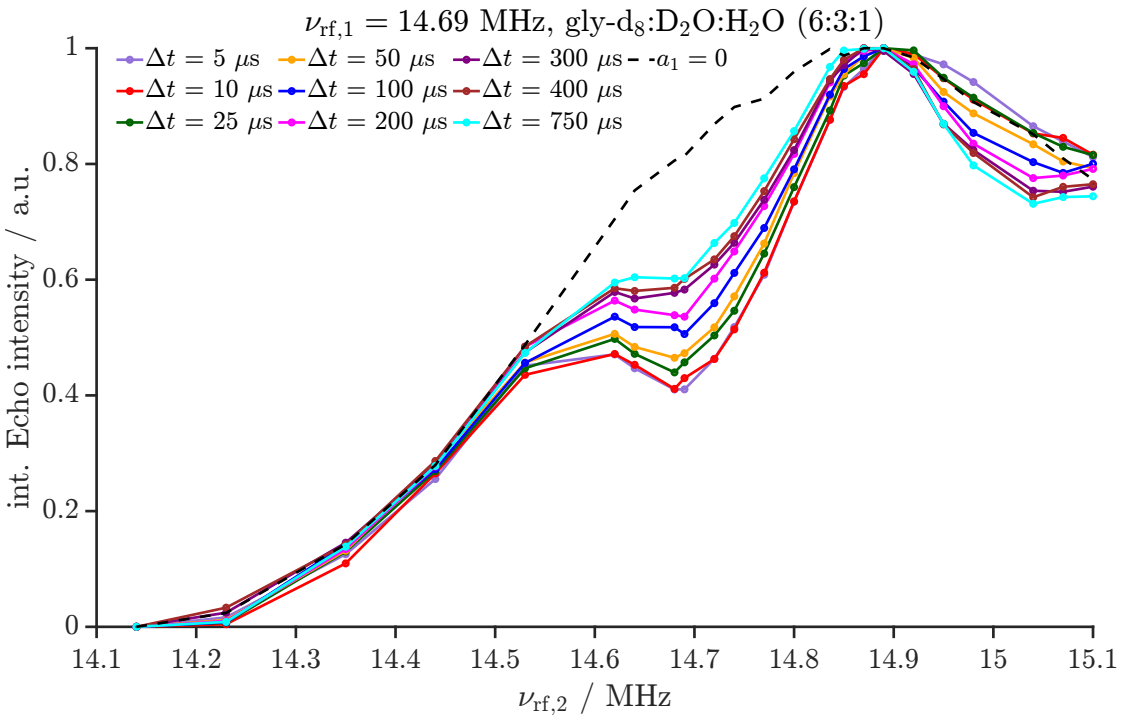

Figure S54: Hole burning spectra for delays Δt between the two Gauss pulses varying from 5 to 750 μs. The hole was burned at $\nu_{rf,1}$ = 14.69 MHz. The black dashed line is obtained by using the data points in Fig. S53 with $a_1 = 0$. The spectra with a hole burned are obtained by using the data points along the dashed line in Fig. S53. The sample is 5 mM trityl in gly-d$_8$:D$_2$O:H$_2$O (6:3:1). 10 shots were used for each individual data point, t_{del} = 800 μs and t_{SL} = 4000 ns.

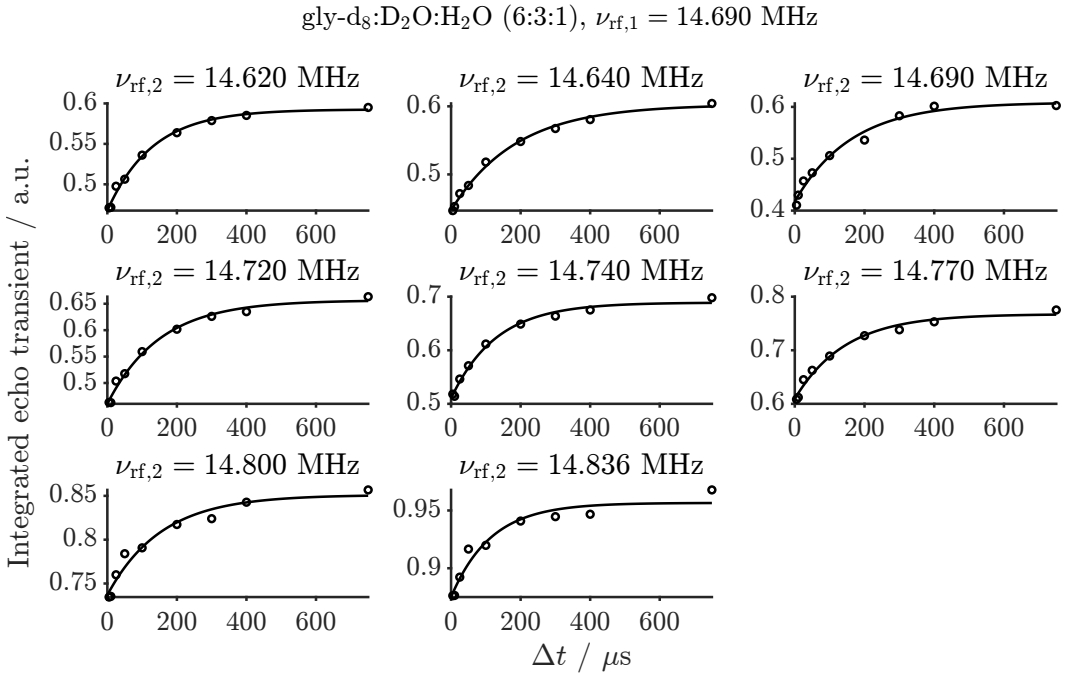

Figure S55: Diffusion traces for the hole burned at $\nu_{rf,1} = 14.69$ MHz using $t_{del} = 800$ μs and $t_{SL} = 4000$ ns. The individual data points are obtained from Fig. S54 for the corresponding frequency $\nu_{rf,2}$. The sample is 5 mM trityl in gly-d_8:D_2O:H_2O (6:3:1) and 10 shots were used for each individual data point. The data points are fitted to the function Eq. S.5 and the corresponding fitting parameters are given in Tab. S15.

$\nu_{\mathrm{rf},2}$ / MHz	ΔI / a.u.	τ / μs	I_0 / a.u.
14.620	0.125	130.118	0.467
14.640	0.155	186.420	0.447
14.690	0.191	163.252	0.418
14.720	0.196	151.483	0.461
14.740	0.179	129.562	0.510
14.770	0.158	145.111	0.609
14.800	0.114	154.546	0.737
14.836	0.082	114.475	0.875

Table S15: Extracted fit parameters from a mono-exponential build-up as given in Eq. S.5 and shown in Fig. S55 for the hole burning at spectral position $\nu_{\mathrm{rf},1}$ = 14.69 MHz. The sample is 5 mM trityl in gly-d_8:D_2O:H_2O (6:3:1).

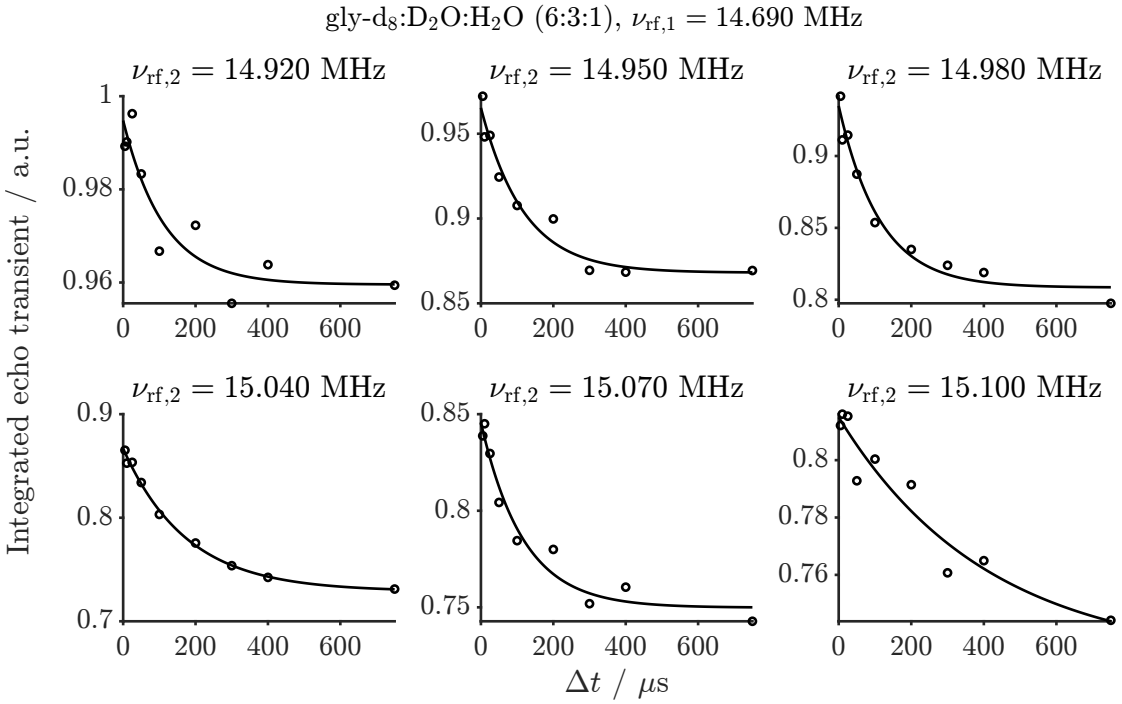

Figure S56: Diffusion traces for the hole burned at $\nu_{rf,1} = 14.69$ MHz using $t_{del} = 800$ μs and $t_{SL} = 4000$ ns. The individual data points are obtained from Fig. S54 for the corresponding frequency $\nu_{rf,2}$. The sample is 5 mM trityl in gly-d_8:D_2O:H_2O (6:3:1) and 10 shots were used for each individual data point. The data points are fitted to the function Eq. S.6 and the corresponding fitting parameters are given in Tab. S16.

$\nu_{rf,2}$ / MHz	ΔI / a.u.	τ / μs	I_∞ / a.u.
14.920	0.035	112.860	0.960
14.950	0.097	118.322	0.868
14.980	0.126	114.097	0.808
15.040	0.138	176.162	0.729
15.070	0.096	117.224	0.750
15.100	0.085	409.900	0.730

Table S16: Extracted fit parameters from a mono-exponential decay as given in Eq. S.6 and shown in Fig. S56 for the hole burning at spectral position $\nu_{rf,1} = 14.69$ MHz. The sample is 5 mM trityl in gly-d_8:D_2O:H_2O (6:3:1).

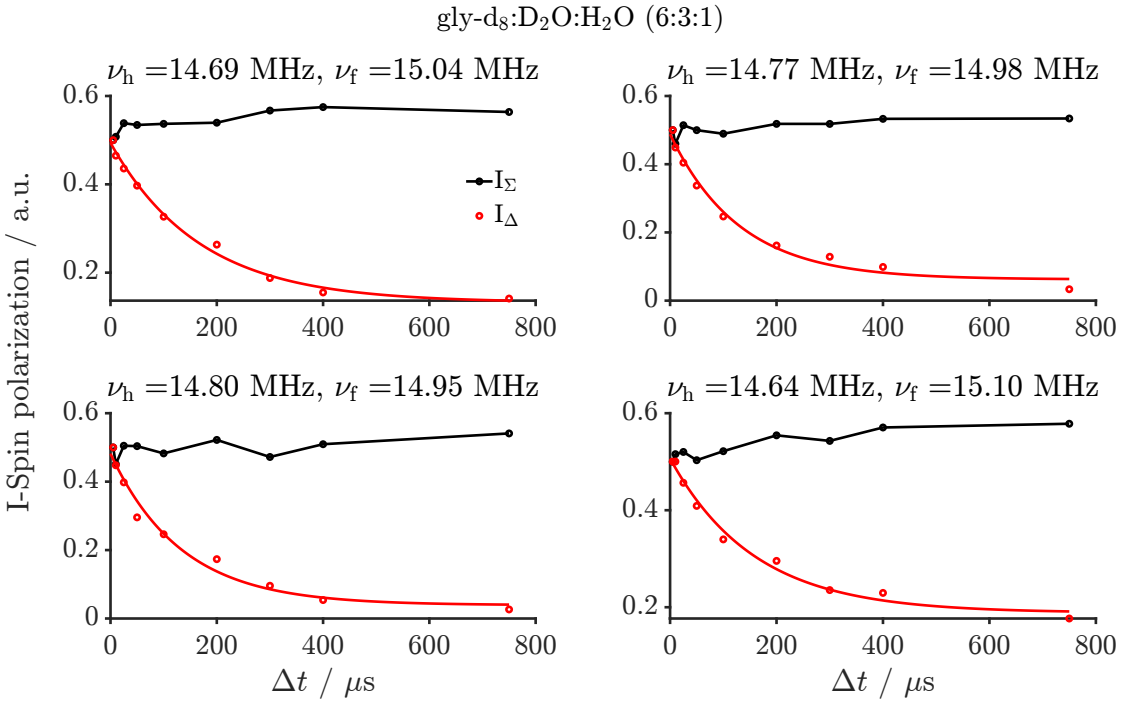

Figure S57: Sum and difference magnetization according to Eqs. (2)-(3) in the main text for different combinations of ν_h and ν_f. The hole is burned at $\nu_{rf,1} = 14.69$ MHz. The sample is 5 mM trityl in gly-d_8:D_2O:H_2O (6:3:1).

ν_h / MHz	ν_f / MHz	ΔI / a.u.	τ / μs	I_∞ / a.u.
14.69	15.04	0.361	168.499	0.132
14.77	14.98	0.426	130.713	0.062
14.80	14.95	0.443	133.227	0.039
14.64	15.10	0.318	158.369	0.189

Table S17: Extracted fit parameters from a mono-exponential decay as given in Eq. S.6 and shown in Fig. S57 for difference magnetization I_Δ as given in Eq. (3) in the main text. The hole is burned at $\nu_{rf,1} = 14.69$ MHz. The sample is 5 mM trityl in gly-d_8:D_2O:H_2O (6:3:1).

$\nu_{rf,1}$ **= 14.89 MHz**

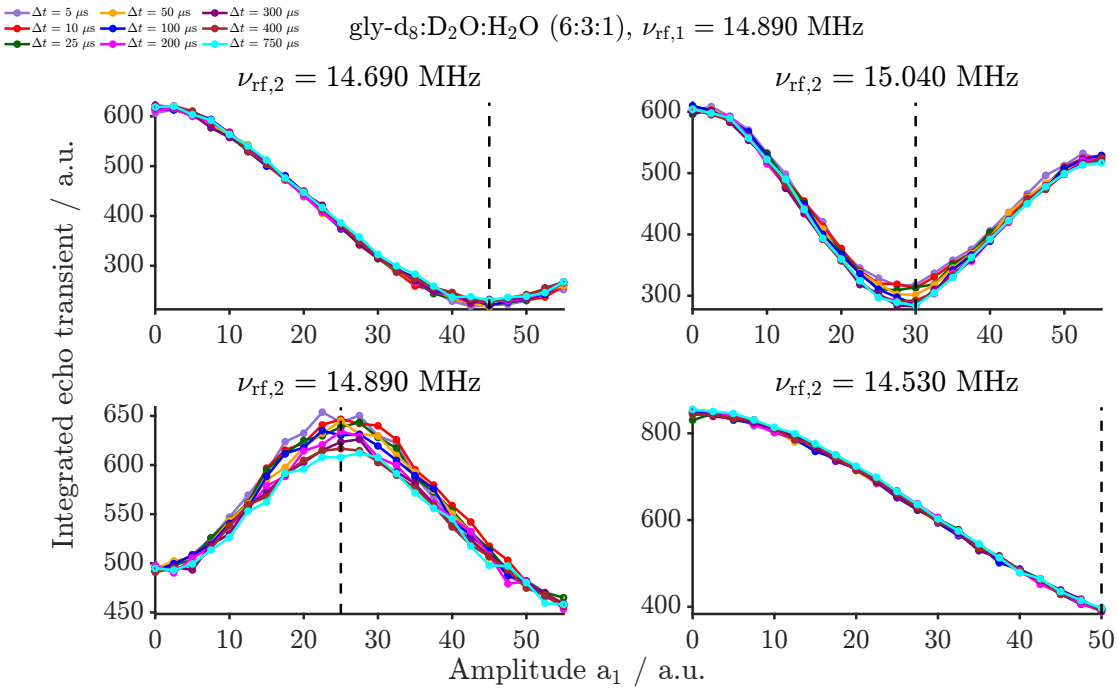

Figure S58: Amplitude traces recorded by sweeping the amplitude a_1 of the first Gauss pulse in steps of 2.5 for $\nu_{rf,1}$ = 14.89 MHz. An amplitude a_1 of 30 corresponds to a Rabi frequency of 100 kHz. The delay Δt between the first and second Gauss pulse was varied from 5 to 750 μs and is indicated in the legend of the figure. Here four different frequencies as examples are shown for the second Gauss pulse $\nu_{rf,2}$ = 14.53, 14.69, 14.89 and 15.04 MHz for the matrix gly-d_8:D_2O:H_2O (6:3:1). 10 shots were used for each individual data point, t_{del} = 800 μs and t_{SL} = 4000 ns.

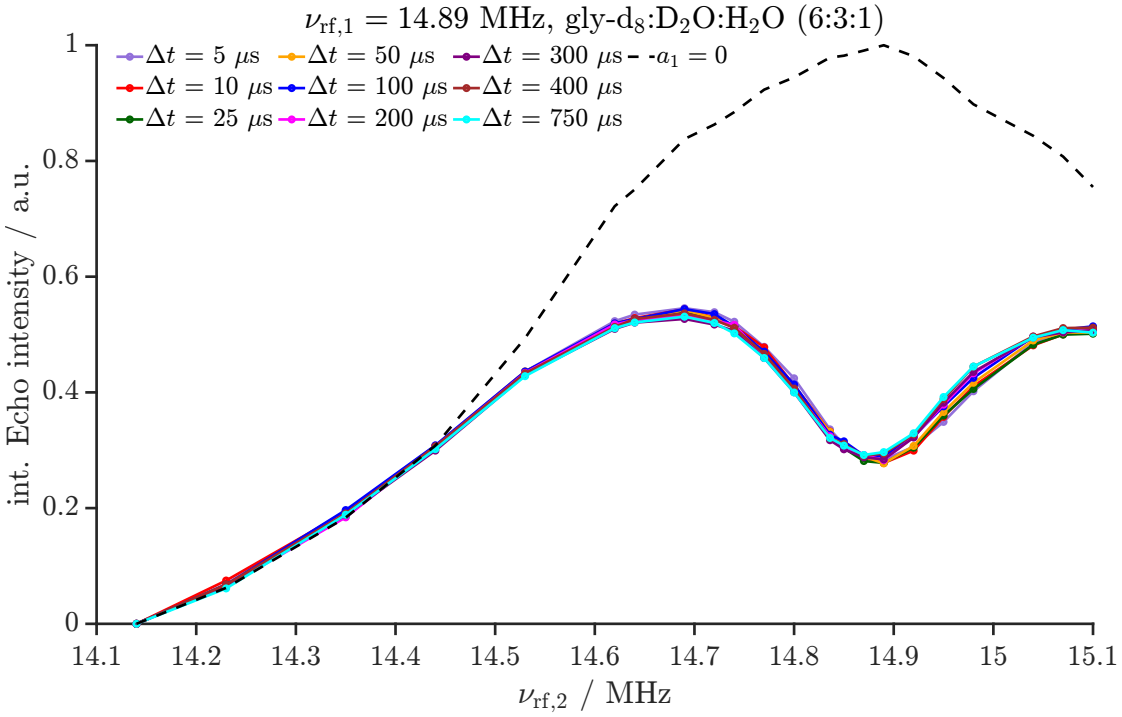

Figure S59: Hole burning spectra for delays Δt between the two Gauss pulses varying from 5 to 750 μs. The hole was burned at $\nu_{rf,1}$ = 14.89 MHz. The black dashed line is obtained by using the data points in Fig. S58 with $a_1 = 0$. The spectra with a hole burned are obtained by using the data points along the dashed line in Fig. S58. The sample is 5 mM trityl in gly-d$_8$:D$_2$O:H$_2$O (6:3:1). 10 shots were used for each individual data point, t_{del} = 800 μs and t_{SL} = 4000 ns.

$\nu_{rf,1}$ **= 15.04 MHz**

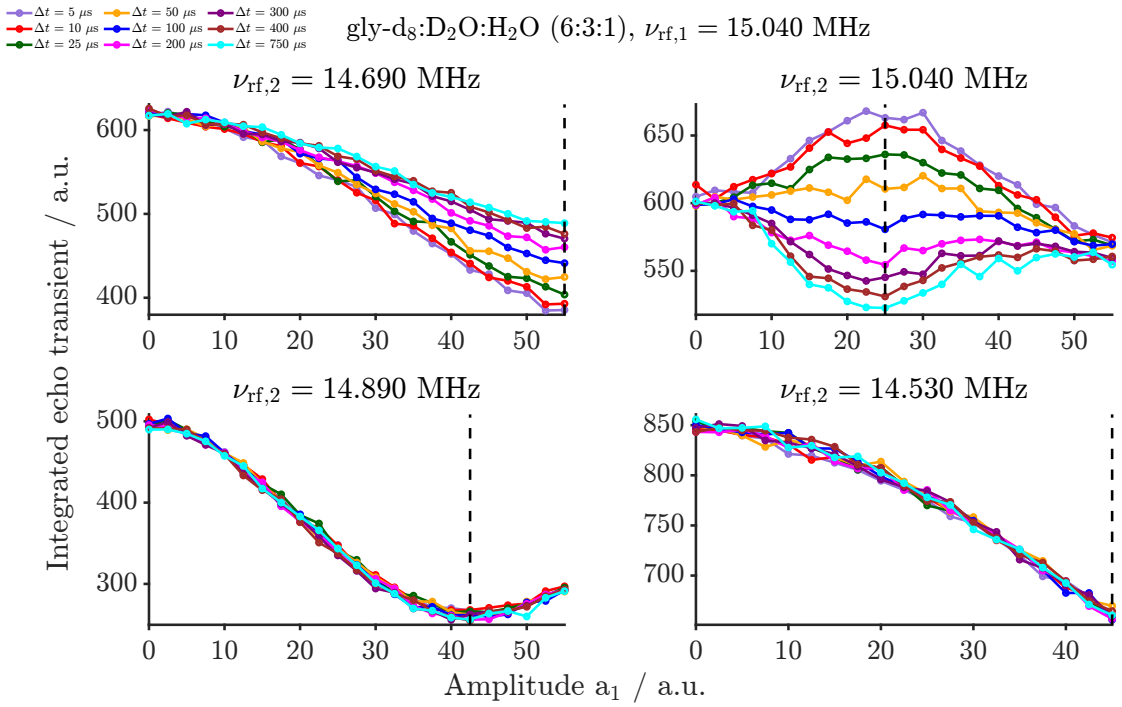

Figure S60: Amplitude traces recorded by sweeping the amplitude a_1 of the first Gauss pulse in steps of 2.5 for $\nu_{rf,1}$ = 15.04 MHz. An amplitude a_1 of 30 corresponds to a Rabi frequency of 100 kHz. The delay Δt between the first and second Gauss pulse was varied from 5 to 750 μs and is indicated in the legend of the figure. Here four different frequencies as examples are shown for the second Gauss pulse $\nu_{rf,2}$ = 14.53, 14.69, 14.89 and 15.04 MHz for the matrix gly-d_8:D_2O:H_2O (6:3:1). 10 shots were used for each individual data point, t_{del} = 800 μs and t_{SL} = 4000 ns.

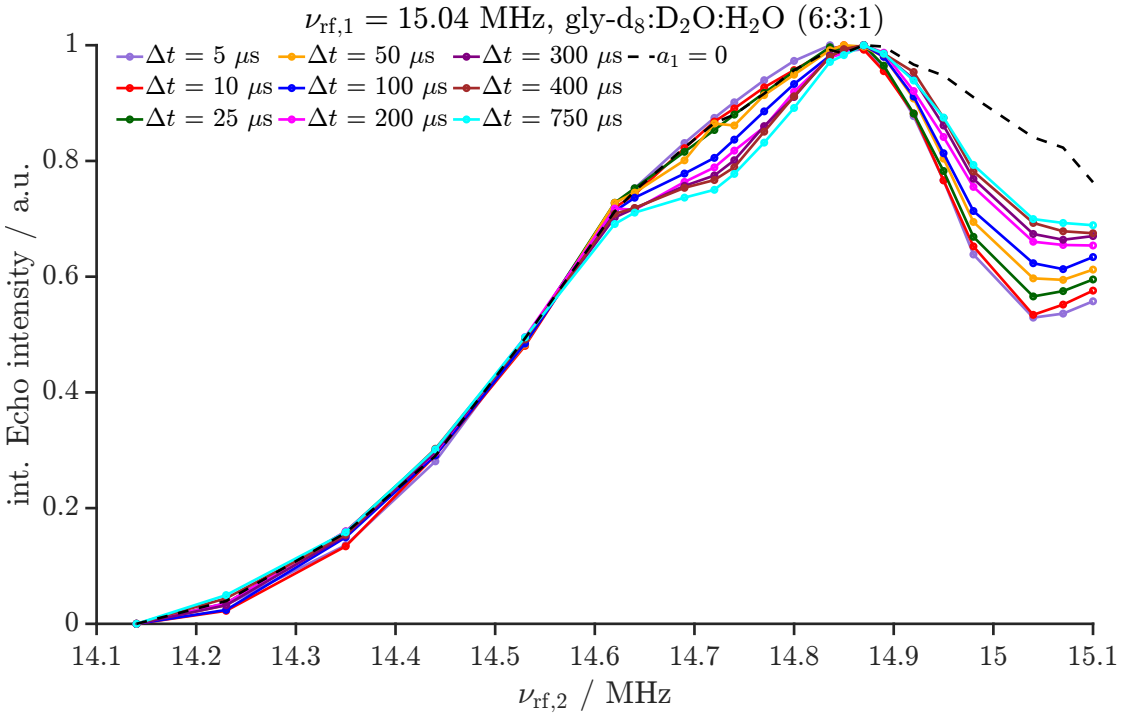

Figure S61: Hole burning spectra for delays Δt between the two Gauss pulses varying from 5 to 750 μs. The hole was burned at $\nu_{rf,1}$ = 15.04 MHz. The black dashed line is obtained by using the data points in Fig. S60 with $a_1 = 0$. The spectra with a hole burned are obtained by using the data points along the dashed line in Fig. S60. The sample is 5 mM trityl in gly-d$_8$:D$_2$O:H$_2$O (6:3:1). 10 shots were used for each individual data point, t_{del} = 800 μs and t_{SL} = 4000 ns.

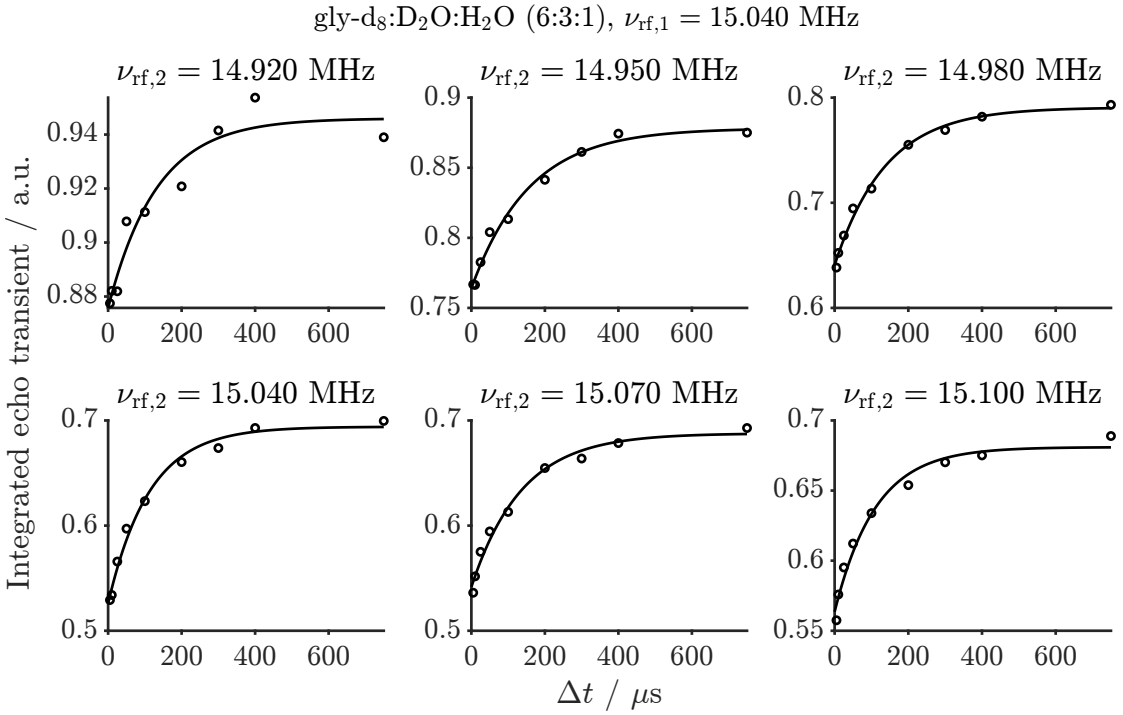

Figure S62: Diffusion traces for the hole burned at $\nu_{rf,1} = 15.04$ MHz using $t_{del} = 800$ μs and $t_{SL} = 4000$ ns. The individual data points are obtained from Fig. S61 for the corresponding frequency $\nu_{rf,2}$. The sample is 5 mM trityl in gly-d_8:D_2O:H_2O (6:3:1) and 10 shots were used for each individual data point. The data points are fitted to the function Eq. S.5 and the corresponding fitting parameters are given in Tab. S18.

$\nu_{rf,2}$ / MHz	ΔI / a.u.	τ / μs	I_0 / a.u.
14.920	0.070	132.245	0.876
14.950	0.114	157.851	0.764
14.980	0.150	138.858	0.641
15.040	0.168	112.160	0.526
15.070	0.146	137.191	0.542
15.100	0.117	110.845	0.564

Table S18: Extracted fit parameters from a mono-exponential build up as given in Eq. S.5 and shown in Fig. S62 for the hole burning at spectral position $\nu_{rf,1} = 15.04$ MHz. The sample is 5 mM trityl in gly-d_8:D_2O:H_2O (6:3:1).

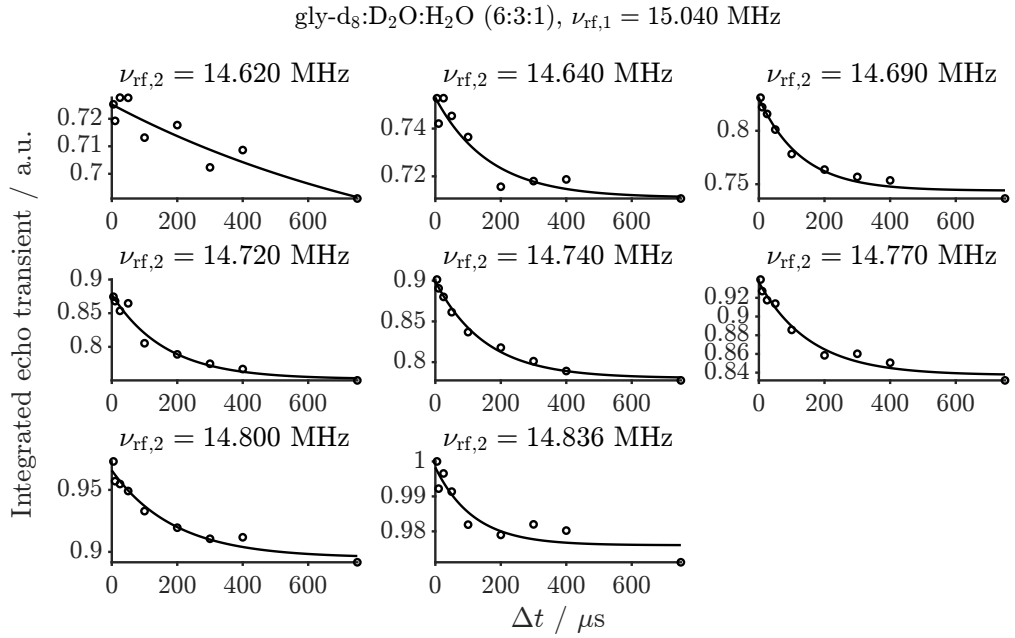

Figure S63: Diffusion traces for the hole burned at $\nu_{rf,1} = 15.04$ MHz using $t_{del} = 800$ μs and $t_{SL} = 4000$ ns. The individual data points are obtained from Fig. S61 for the corresponding frequency $\nu_{rf,2}$. The sample is 5 mM trityl in gly-d_8:D_2O:H_2O (6:3:1) and 10 shots were used for each individual data point. The data points are fitted to the function Eq. S.6 and the corresponding fitting parameters are given in Tab. S19.

$\nu_{rf,2}$ / MHz	ΔI / a.u.	τ / μs	I_∞ / a.u.
14.620	0.065	1029.419	0.660
14.640	0.042	163.929	0.711
14.690	0.087	128.194	0.744
14.720	0.126	163.368	0.752
14.740	0.119	152.907	0.780
14.770	0.099	156.340	0.837
14.800	0.070	191.060	0.895
14.836	0.022	116.808	0.976

Table S19: Extracted fit parameters from a mono-exponential decay as given in Eq. S.6 and shown in Fig. S63 for the hole burning at spectral position $\nu_{rf,1} = 15.04$ MHz. The sample is 5 mM trityl in gly-d_8:D_2O:H_2O (6:3:1).

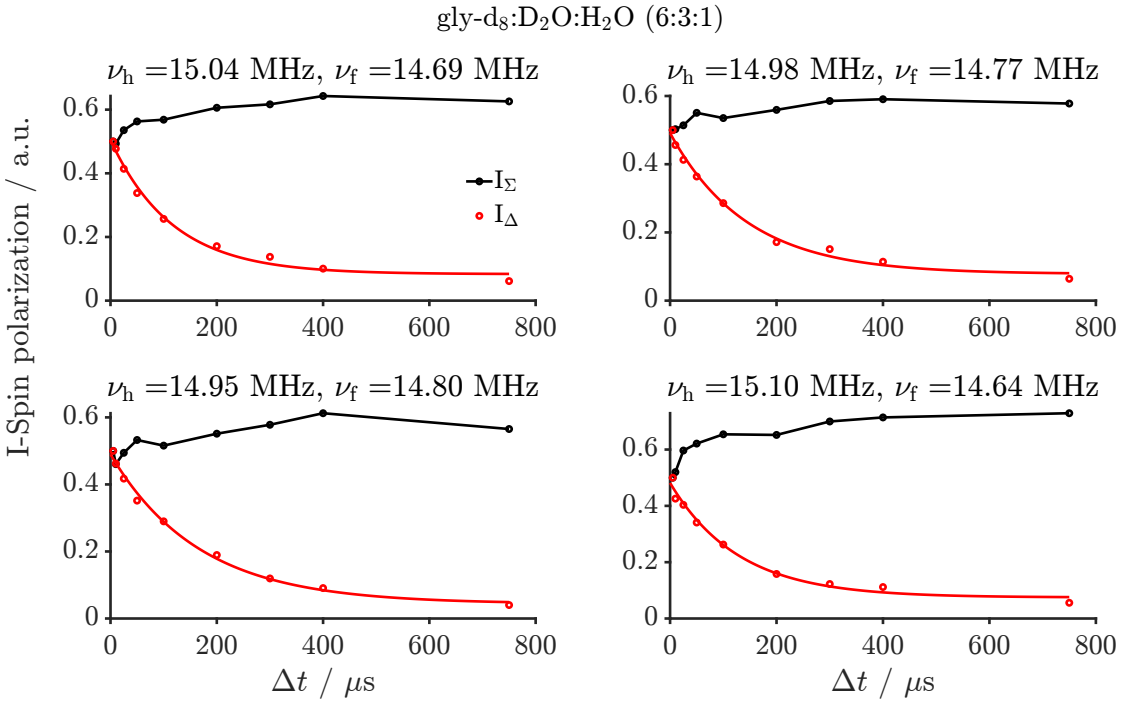

Figure S64: Sum and difference magnetization according to Eqs. (2)-(3) in the main text for different combinations of ν_h and ν_f. The hole is burned at $\nu_{rf,1} = 15.04$ MHz. The sample is 5 mM trityl in gly-d_8:D_2O:H_2O (6:3:1).

ν_h / MHz	ν_f / MHz	ΔI / a.u.	τ / μs	I_∞ / a.u.
15.04	14.69	0.421	116.877	0.083
14.98	14.77	0.413	144.957	0.078
14.95	14.80	0.446	166.816	0.044
15.10	14.64	0.434	144.381	0.053

Table S20: Extracted fit parameters from a mono-exponential decay as given in Eq. S.6 and shown in Fig. S64 for difference magnetization I_Δ as given in Eq. (3) in the main text. The hole is burned at $\nu_{rf,1} = 15.04$ MHz. The sample is 5 mM trityl in gly-d_8:D_2O:H_2O (6:3:1).

E.3. 5 mM trityl in gly-d_8:D_2O (6:4)

$\nu_{rf,1}$ = 14.69 MHz

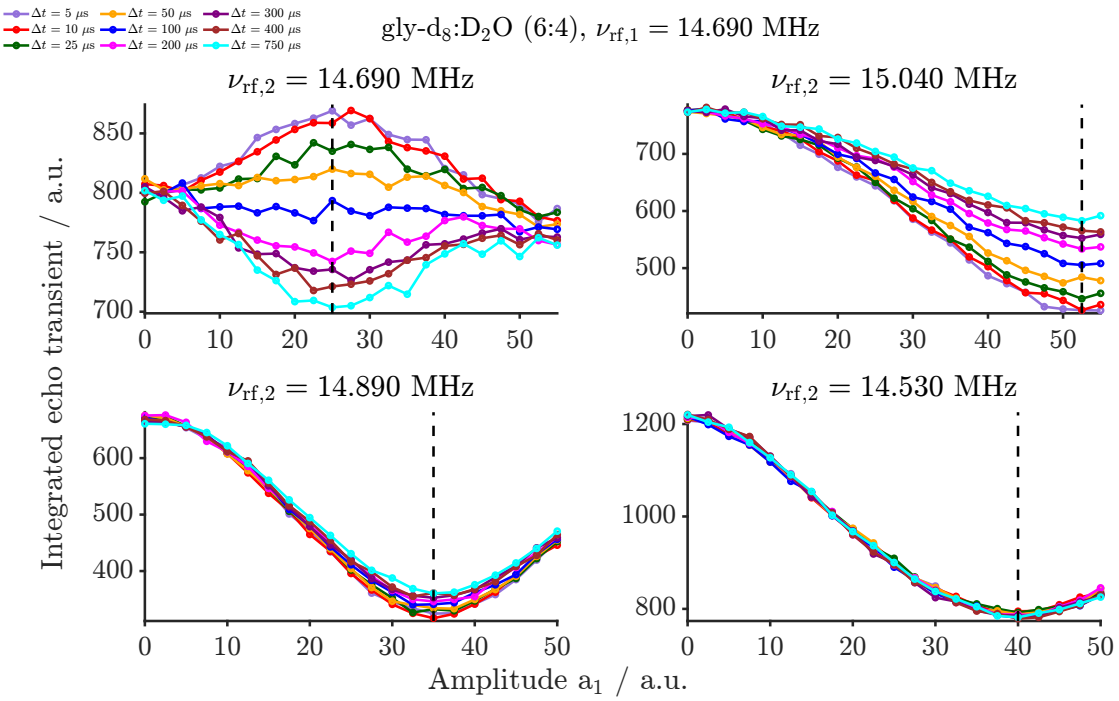

Figure S65: Amplitude traces recorded by sweeping the amplitude a_1 of the first Gauss pulse in steps of 2.5 for $\nu_{rf,1}$ = 14.69 MHz. An amplitude a_1 of 30 corresponds to a Rabi frequency of 100 kHz. The delay Δt between the first and second Gauss pulse was varied from 5 to 750 μs and is indicated in the legend of the figure. Here four different frequencies as examples are shown for the second Gauss pulse $\nu_{rf,2}$ = 14.53, 14.69, 14.89 and 15.04 MHz for the matrix gly-d_8:D_2O (6:4). 10 shots were used for each individual data point, t_{del} = 800 μs and t_{SL} = 4000 ns.

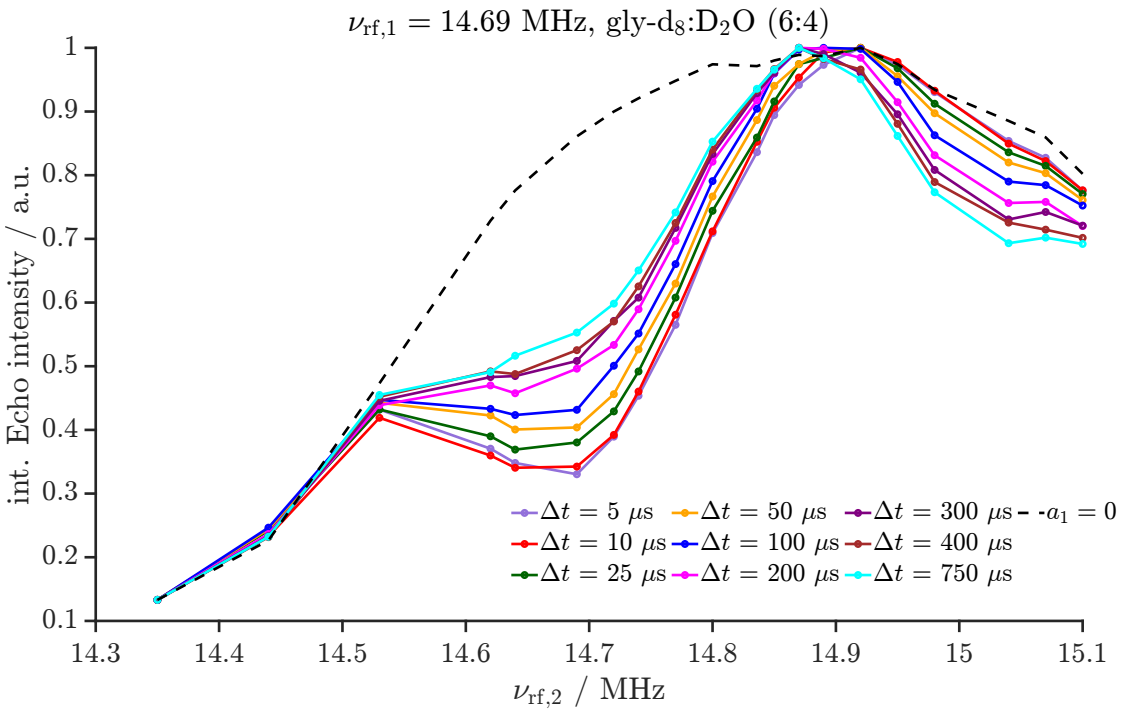

Figure S66: Hole burning spectra for delays Δt between the two Gauss pulses varying from 5 to 750 μs. The hole was burned at $\nu_{rf,1}$ = 14.69 MHz. The black dashed line is obtained by using the data points in Fig. S65 with $a_1 = 0$. The spectra with a hole burned are obtained by using the data points along the dashed line in Fig. S65. The sample is 5 mM trityl in gly-d$_8$:D$_2$O (6:4). 10 shots were used for each individual data point, t_{del} = 800 μs and t_{SL} = 4000 ns.

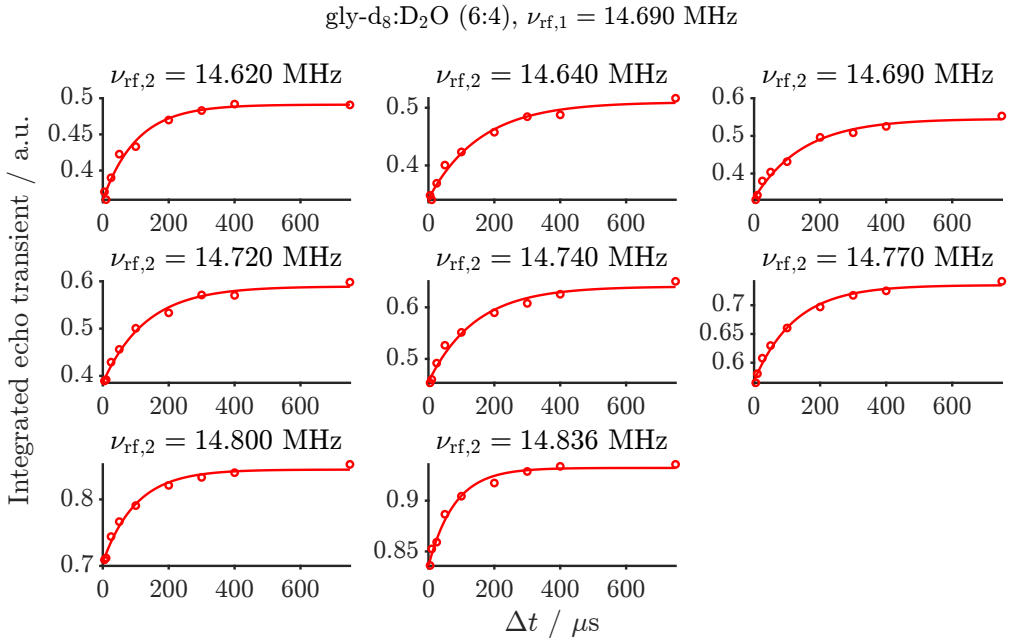

Figure S67: Diffusion traces for the hole burned at $\nu_{rf,1}$ = 14.69 MHz using t_{del} = 800 μs and t_{SL} = 4000 ns. The individual data points are obtained from Fig. S66 for the corresponding frequency $\nu_{rf,2}$. The sample is 5 mM trityl in gly-d_8:D_2O (6:4) and 10 shots were used for each individual data point. The data points are fitted to the function Eq. S.5 and the corresponding fitting parameters are given in Tab. S21.

$\nu_{rf,2}$ / MHz	ΔI / a.u.	τ / μs	I_0 / a.u.
14.620	0.132	103.674	0.360
14.640	0.168	157.428	0.342
14.690	0.212	147.911	0.334
14.720	0.204	130.825	0.385
14.740	0.185	141.828	0.455
14.770	0.167	123.584	0.568
14.800	0.140	100.873	0.705
14.836	0.096	79.533	0.836

Table S21: Extracted fit parameters from a mono-exponential build up as given in Eq. S.5 and shown in Fig. S67 for the hole burning at spectral position $\nu_{rf,1}$ = 14.69 MHz. The sample is 5 mM trityl in gly-d_8:D_2O (6:4).

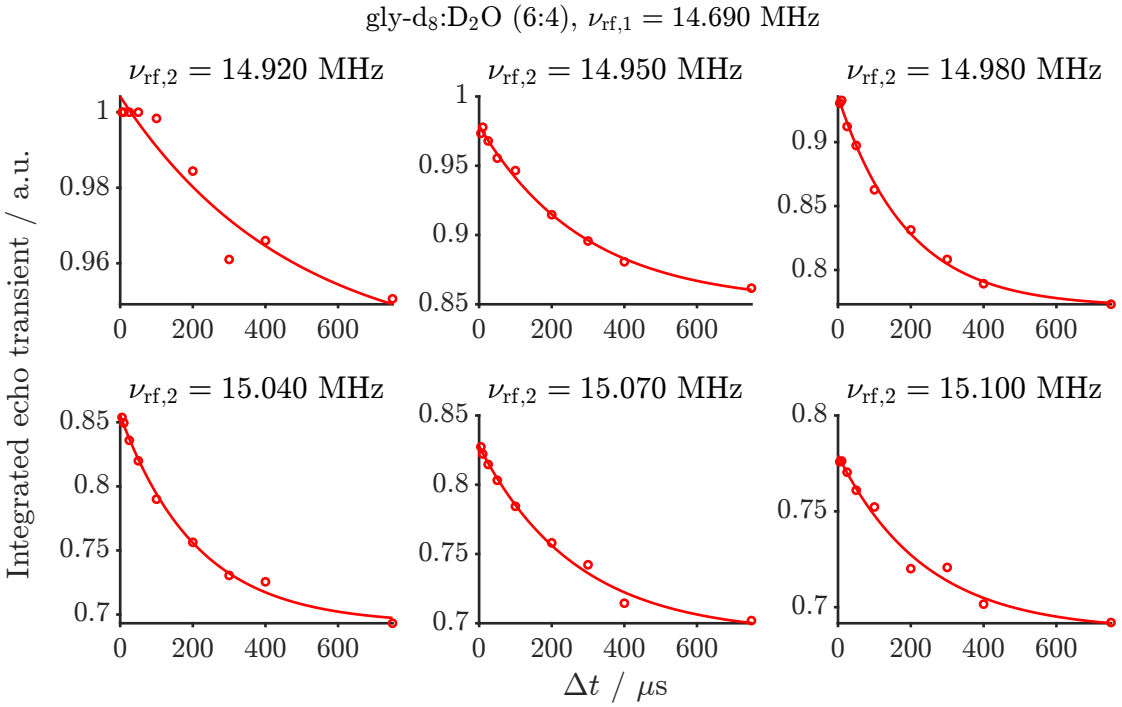

Figure S68: Diffusion traces for the hole burned at $\nu_{rf,1}$ = 14.69 MHz using t_{del} = 800 μs and t_{SL} = 4000 ns. The individual data points are obtained from Fig. S66 for the corresponding frequency $\nu_{rf,2}$. The sample is 5 mM trityl in gly-d_8:D_2O (6:4) and 10 shots were used for each individual data point. The data points are fitted to the function Eq. S.6 and the corresponding fitting parameters are given in Tab. S22.

$\nu_{rf,2}$ / MHz	ΔI / a.u.	τ / μs	I_∞ / a.u.
14.920	0.069	469.094	0.935
14.950	0.128	289.030	0.851
14.980	0.165	188.906	0.771
15.040	0.163	212.152	0.693
15.070	0.136	267.256	0.692
15.100	0.092	238.934	0.688

Table S22: Extracted fit parameters from a mono-exponential decay as given in Eq. S.6 and shown in Fig. S68 for the hole burning at spectral position $\nu_{rf,1}$ = 14.69 MHz. The sample is 5 mM trityl in gly-d_8:D_2O (6:4).

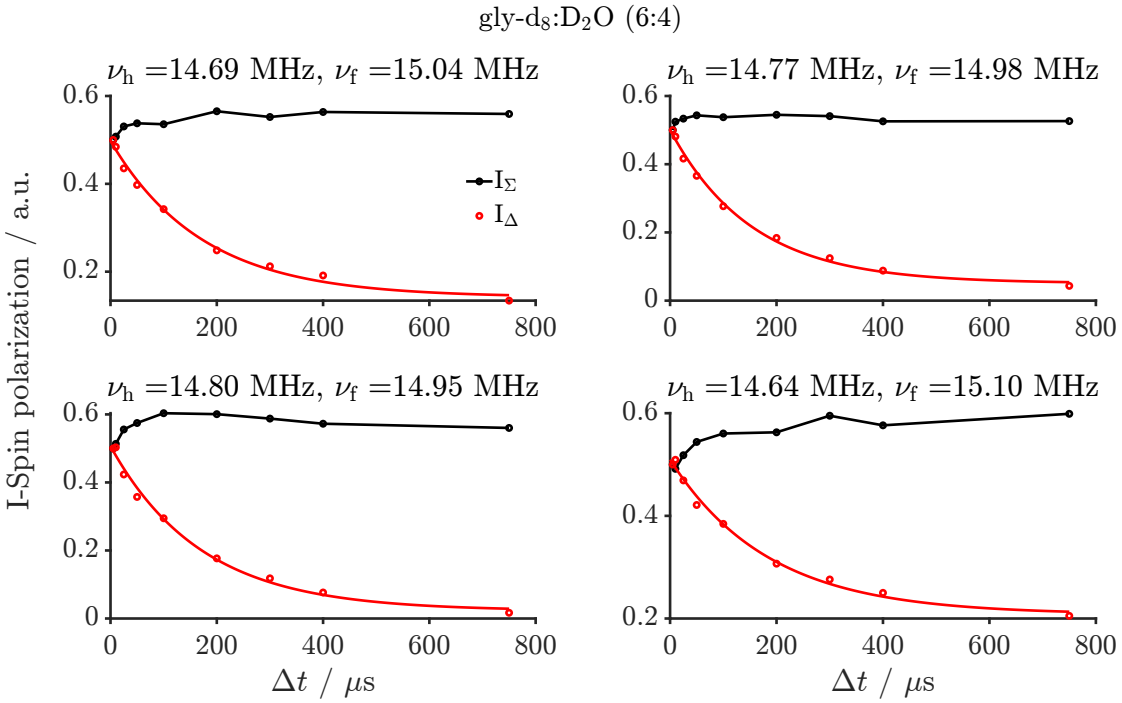

Figure S69: Sum and difference magnetization according to Eqs. (2)-(3) in the main text for different combinations of ν_h and ν_f. The hole is burned at $\nu_{rf,1} = 14.69$ MHz. The sample is 5 mM trityl in gly-d_8:D_2O (6:4).

ν_h / MHz	ν_f / MHz	ΔI / a.u.	τ / μs	I_∞ / a.u.
14.69	15.04	0.356	172.961	0.142
14.77	14.98	0.450	154.005	0.051
14.80	14.95	0.484	171.248	0.023
14.64	15.10	0.302	184.828	0.208

Table S23: Extracted fit parameters from a mono-exponential decay as given in Eq. S.6 and shown in Fig. S69 for difference magnetization I_Δ as given in Eq. (3) in the main text. The hole is burned at $\nu_{rf,1} = 14.69$ MHz. The sample is 5 mM trityl in gly-d_8:D_2O (6:4).

$\nu_{rf,1}$ = 14.89 MHz

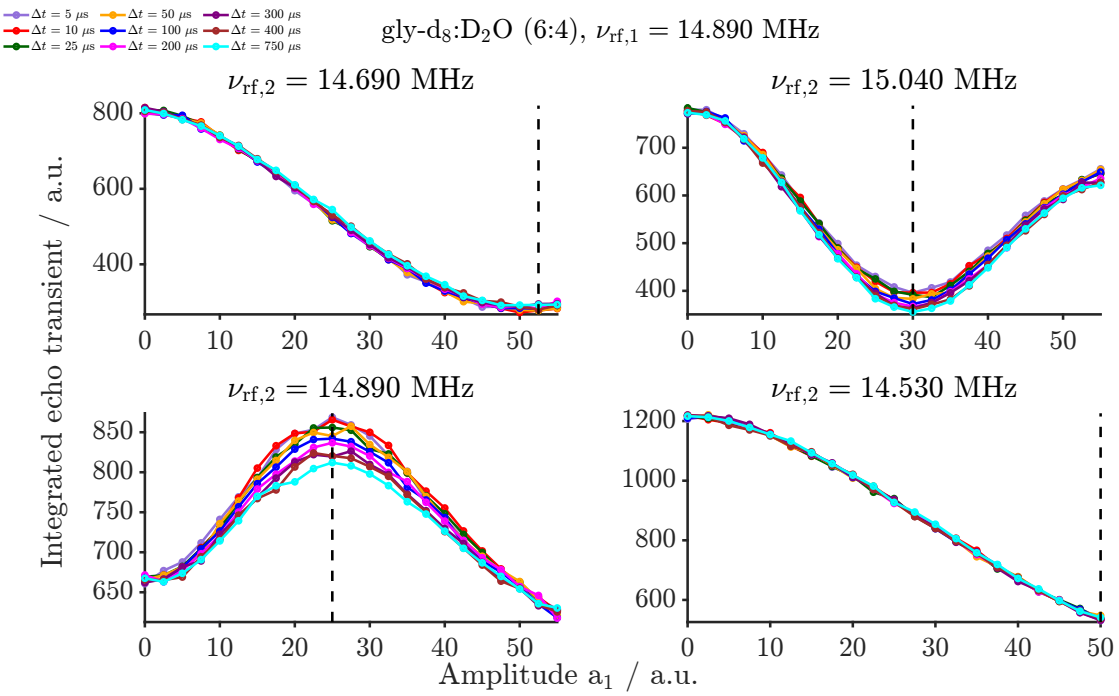

Figure S70: Amplitude traces recorded by sweeping the amplitude a_1 of the first Gauss pulse in steps of 2.5 for $\nu_{rf,1}$ = 14.89 MHz. An amplitude a_1 of 30 corresponds to a Rabi frequency of 100 kHz. The delay Δt between the first and second Gauss pulse was varied from 5 to 750 μs and is indicated in the legend of the figure. Here four different frequencies as examples are shown for the second Gauss pulse $\nu_{rf,2}$ = 14.53, 14.69, 14.89 and 15.04 MHz for the matrix gly-d_8:D_2O (6:4). 10 shots were used for each individual data point, t_{del} = 800 μs and t_{SL} = 4000 ns.

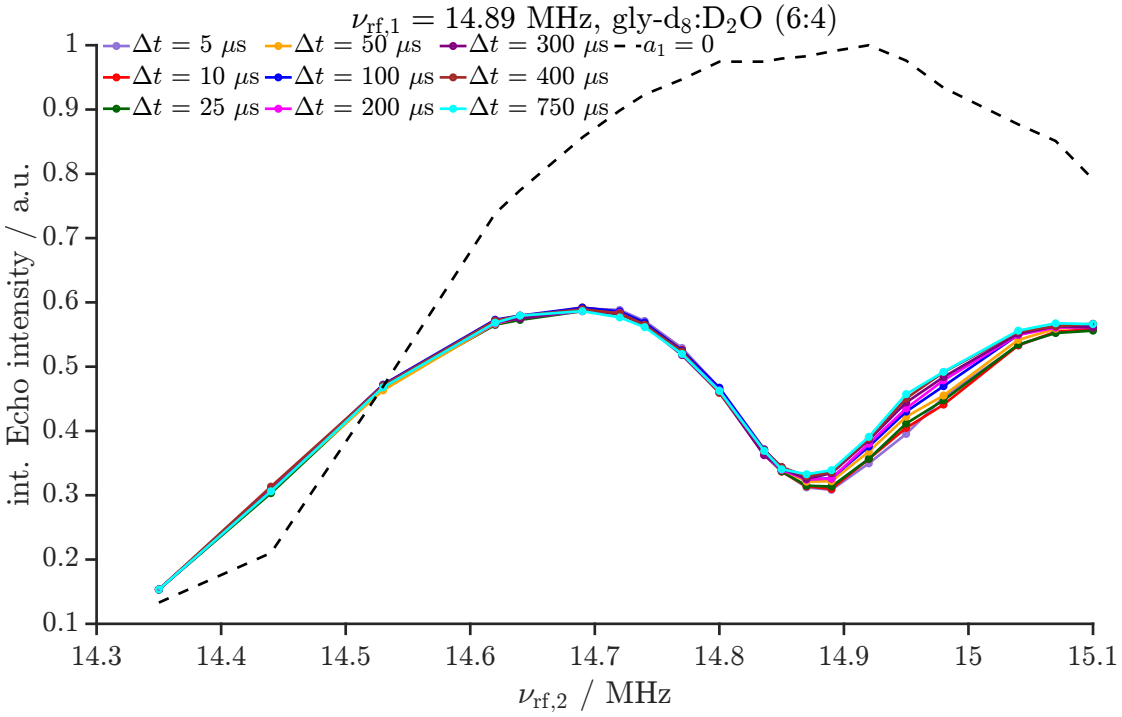

Figure S71: Hole burning spectra for delays Δt between the two Gauss pulses varying from 5 to 750 μs. The hole was burned at $\nu_{rf,1}$ = 14.89 MHz. The black dashed line is obtained by using the data points in Fig. S70 with a_1 = 0. The spectra with a hole burned are obtained by using the data points along the dashed line in Fig. S70. The sample is 5 mM trityl in gly-d$_8$:D$_2$O (6:4). 10 shots were used for each individual data point, t_{del} = 800 μs and t_{SL} = 4000 ns.

$\nu_{rf,1}$ **= 15.04 MHz**

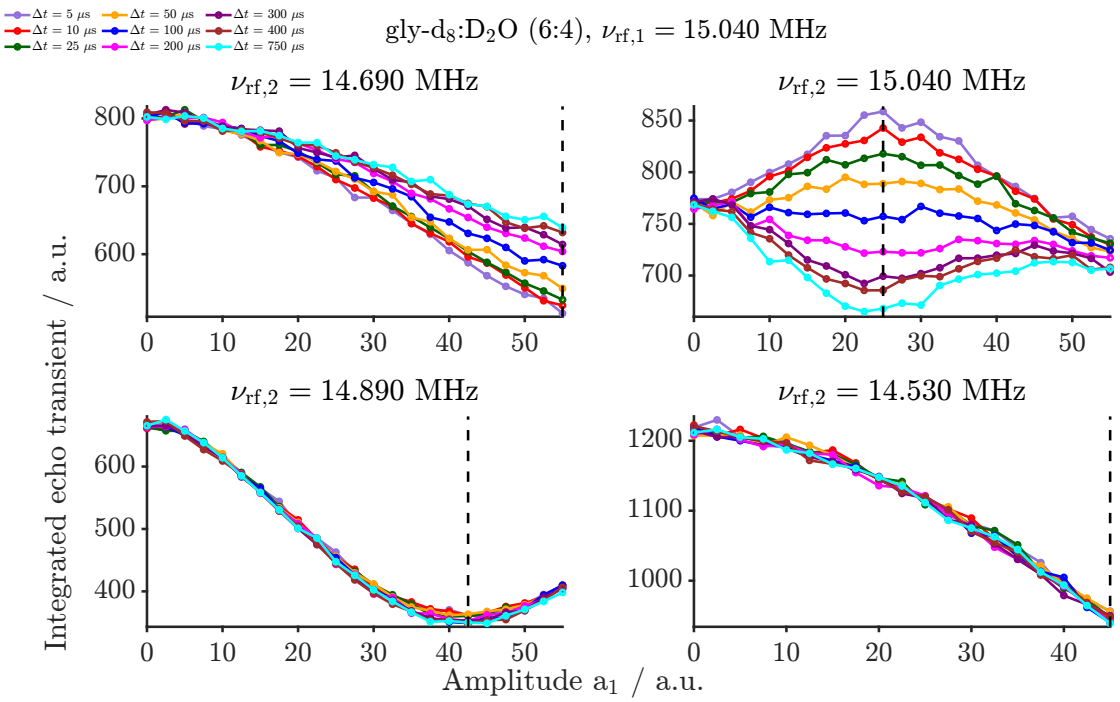

Figure S72: Amplitude traces recorded by sweeping the amplitude a_1 of the first Gauss pulse in steps of 2.5 for $\nu_{rf,1}$ = 15.04 MHz. An amplitude a_1 of 30 corresponds to a Rabi frequency of 100 kHz. The delay Δt between the first and second Gauss pulse was varied from 5 to 750 μs and is indicated in the legend of the figure. Here four different frequencies as examples are shown for the second Gauss pulse $\nu_{rf,2}$ = 14.53, 14.69, 14.89 and 15.04 MHz for the matrix gly-d_8:D_2O (6:4). 10 shots were used for each individual data point, t_{del} = 800 μs and t_{SL} = 4000 ns.

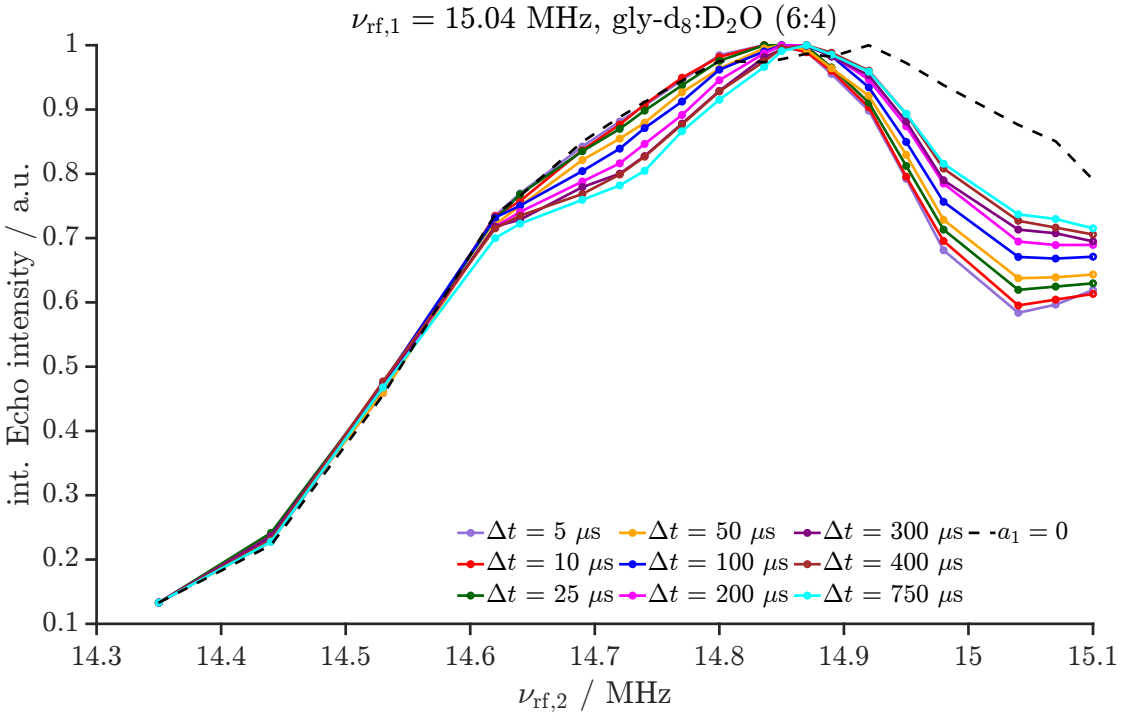

Figure S73: Hole burning spectra for delays Δt between the two Gauss pulses varying from 5 to 750 μs. The hole was burned at $\nu_{rf,1}$ = 15.04 MHz. The black dashed line is obtained by using the data points in Fig. S72 with $a_1 = 0$. The spectra with a hole burned are obtained by using the data points along the dashed line in Fig. S72. The sample is 5 mM trityl in gly-d$_8$:D$_2$O (6:4). 10 shots were used for each individual data point, t_{del} = 800 μs and t_{SL} = 4000 ns.

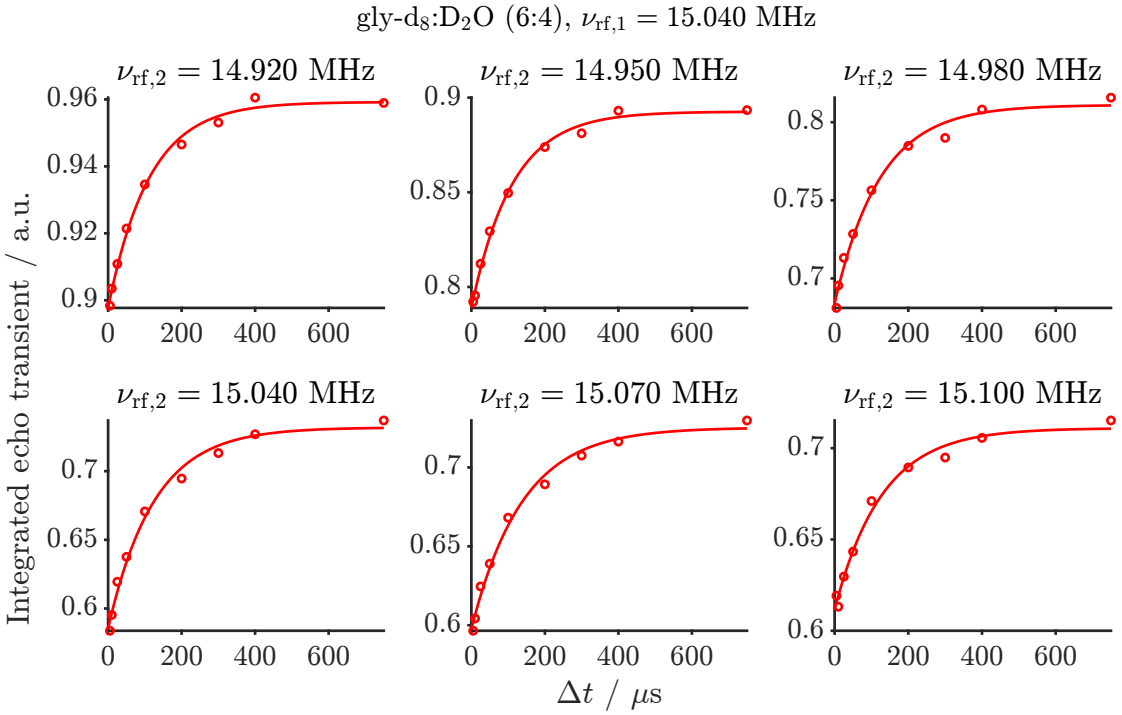

Figure S74: Diffusion traces for the hole burned at $\nu_{rf,1}$ = 15.04 MHz using t_{del} = 800 μs and t_{SL} = 4000 ns. The individual data points are obtained from Fig. S73 for the corresponding frequency $\nu_{rf,2}$. The sample is 5 mM trityl in gly-d_8:D_2O (6:4) and 10 shots were used for each individual data point. The data points are fitted to the function Eq. S.5 and the corresponding fitting parameters are given in Tab. S24.

$\nu_{rf,2}$ / MHz	ΔI / a.u.	τ / μs	I_0 / a.u.
14.920	0.062	112.027	0.898
14.950	0.104	111.691	0.789
14.980	0.127	123.607	0.684
15.040	0.146	124.860	0.586
15.070	0.128	138.397	0.598
15.100	0.099	128.421	0.612

Table S24: Extracted fit parameters from a mono-exponential build up as given in Eq. S.5 and shown in Fig. S74 for the hole burning at spectral position $\nu_{rf,1}$ = 15.04 MHz. The sample is 5 mM trityl in gly-d_8:D_2O (6:4).

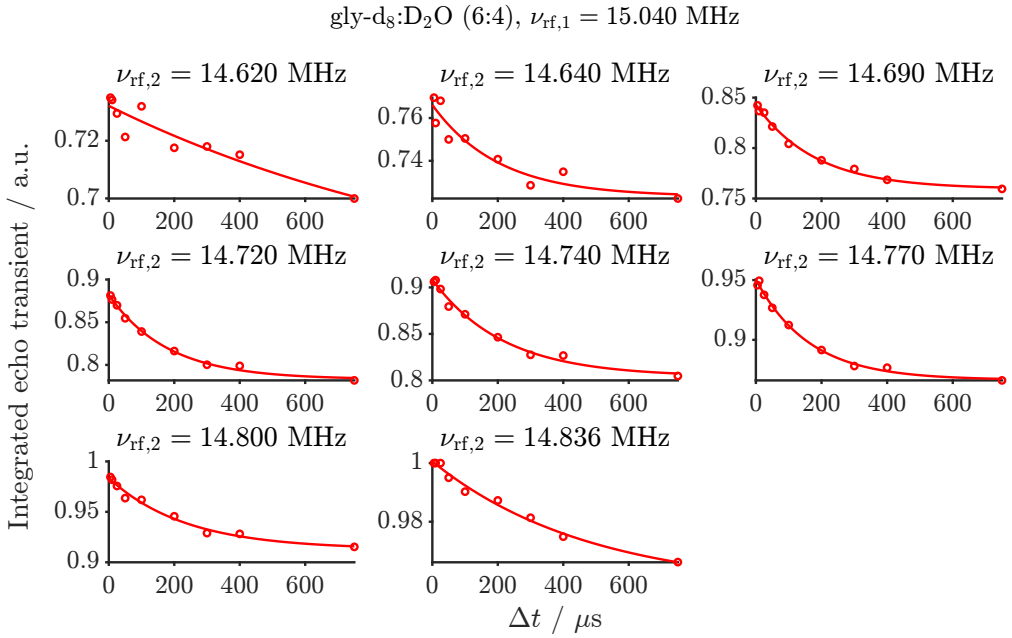

Figure S75: Diffusion traces for the hole burned at $\nu_{rf,1}$ = 15.04 MHz using t_{del} = 800 μs and t_{SL} = 4000 ns. The individual data points are obtained from Fig. S73 for the corresponding frequency $\nu_{rf,2}$. The sample is 5 mM trityl in gly-d_8:D_2O (6:4) and 10 shots were used for each individual data point. The data points are fitted to the function Eq. S.6 and the corresponding fitting parameters are given in Tab. S25.

$\nu_{rf,2}$ / MHz	ΔI / a.u.	τ / μs	I_∞ / a.u.
14.620	0.068	1209.965	0.664
14.640	0.043	202.472	0.723
14.690	0.083	182.290	0.760
14.720	0.099	179.660	0.783
14.740	0.104	217.458	0.804
14.770	0.084	163.212	0.867
14.800	0.071	234.761	0.913
14.836	0.044	480.700	0.957

Table S25: Extracted fit parameters from a mono-exponential decay as given in Eq. S.6 and shown in Fig. S75 for the hole burning at spectral position $\nu_{rf,1}$ = 15.04 MHz. The sample is 5 mM trityl in gly-d_8:D_2O (6:4).

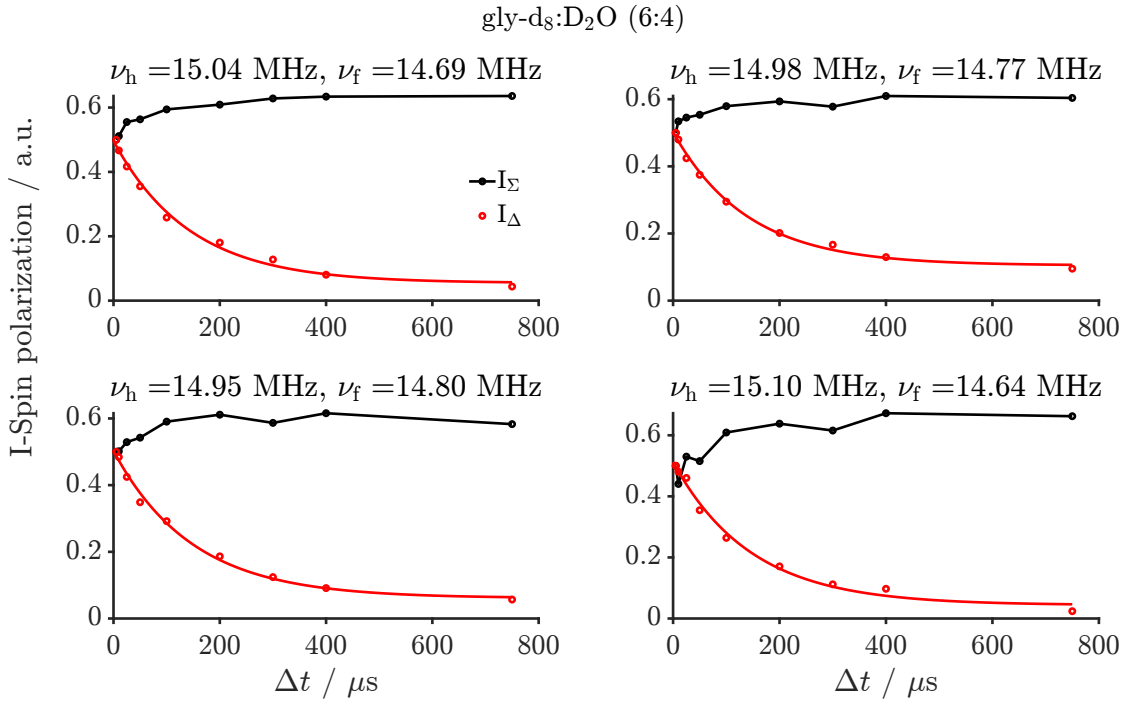

Figure S76: Sum and difference magnetization according to Eqs. (2)-(3) in the main text for different combinations of ν_h and ν_f. The hole is burned at $\nu_{rf,1} = 15.04$ MHz. The sample is 5 mM trityl in gly-d_8:D_2O (6:4).

ν_h / MHz	ν_f / MHz	ΔI / a.u.	τ / μs	I_∞ / a.u.
15.04	14.69	0.442	144.066	0.055
14.98	14.77	0.398	139.507	0.105
14.95	14.80	0.442	148.109	0.061
15.10	14.64	0.469	146.387	0.044

Table S26: Extracted fit parameters from a mono-exponential decay as given in Eq. S.6 and shown in Fig. S76 for difference magnetization I_Δ as given in Eq. (3) in the main text. The hole is burned at $\nu_{rf,1} = 15.04$ MHz. The sample is 5 mM trityl in gly-d_8:D_2O (6:4).

E.4. 5 mM trityl in gly-d_8:H_2O (6:4), t_{SL} = 4000 ns

$\nu_{rf,1}$ = 14.69 MHz

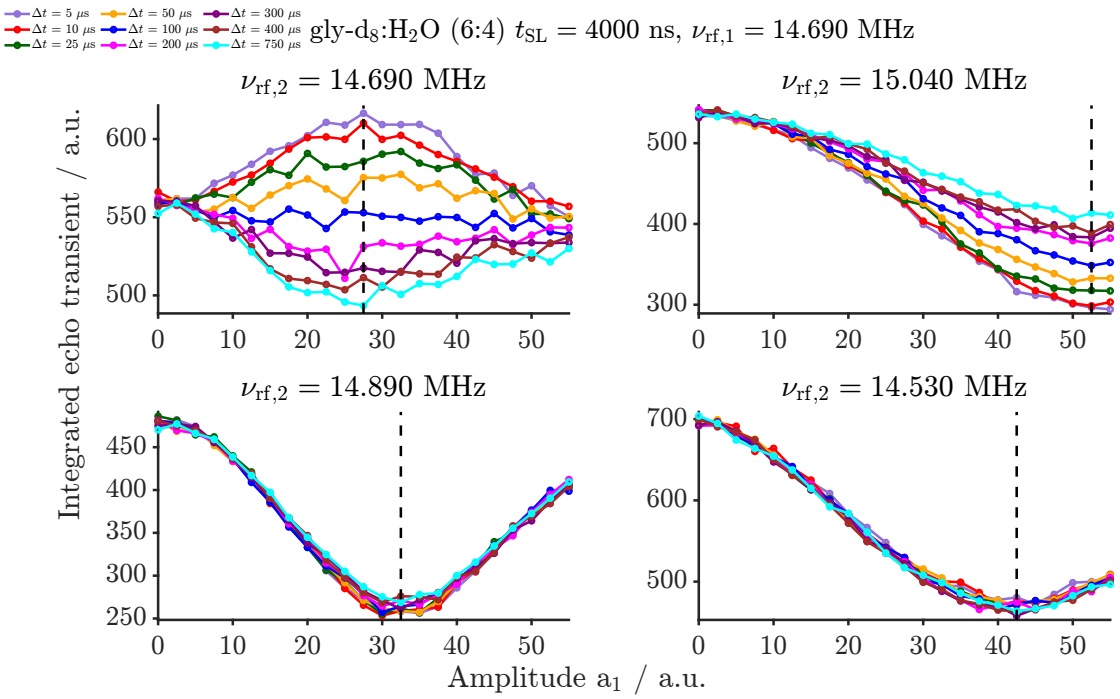

Figure S77: Amplitude traces recorded by sweeping the amplitude a_1 of the first Gauss pulse in steps of 2.5 for $\nu_{rf,1}$ = 14.69 MHz. An amplitude a_1 of 30 corresponds to a Rabi frequency of 100 kHz. The delay Δt between the first and second Gauss pulse was varied from 5 to 750 μs and is indicated in the legend of the figure. Here four different frequencies as examples are shown for the second Gauss pulse $\nu_{rf,2}$ = 14.53, 14.69, 14.89 and 15.04 MHz for the matrix gly-d_8:H_2O (6:4). 10 shots were used for each individual data point, t_{del} = 800 μs and t_{SL} = 4000 ns.

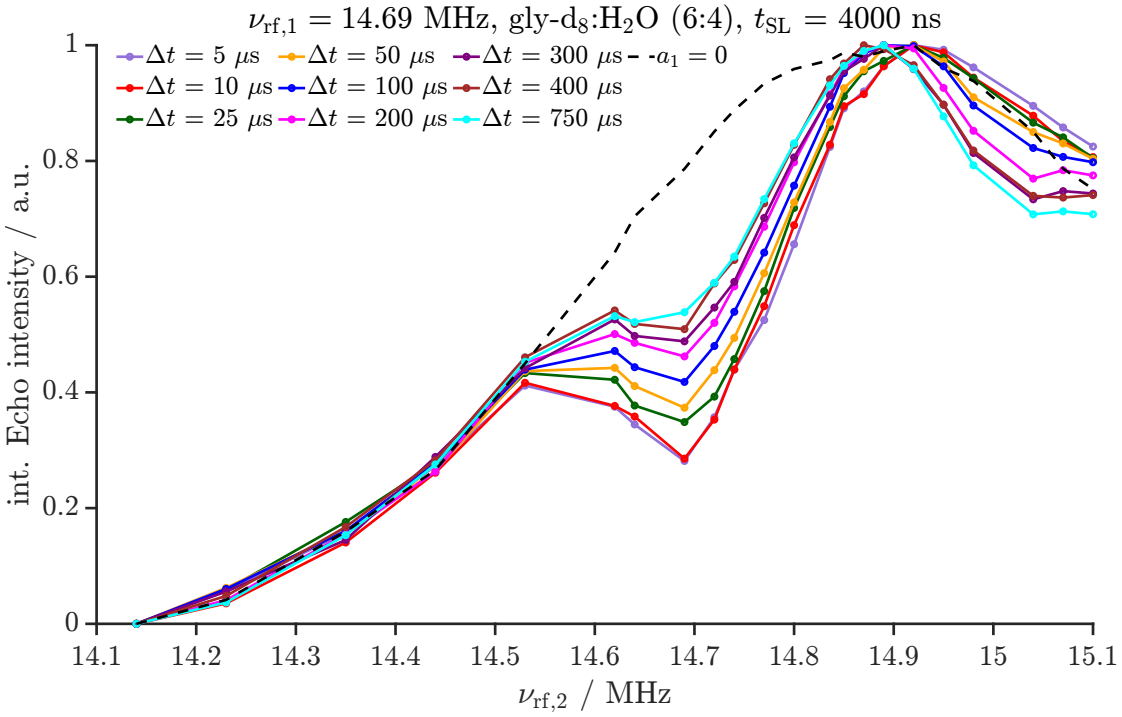

Figure S78: Hole burning spectra for delays Δt between the two Gauss pulses varying from 5 to 750 μs. The hole was burned at $\nu_{rf,1}$ = 14.69 MHz. The black dashed line is obtained by using the data points in Fig. S77 with a_1 = 0. The spectra with a hole burned are obtained by using the data points along the dashed line in Fig. S77. The sample is 5 mM trityl in gly-d$_8$:H$_2$O (6:4). 10 shots were used for each individual data point, t_{del} = 800 μs and t_{SL} = 4000 ns.

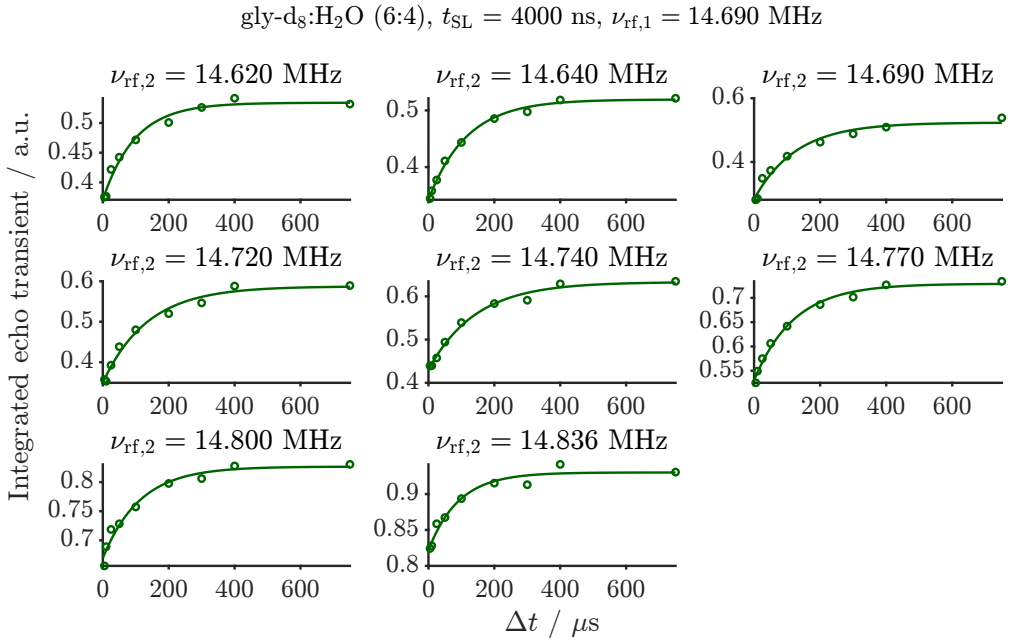

Figure S79: Diffusion traces for the hole burned at $\nu_{rf,1}$ = 14.69 MHz using t_{del} = 800 μs and t_{SL} = 4000 ns. The individual data points are obtained from Fig. S78 for the corresponding frequency $\nu_{rf,2}$. The sample is 5 mM trityl in gly-d_8:H_2O (6:4) and 10 shots were used for each individual data point. The data points are fitted to the function Eq. S.5 and the corresponding fitting parameters are given in Tab. S27.

$\nu_{rf,2}$ / MHz	ΔI / a.u.	τ / μs	I_0 / a.u.
14.620	0.163	98.370	0.371
14.640	0.177	116.445	0.342
14.690	0.240	127.332	0.283
14.720	0.238	135.273	0.349
14.740	0.203	142.898	0.430
14.770	0.199	120.919	0.530
14.800	0.157	112.170	0.669
14.836	0.108	91.479	0.822

Table S27: Extracted fit parameters from a mono-exponential build up as given in Eq. S.5 and shown in Fig. S79 for the hole burning at spectral position $\nu_{rf,1}$ = 14.69 MHz. The sample is 5 mM trityl in gly-d_8:H_2O (6:4).

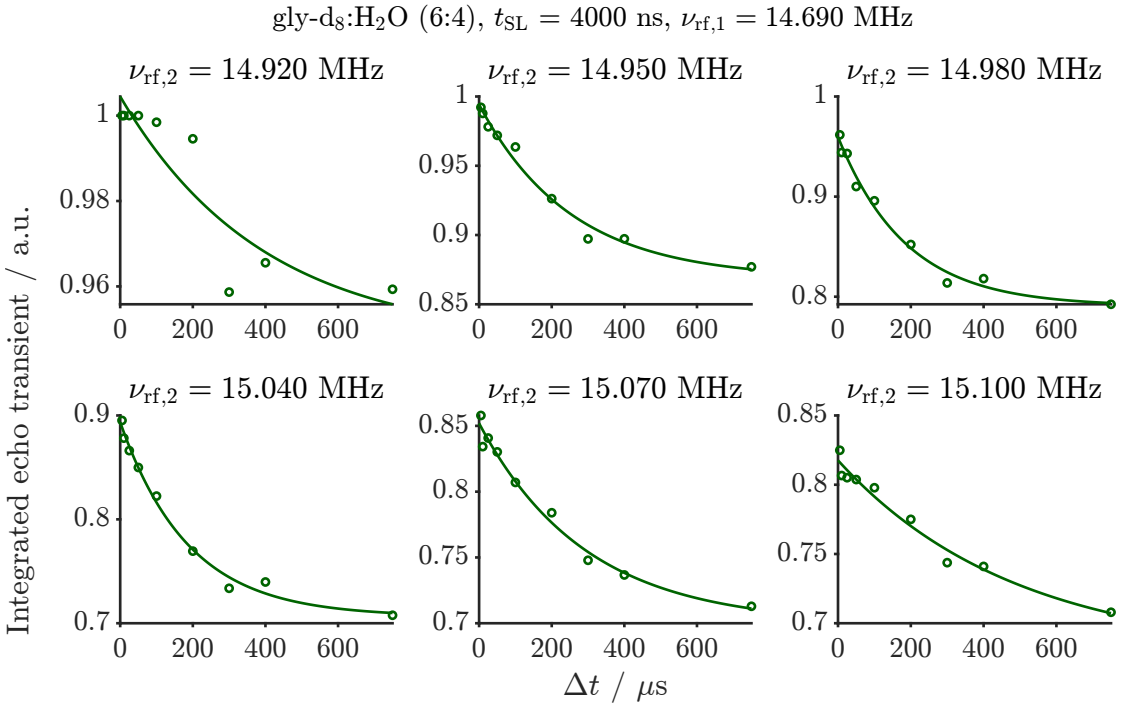

Figure S80: Diffusion traces for the hole burned at $\nu_{rf,1}$ = 14.69 MHz using t_{del} = 800 μs and t_{SL} = 4000 ns. The individual data points are obtained from Fig. S78 for the corresponding frequency $\nu_{rf,2}$. The sample is 5 mM trityl in gly-d_8:H_2O (6:4) and 10 shots were used for each individual data point. The data points are fitted to the function Eq. S.6 and the corresponding fitting parameters are given in Tab. S28.

$\nu_{rf,2}$ / MHz	ΔI / a.u.	τ / μs	I_∞ / a.u.
14.920	0.057	393.560	0.947
14.950	0.125	253.789	0.869
14.980	0.169	186.694	0.791
15.040	0.187	187.826	0.706
15.070	0.153	293.033	0.699
15.100	0.140	484.464	0.677

Table S28: Extracted fit parameters from a mono-exponential build up as given in Eq. S.6 and shown in Fig. S80 for the hole burning at spectral position $\nu_{rf,1}$ = 14.69 MHz. The sample is 5 mM trityl in gly-d_8:H_2O (6:4).

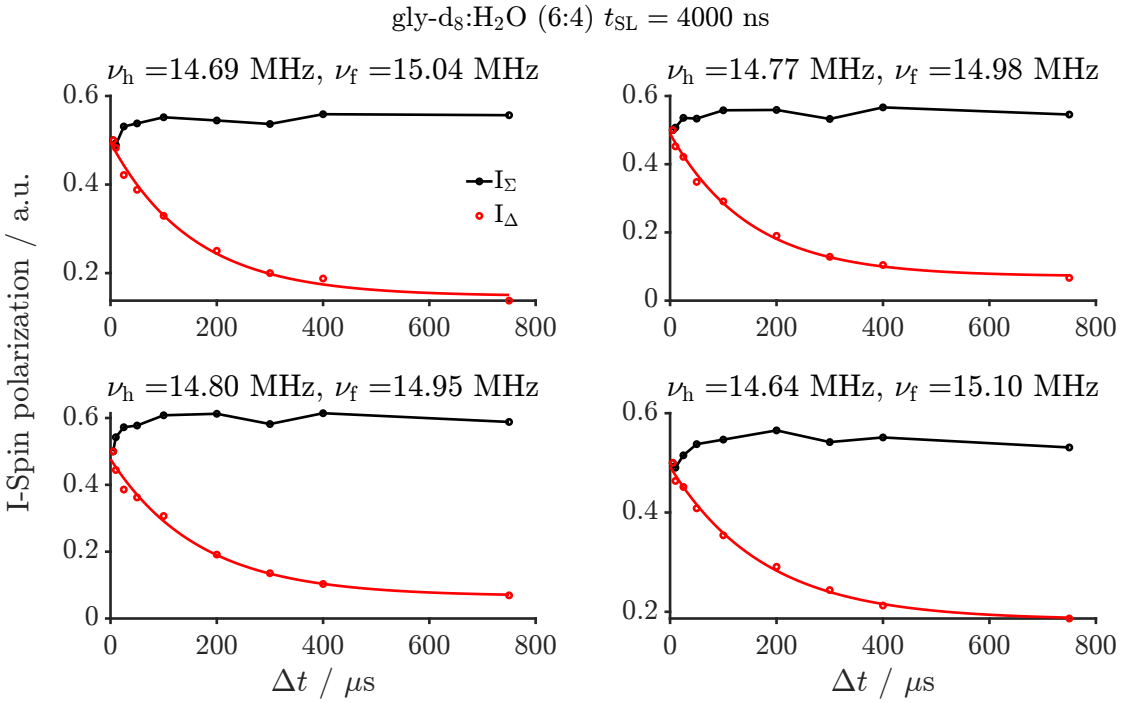

Figure S81: Sum and difference magnetization according to Eqs. (2)-(3) in the main text for different combinations of ν_h and ν_f. The hole is burned at $\nu_{rf,1} = 14.69$ MHz. The sample is 5 mM trityl in gly-d$_8$:H$_2$O (6:4) and $t_{SL} = 4000$ ns.

ν_h / MHz	ν_f / MHz	ΔI / a.u.	τ / μs	I_∞ / a.u.
14.69	15.04	0.347	155.591	0.148
14.77	14.98	0.418	149.555	0.071
14.80	14.95	0.410	166.270	0.067
14.64	15.10	0.308	176.100	0.184

Table S29: Extracted fit parameters from a mono-exponential decay as given in Eq. S.6 and shown in Fig. S81 for difference magnetization I_Δ as given in Eq. (3) in the main text. The hole is burned at $\nu_{rf,1} = 14.69$ MHz. The sample is 5 mM trityl in gly-d$_8$:H$_2$O (6:4) $t_{SL} = 4000$ ns.

$\nu_{rf,1}$ = 14.89 MHz

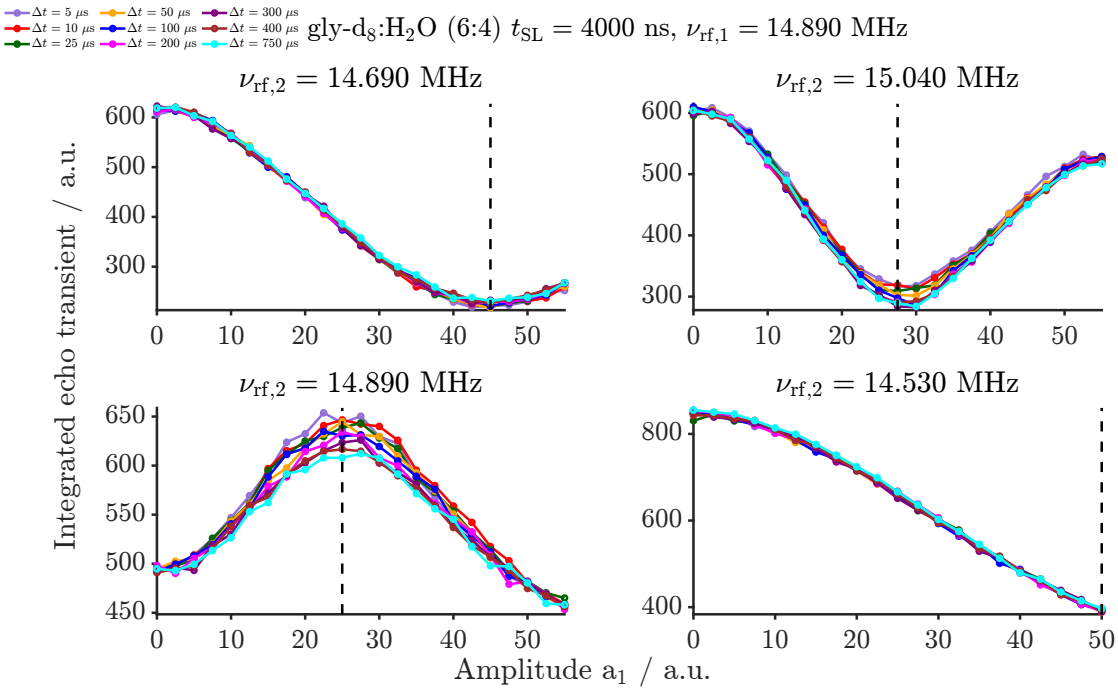

Figure S82: Amplitude traces recorded by sweeping the amplitude a_1 of the first Gauss pulse in steps of 2.5 for $\nu_{rf,1}$ = 14.89 MHz. An amplitude a_1 of 30 corresponds to a Rabi frequency of 100 kHz. The delay Δt between the first and second Gauss pulse was varied from 5 to 750 μs and is indicated in the legend of the figure. Here four different frequencies as examples are shown for the second Gauss pulse $\nu_{rf,2}$ = 14.53, 14.69, 14.89 and 15.04 MHz for the matrix gly-d_8:H_2O (6:4). 10 shots were used for each individual data point, t_{del} = 800 μs and t_{SL} = 4000 ns.

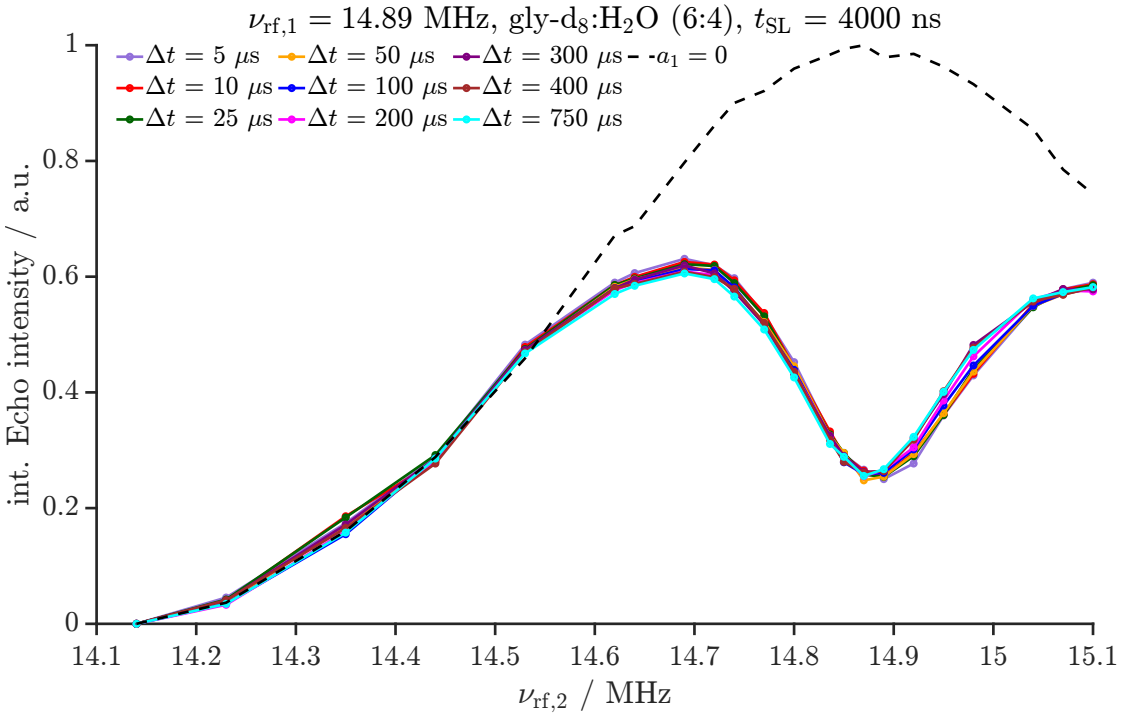

Figure S83: Hole burning spectra for delays Δt between the two Gauss pulses varying from 5 to 750 μs. The hole was burned at $\nu_{rf,1}$ = 14.89 MHz. The black dashed line is obtained by using the data points in Fig. S82 with $a_1 = 0$. The spectra with a hole burned are obtained by using the data points along the dashed line in Fig. S82. The sample is 5 mM trityl in gly-d$_8$:H$_2$O (6:4). 10 shots were used for each individual data point, t_{del} = 800 μs and t_{SL} = 4000 ns.

$\nu_{rf,1}$ **= 15.04 MHz**

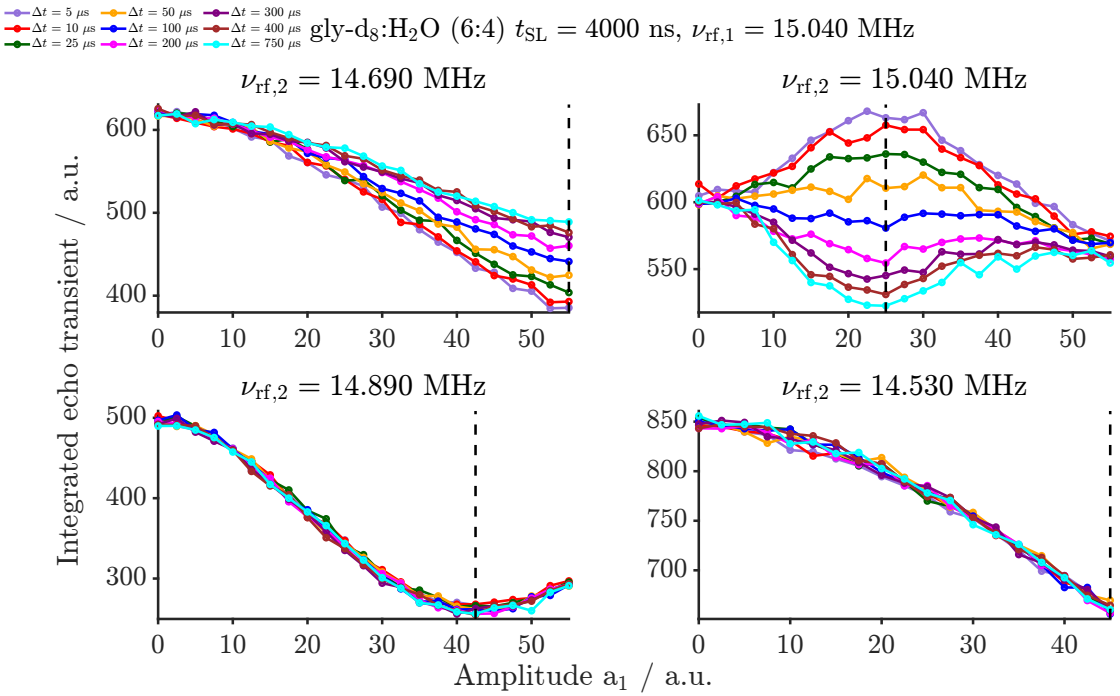

Figure S84: Amplitude traces recorded by sweeping the amplitude a_1 of the first Gauss pulse in steps of 2.5 for $\nu_{rf,1}$ = 15.04 MHz. An amplitude a_1 of 30 corresponds to a Rabi frequency of 100 kHz. The delay Δt between the first and second Gauss pulse was varied from 5 to 750 μs and is indicated in the legend of the figure. Here four different frequencies as examples are shown for the second Gauss pulse $\nu_{rf,2}$ = 14.53, 14.69, 14.89 and 15.04 MHz for the matrix gly-d_8:H_2O (6:4). 10 shots were used for each individual data point, t_{del} = 800 μs and t_{SL} = 4000 ns.

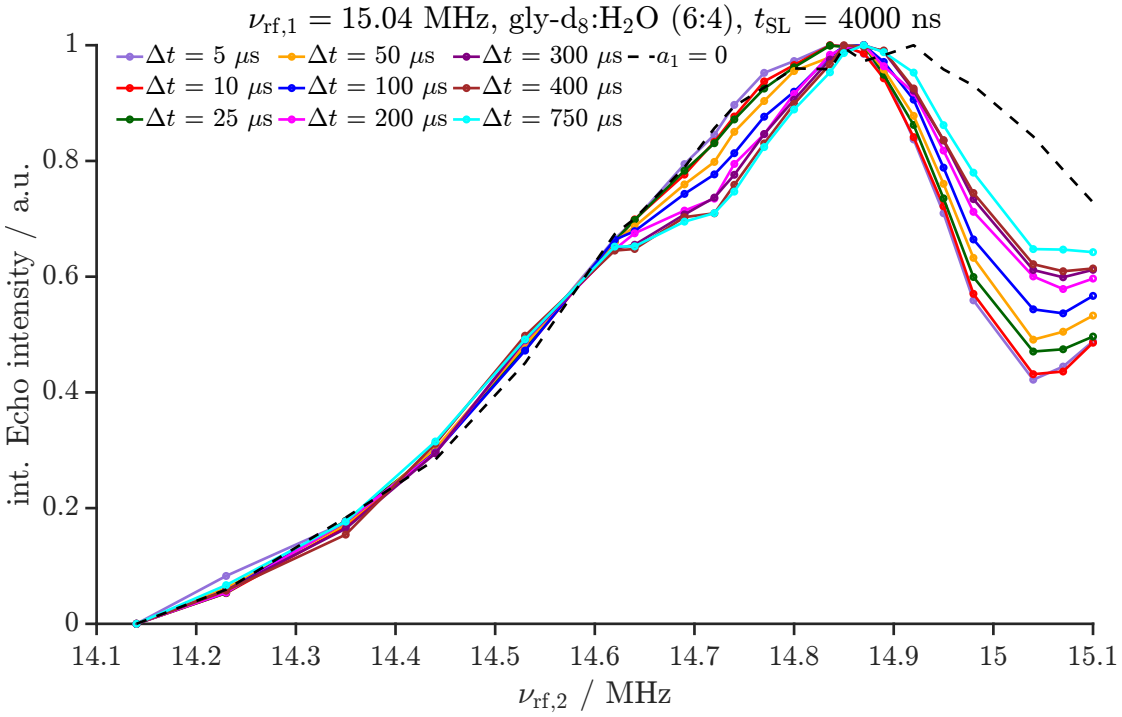

Figure S85: Hole burning spectra for delays Δt between the two Gauss pulses varying from 5 to 750 μs. The hole was burned at $\nu_{rf,1}$ = 15.04 MHz. The black dashed line is obtained by using the data points in Fig. S84 with $a_1 = 0$. The spectra with a hole burned are obtained by using the data points along the dashed line in Fig. S84. The sample is 5 mM trityl in gly-d$_8$:H$_2$O (6:4). 10 shots were used for each individual data point, t_{del} = 800 μs and t_{SL} = 4000 ns.

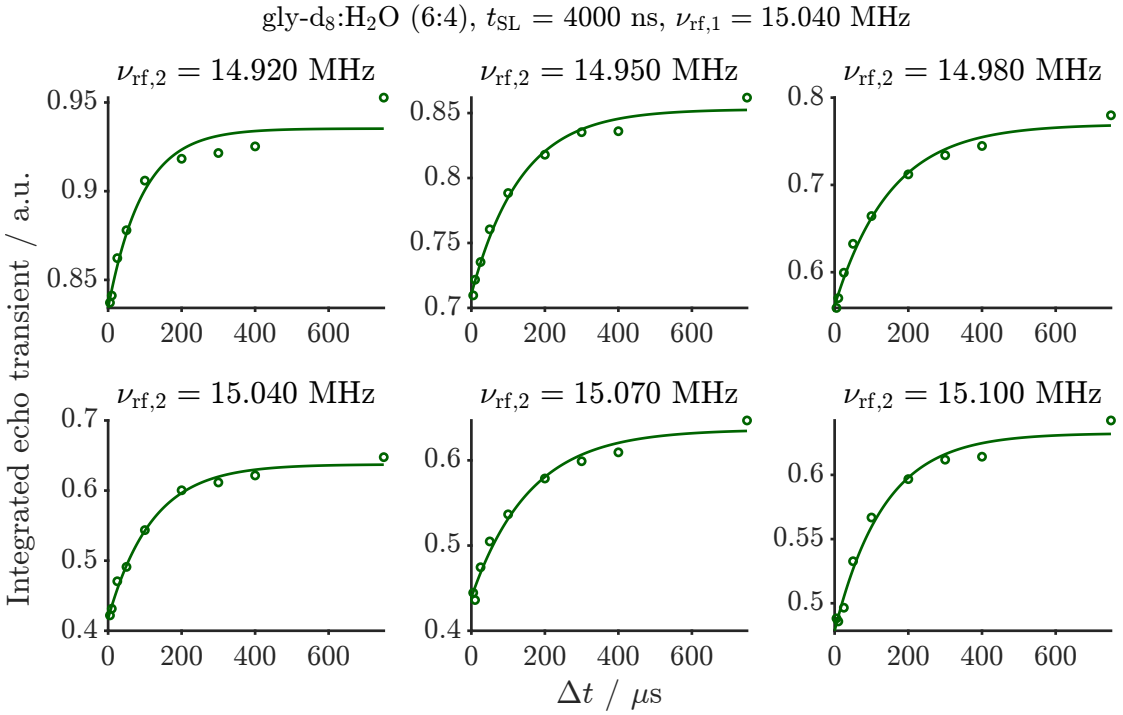

Figure S86: Diffusion traces for the hole burned at $\nu_{rf,1}$ = 15.04 MHz using t_{del} = 800 μs and t_{SL} = 4000 ns. The individual data points are obtained from Fig. S85 for the corresponding frequency $\nu_{rf,2}$. The sample is 5 mM trityl in gly-d_8:H_2O (6:4) and 10 shots were used for each individual data point. The data points are fitted to the function Eq. S.5 and the corresponding fitting parameters are given in Tab. S30.

$\nu_{rf,2}$ / MHz	ΔI / a.u.	τ / μs	I_0 / a.u.
14.920	0.101	93.465	0.834
14.950	0.142	135.180	0.711
14.980	0.208	151.521	0.562
15.040	0.220	118.880	0.418
15.070	0.197	158.365	0.439
15.100	0.154	133.989	0.479

Table S30: Extracted fit parameters from a mono-exponential build up as given in Eq. S.5 and shown in Fig. S86 for the hole burning at spectral position $\nu_{rf,1}$ = 15.04 MHz. The sample is 5 mM trityl in gly-d_8:H_2O (6:4).

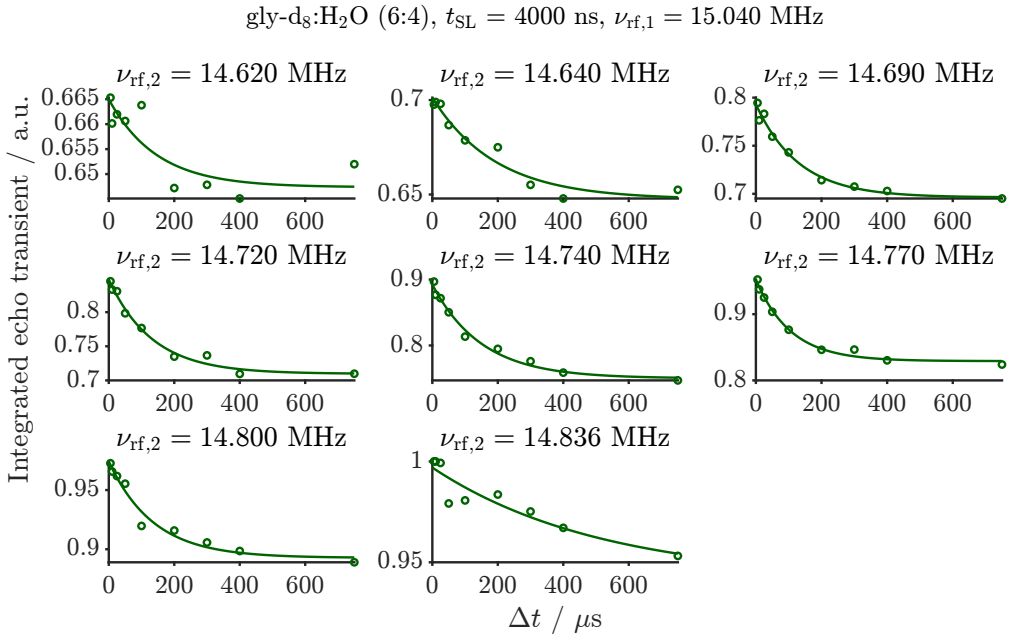

Figure S87: Diffusion traces for the hole burned at $\nu_{rf,1}$ = 15.04 MHz using t_{del} = 800 μs and t_{SL} = 4000 ns. The individual data points are obtained from Fig. S85 for the corresponding frequency $\nu_{rf,2}$. The sample is 5 mM trityl in gly-d_8:H_2O (6:4) and 10 shots were used for each individual data point. The data points are fitted to the function Eq. S.6 and the corresponding fitting parameters are given in Tab. S31.

$\nu_{rf,2}$ / MHz	ΔI / a.u.	τ / μs	I_∞ / a.u.
14.620	0.018	146.086	0.647
14.640	0.054	194.439	0.647
14.690	0.097	130.923	0.696
14.720	0.138	132.863	0.710
14.740	0.142	150.896	0.750
14.770	0.123	105.636	0.829
14.800	0.081	135.876	0.893
14.836	0.056	515.369	0.941

Table S31: Extracted fit parameters from a mono-exponential decay as given in Eq. S.6 and shown in Fig. S87 for the hole burning at spectral position $\nu_{rf,1}$ = 15.04 MHz. The sample is 5 mM trityl in gly-d_8:H_2O (6:4).

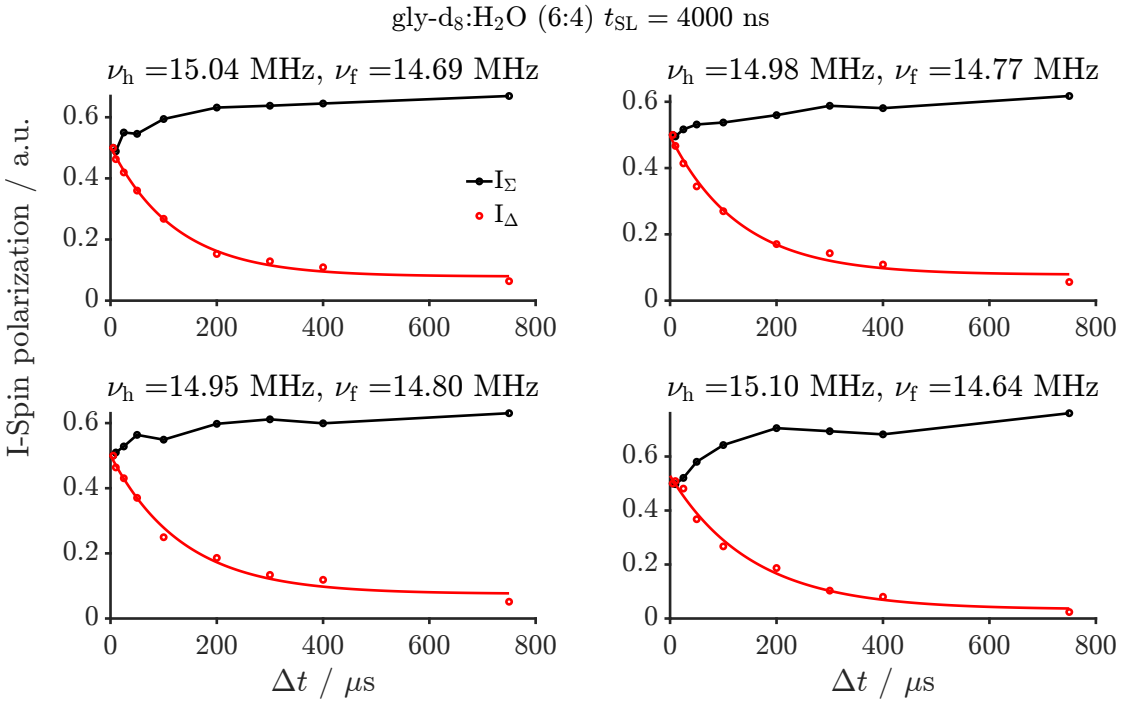

Figure S88: Sum and difference magnetization according to Eqs. (2)-(3) in the main text for different combinations of ν_h and ν_f. The hole is burned at $\nu_{rf,1} = 15.04$ MHz. The sample is 5 mM trityl in gly-d_8:H_2O (6:4) and $t_{SL} = 4000$ ns.

ν_h / MHz	ν_f / MHz	ΔI / a.u.	τ / μs	I_∞ / a.u.
15.04	14.69	0.425	122.797	0.079
14.98	14.77	0.418	130.949	0.078
14.95	14.80	0.426	135.442	0.076
15.10	14.64	0.495	152.299	0.033

Table S32: Extracted fit parameters from a mono-exponential decay as given in Eq. S.6 and shown in Fig. S88 for difference magnetization I_Δ as given in Eq. (3) in the main text. The hole is burned at $\nu_{rf,1} = 15.04$ MHz. The sample is 5 mM trityl in gly-d_8:H_2O (6:4) $t_{SL} = 4000$ ns.

E.5. 5 mM trityl in gly-d_8:H_2O (6:4), t_{SL} = 800 ns

$\nu_{rf,1}$ = 14.69 MHz

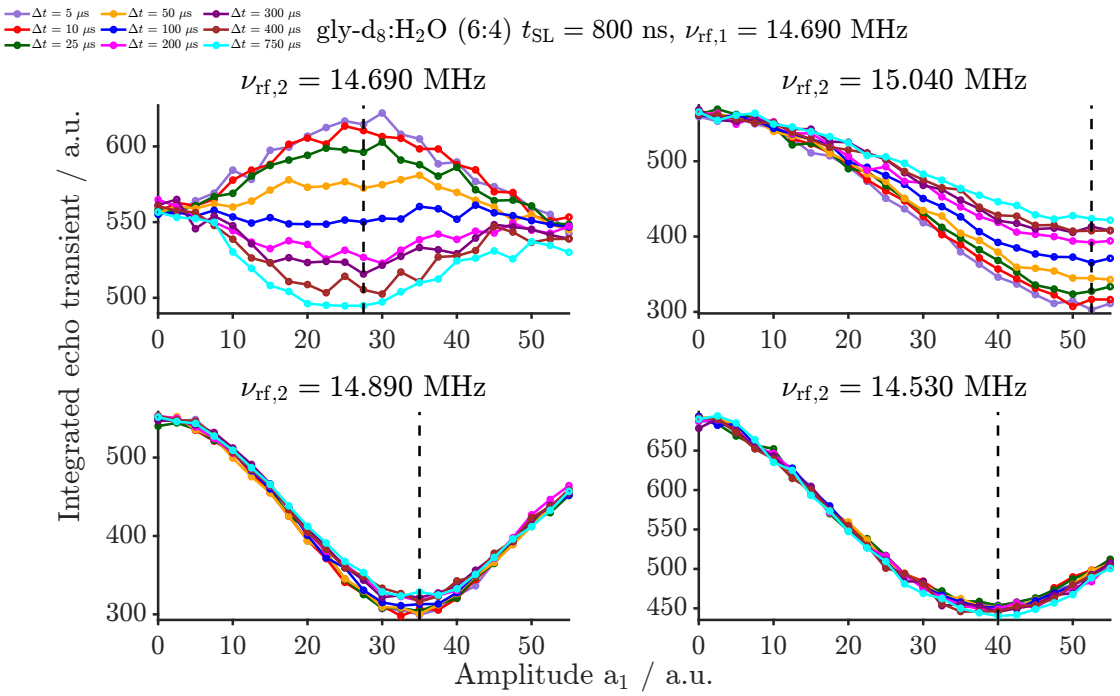

Figure S89: Amplitude traces recorded by sweeping the amplitude a_1 of the first Gauss pulse in steps of 2.5 for $\nu_{rf,1}$ = 14.69 MHz. An amplitude a_1 of 30 corresponds to a Rabi frequency of 100 kHz. The delay Δt between the first and second Gauss pulse was varied from 5 to 750 μs and is indicated in the legend of the figure. Here four different frequencies as examples are shown for the second Gauss pulse $\nu_{rf,2}$ = 14.53, 14.69, 14.89 and 15.04 MHz for the matrix gly-d_8:H_2O (6:4). 10 shots were used for each individual data point, t_{del} = 800 μs and t_{SL} = 800 ns.

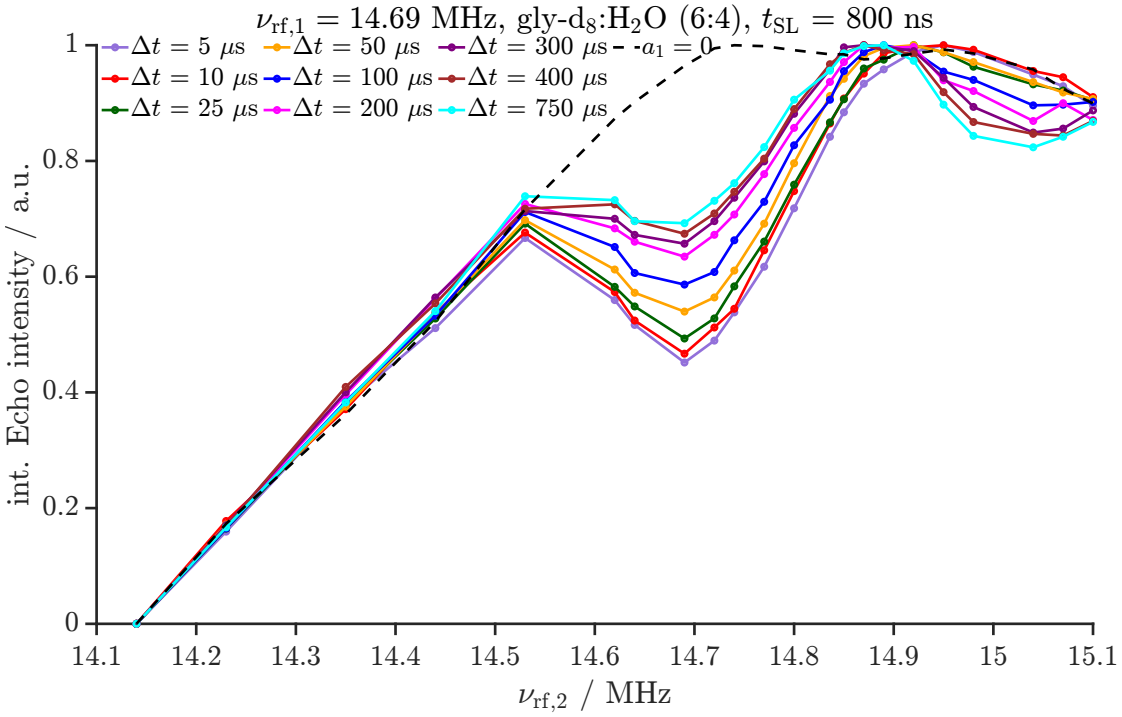

Figure S90: Hole burning spectra for delays Δt between the two Gauss pulses varying from 5 to 750 μs. The hole was burned at $\nu_{rf,1}$ = 14.69 MHz. The black dashed line is obtained by using the data points in Fig. S89 with $a_1 = 0$. The spectra with a hole burned are obtained by using the data points along the dashed line in Fig. S89. The sample is 5 mM trityl in gly-d$_8$:H$_2$O (6:4). 10 shots were used for each individual data point, t_{del} = 800 μs and t_{SL} = 800 ns.

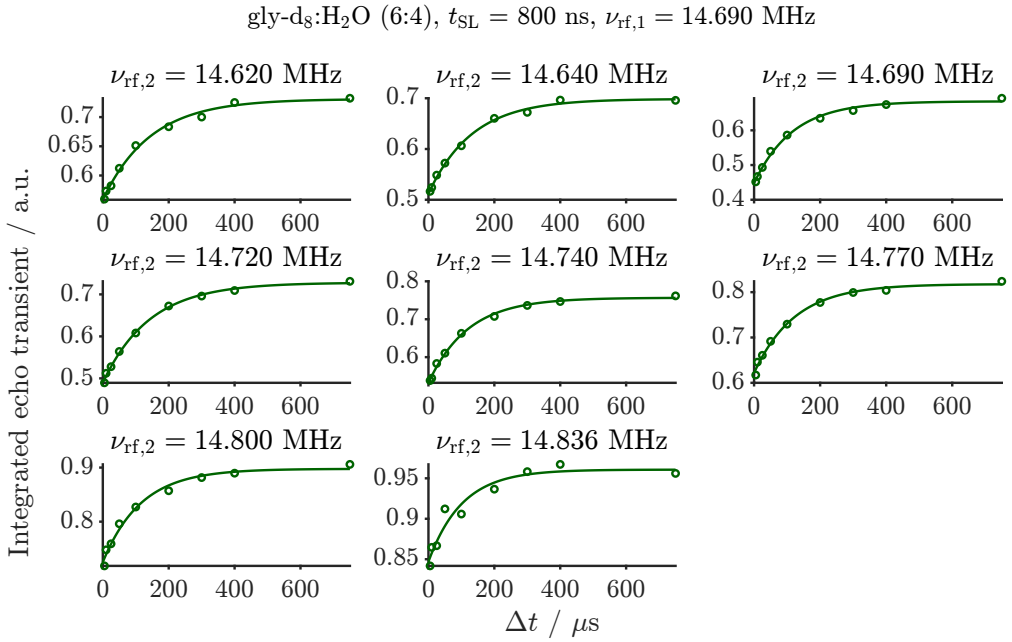

Figure S91: Diffusion traces for the hole burned at $\nu_{rf,1} = 14.69$ MHz using $t_{del} = 800$ μs and $t_{SL} = 800$ ns. The individual data points are obtained from Fig. S90 for the corresponding frequency $\nu_{rf,2}$. The sample is 5 mM trityl in gly-d_8:H_2O (6:4) and 10 shots were used for each individual data point. The data points are fitted to the function Eq. S.5 and the corresponding fitting parameters are given in Tab. S33.

$\nu_{rf,2}$ / MHz	ΔI / a.u.	τ / μs	I_0 / a.u.
14.620	0.173	145.027	0.558
14.640	0.187	133.046	0.512
14.690	0.236	117.030	0.448
14.720	0.238	142.079	0.489
14.740	0.224	119.844	0.532
14.770	0.196	123.738	0.622
14.800	0.172	115.775	0.725
14.836	0.114	102.004	0.847

Table S33: Extracted fit parameters from a mono-exponential build up as given in Eq. S.5 and shown in Fig. S91 for the hole burning at spectral position $\nu_{rf,1} = 14.69$ MHz. The sample is 5 mM trityl in gly-d_8:H_2O (6:4).

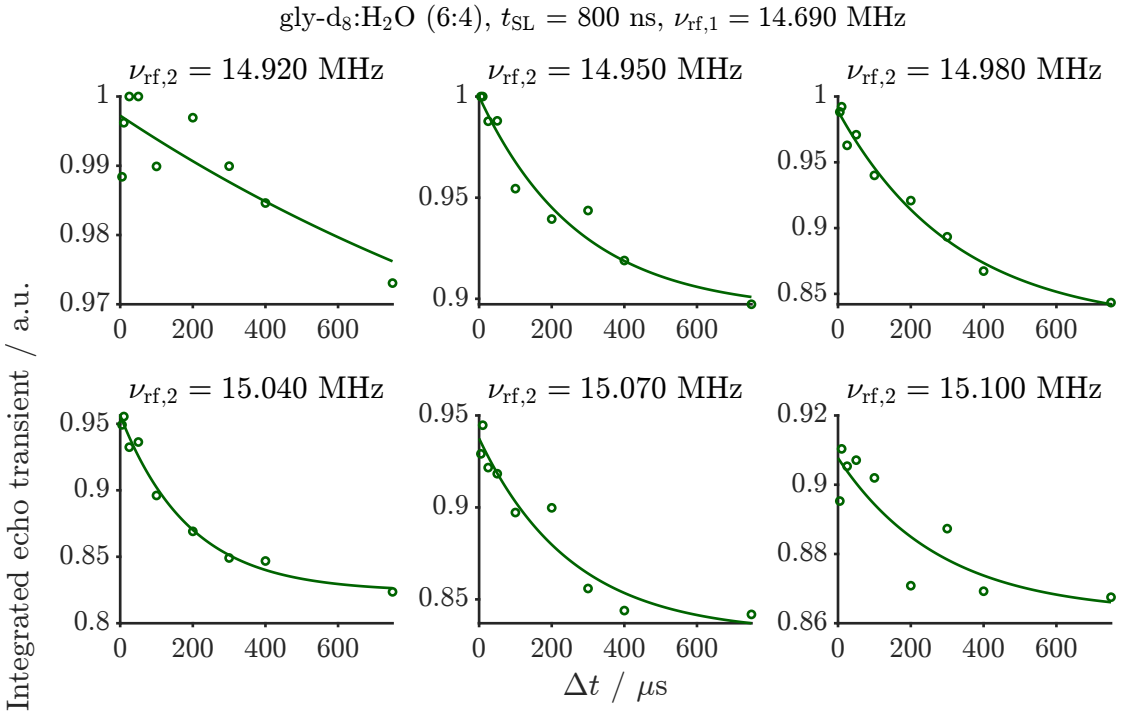

Figure S92: Diffusion traces for the hole burned at $\nu_{rf,1} = 14.69$ MHz using $t_{del} = 800$ μs and $t_{SL} = 800$ ns. The individual data points are obtained from Fig. S90 for the corresponding frequency $\nu_{rf,2}$. The sample is 5 mM trityl in gly-d_8:H_2O (6:4) and 10 shots were used for each individual data point. The data points are fitted to the function Eq. S.6 and the corresponding fitting parameters are given in Tab. S34.

$\nu_{rf,2}$ / MHz	ΔI / a.u.	τ / μs	I_∞ / a.u.
14.920	0.058	1648.225	0.940
14.950	0.106	274.724	0.894
14.980	0.163	324.915	0.826
15.040	0.132	190.575	0.824
15.070	0.106	254.524	0.831
15.100	0.045	282.236	0.863

Table S34: Extracted fit parameters from a mono-exponential decay as given in Eq. S.6 and shown in Fig. S92 for the hole burning at spectral position $\nu_{rf,1} = 14.69$ MHz. The sample is 5 mM trityl in gly-d_8:H_2O (6:4).

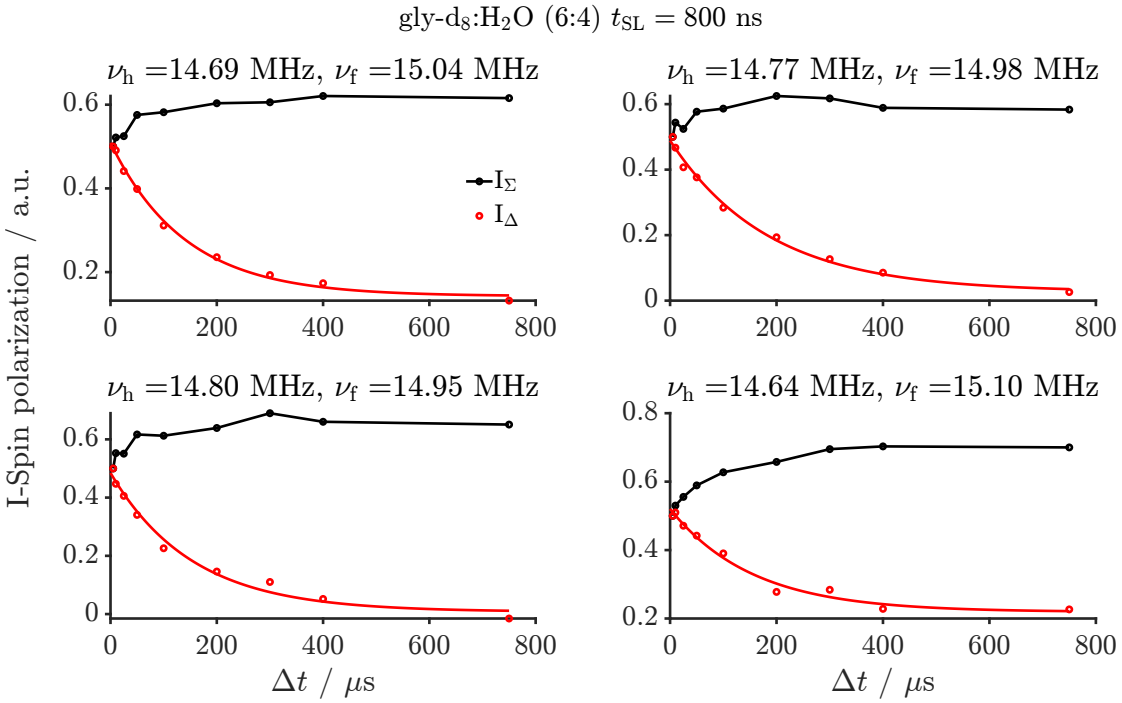

Figure S93: Sum and difference magnetization according to Eqs. (2)-(3) in the main text for different combinations of ν_h and ν_f. The hole is burned at $\nu_{rf,1} = 14.69$ MHz. The sample is 5 mM trityl in gly-d$_8$:H$_2$O (6:4) and t_{SL}= 800 ns.

ν_h / MHz	ν_f / MHz	ΔI / a.u.	τ / μs	I_∞ / a.u.
14.69	15.04	0.367	140.626	0.142
14.77	14.98	0.462	185.395	0.027
14.80	14.95	0.477	153.384	0.008
14.64	15.10	0.301	155.195	0.219

Table S35: Extracted fit parameters from a mono-exponential decay as given in Eq. S.6 and shown in Fig. S93 for difference magnetization I_Δ as given in Eq. (3) in the main text. The hole is burned at $\nu_{rf,1} = 14.69$ MHz. The sample is 5 mM trityl in gly-d$_8$:H$_2$O (6:4) $t_{SL} = 800$ ns.

$\nu_{rf,1}$ = 14.89 MHz

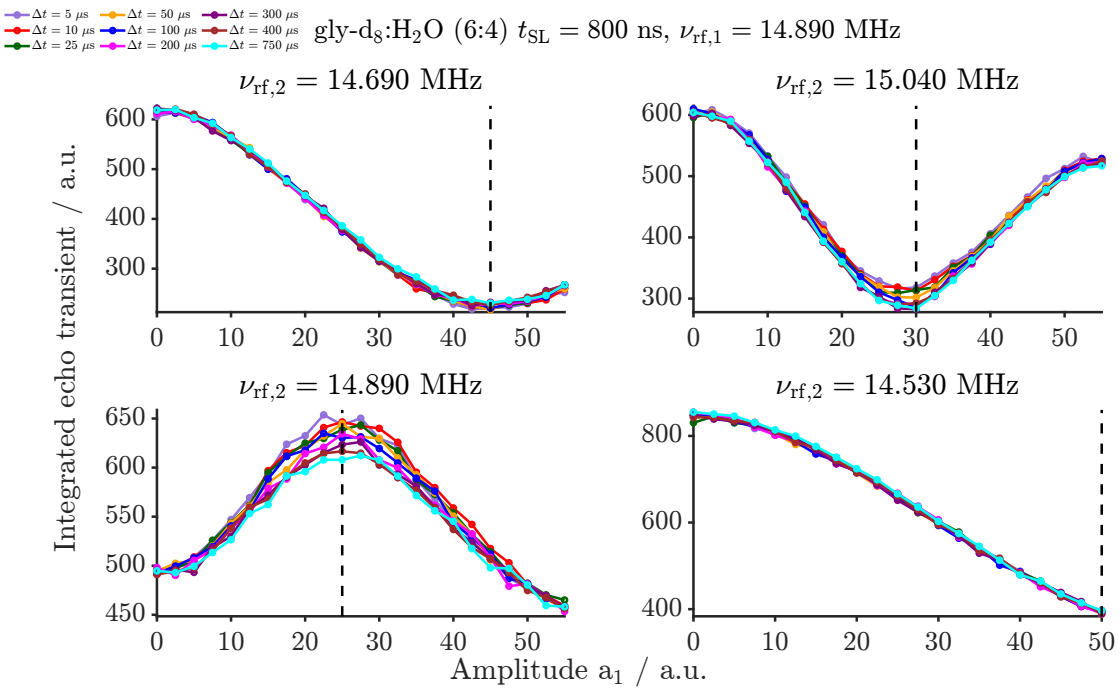

Figure S94: Amplitude traces recorded by sweeping the amplitude a_1 of the first Gauss pulse in steps of 2.5 for $\nu_{rf,1}$ = 14.89 MHz. An amplitude a_1 of 30 corresponds to a Rabi frequency of 100 kHz. The delay Δt between the first and second Gauss pulse was varied from 5 to 750 μs and is indicated in the legend of the figure. Here four different frequencies as examples are shown for the second Gauss pulse $\nu_{rf,2}$ = 14.53, 14.69, 14.89 and 15.04 MHz for the matrix gly-d_8:H_2O (6:4). 10 shots were used for each individual data point, t_{del} = 800 μs and t_{SL} = 800 ns.

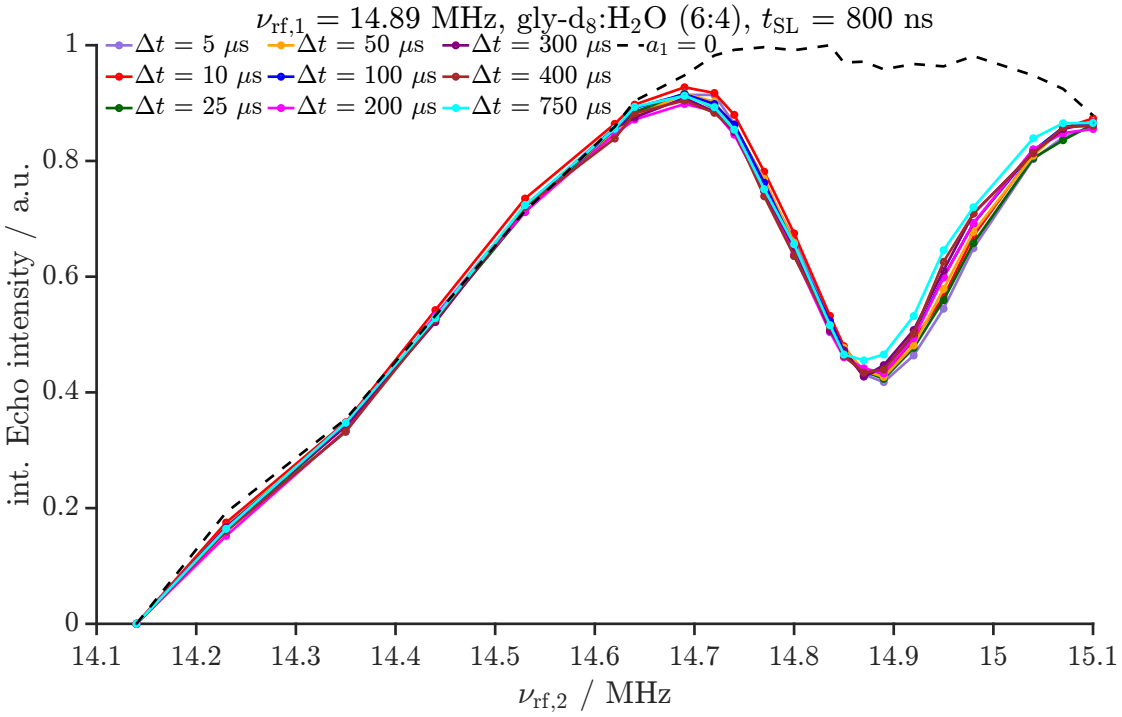

Figure S95: Hole burning spectra for delays Δt between the two Gauss pulses varying from 5 to 750 μs. The hole was burned at $\nu_{rf,1}$ = 14.89 MHz. The black dashed line is obtained by using the data points in Fig. S94 with $a_1 = 0$. The spectra with a hole burned are obtained by using the data points along the dashed line in Fig. S94. The sample is 5 mM trityl in gly-d$_8$:H$_2$O (6:4). 10 shots were used for each individual data point, t_{del} = 800 μs and t_{SL} = 800 ns.

$\nu_{rf,1}$ **= 15.04 MHz**

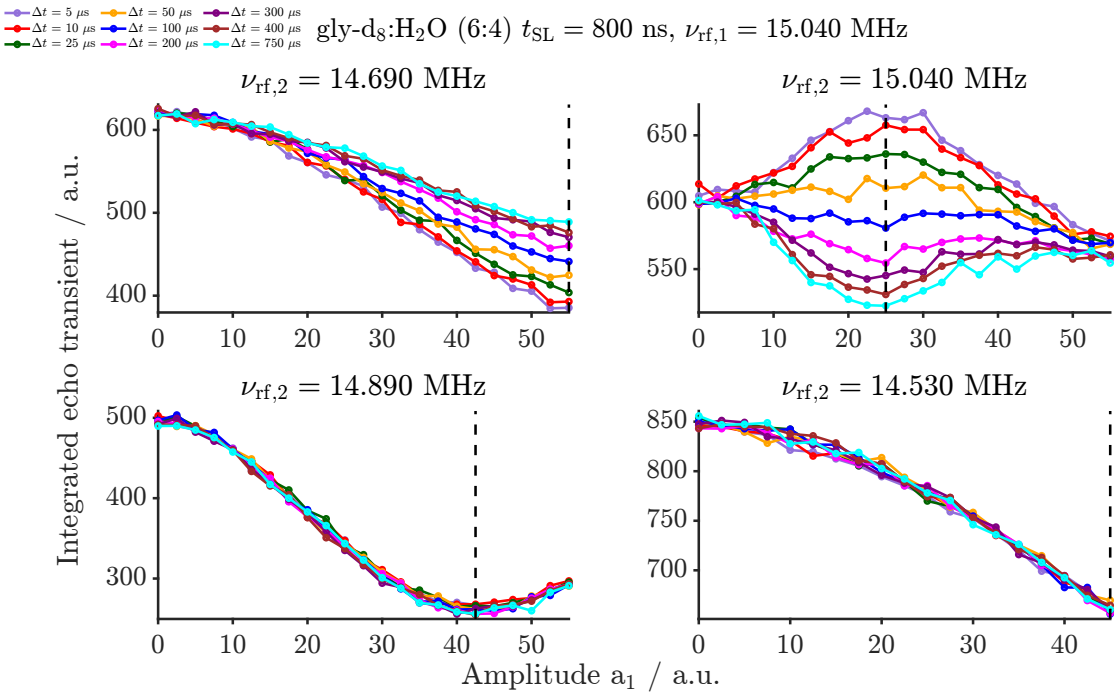

Figure S96: Amplitude traces recorded by sweeping the amplitude a_1 of the first Gauss pulse in steps of 2.5 for $\nu_{rf,1}$ = 15.04 MHz. An amplitude a_1 of 30 corresponds to a Rabi frequency of 100 kHz. The delay Δt between the first and second Gauss pulse was varied from 5 to 750 μs and is indicated in the legend of the figure. Here four different frequencies as examples are shown for the second Gauss pulse $\nu_{rf,2}$ = 14.53, 14.69, 14.89 and 15.04 MHz for the matrix gly-d_8:H_2O (6:4). 10 shots were used for each individual data point, t_{del} = 800 μs and t_{SL} = 800 ns.

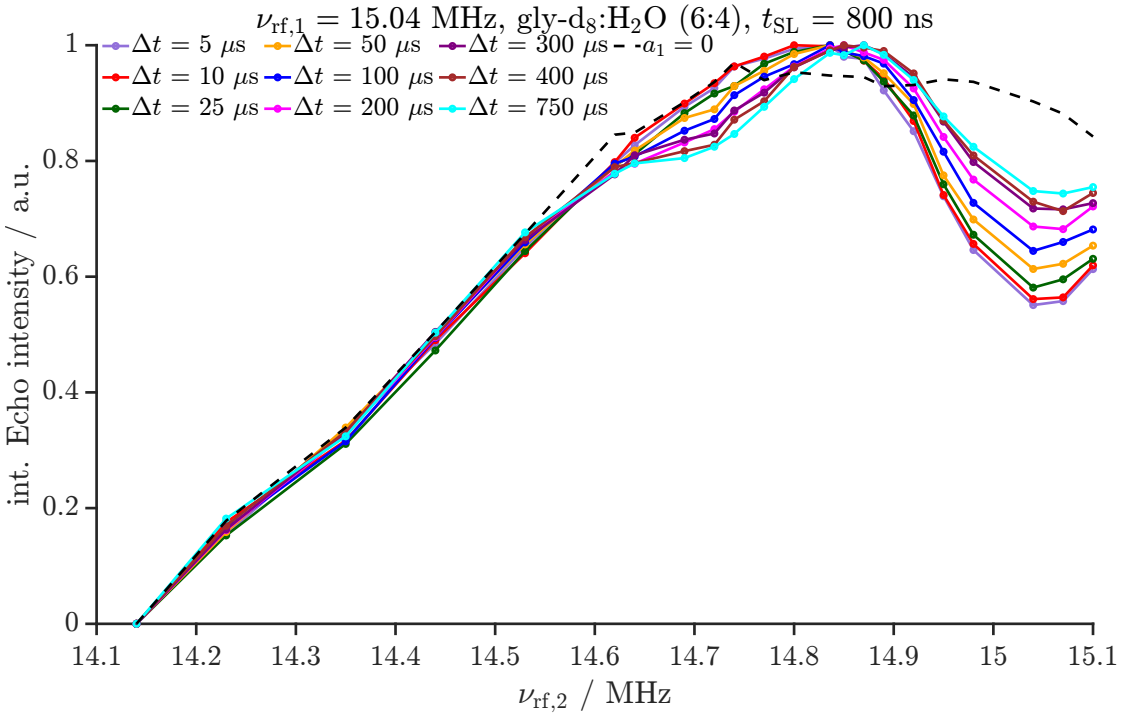

Figure S97: Hole burning spectra for delays Δt between the two Gauss pulses varying from 5 to 750 μs. The hole was burned at $\nu_{rf,1}$ = 15.04 MHz. The black dashed line is obtained by using the data points in Fig. S96 with a_1 = 0. The spectra with a hole burned are obtained by using the data points along the dashed line in Fig. S96. The sample is 5 mM trityl in gly-d$_8$:H$_2$O (6:4). 10 shots were used for each individual data point, t_{del} = 800 μs and t_{SL} = 800 ns.

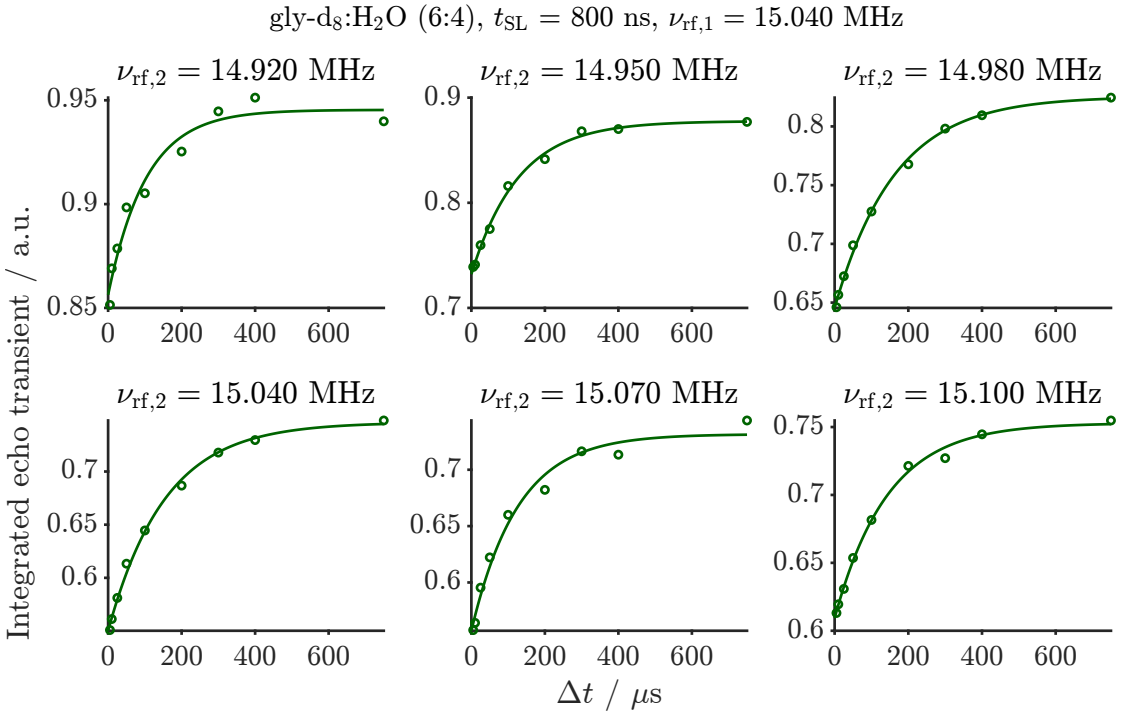

Figure S98: Diffusion traces for the hole burned at $\nu_{rf,1} = 15.04$ MHz using $t_{del} = 800$ μs and $t_{SL} = 800$ ns. The individual data points are obtained from Fig. S97 for the corresponding frequency $\nu_{rf,2}$. The sample is 5 mM trityl in gly-d_8:H_2O (6:4) and 10 shots were used for each individual data point. The data points are fitted to the function Eq. S.5 and the corresponding fitting parameters are given in Tab. S36.

$\nu_{rf,2}$ / MHz	ΔI / a.u.	τ / μs	I_0 / a.u.
14.920	0.089	103.761	0.856
14.950	0.146	128.215	0.732
14.980	0.180	163.406	0.645
15.040	0.196	154.496	0.550
15.070	0.174	126.685	0.557
15.100	0.144	143.870	0.609

Table S36: Extracted fit parameters from a mono-exponential build up as given in Eq. S.5 and shown in Fig. S98 for the hole burning at spectral position $\nu_{rf,1} = 15.04$ MHz. The sample is 5 mM trityl in gly-d_8:H_2O (6:4).

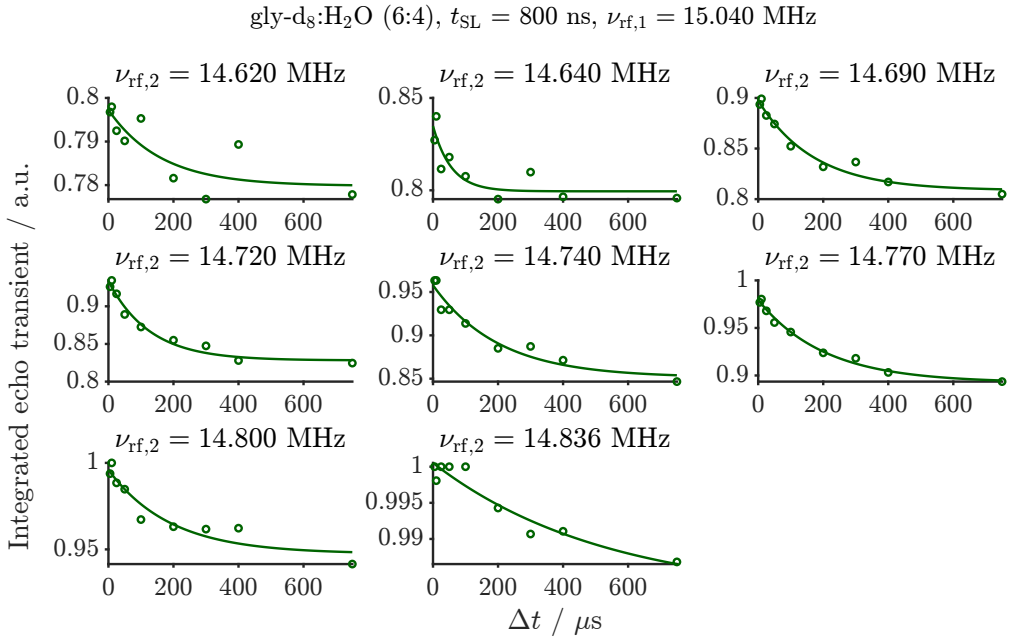

Figure S99: Diffusion traces for the hole burned at $\nu_{rf,1} = 15.04$ MHz using $t_{del} = 800$ μs and $t_{SL} = 800$ ns. The individual data points are obtained from Fig. S97 for the corresponding frequency $\nu_{rf,2}$. The sample is 5 mM trityl in gly-d_8:H_2O (6:4) and 10 shots were used for each individual data point. The data points are fitted to the function Eq. S.6 and the corresponding fitting parameters are given in Tab. S37.

$\nu_{rf,2}$ / MHz	ΔI / a.u.	τ / μs	I_∞ / a.u.
14.620	0.017	161.878	0.780
14.640	0.035	56.620	0.799
14.690	0.089	170.795	0.809
14.720	0.105	126.806	0.828
14.740	0.106	201.126	0.851
14.770	0.087	204.102	0.893
14.800	0.049	190.267	0.947
14.836	0.018	529.999	0.982

Table S37: Extracted fit parameters from a mono-exponential decay as given in Eq. S.6 and shown in Fig. S99 for the hole burning at spectral position $\nu_{rf,1} = 15.04$ MHz. The sample is 5 mM trityl in gly-d_8:H_2O (6:4).

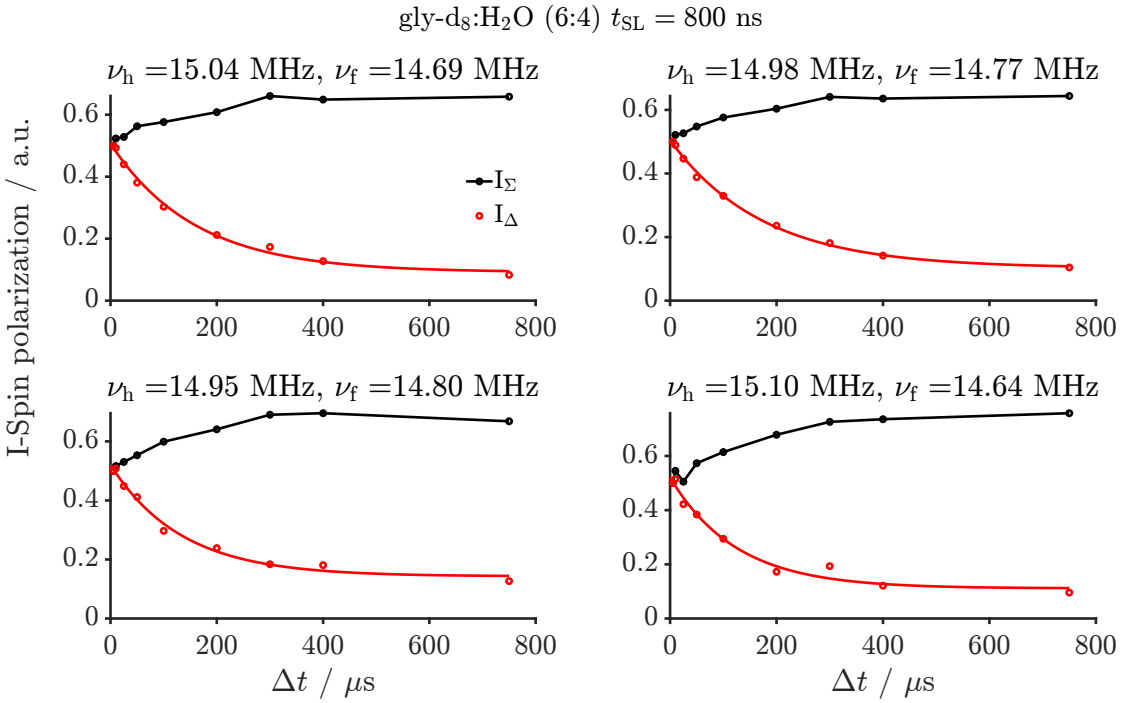

Figure S100: Sum and difference magnetization according to Eqs. (2)-(3) in the main text for different combinations of ν_h and ν_f. The hole is burned at $\nu_{rf,1}$ = 15.04 MHz. The sample is 5 mM trityl in gly-d_8:H_2O (6:4) and t_{SL} = 800 ns.

ν_h / MHz	ν_f / MHz	ΔI / a.u.	τ / μs	I_∞ / a.u.
15.04	14.69	0.415	158.636	0.092
14.98	14.77	0.402	174.666	0.103
14.95	14.80	0.377	133.333	0.143
15.10	14.64	0.409	123.983	0.111

Table S38: Extracted fit parameters from a mono-exponential decay as given in Eq. S.6 and shown in Fig. S100 for difference magnetization I_Δ as given in Eq. (3) in the main text. The hole is burned at $\nu_{rf,1}$ = 15.04 MHz. The sample is 5 mM trityl in gly-d_8:H_2O (6:4) and t_{SL} = 800 ns.

E.6. 100 μM trityl in gly-d_8:D_2O:H_2O (6:3:1)

$\nu_{rf,1}$ = 14.69 MHz

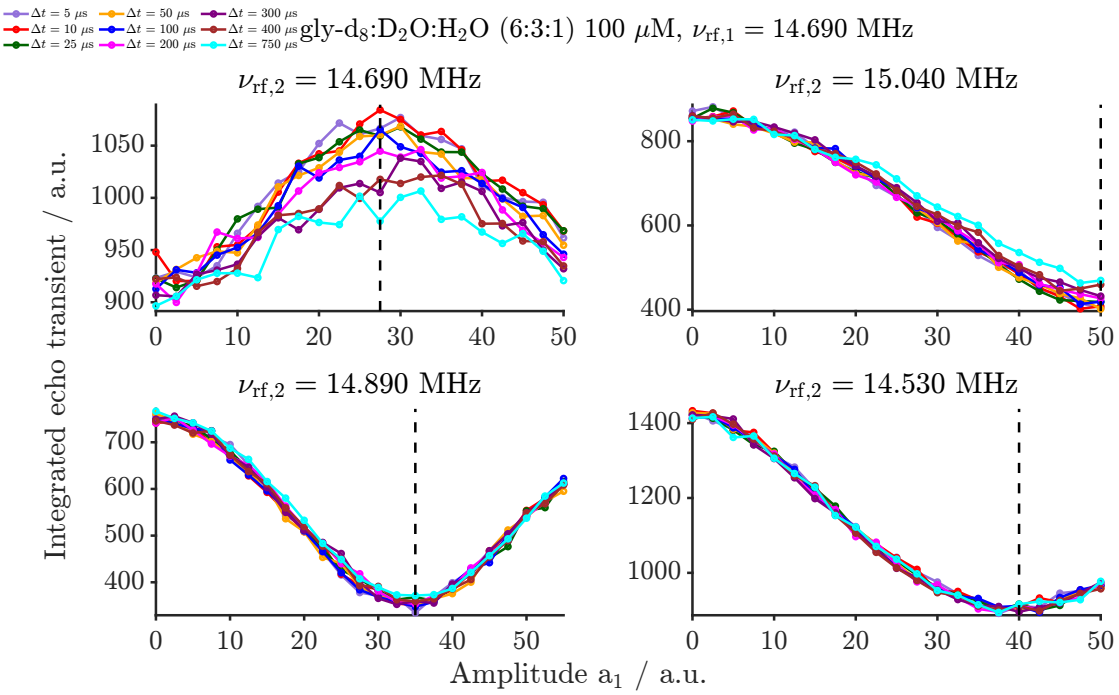

Figure S101: Amplitude traces recorded by sweeping the amplitude a_1 of the first Gauss pulse in steps of 2.5 for $\nu_{rf,1}$ = 14.69 MHz. An amplitude a_1 of 30 corresponds to a Rabi frequency of 100 kHz. The delay Δt between the first and second Gauss pulse was varied from 5 to 750 μs and is indicated in the legend of the figure. Here four different frequencies as examples are shown for the second Gauss pulse $\nu_{rf,2}$ = 14.53, 14.69, 14.89 and 15.04 MHz for the matrix gly-d_8:D_2O:H_2O (6:3:1) and a trityl concentration of 100 μM. 22 shots were used for each individual data point, t_{del} = 800 μs and t_{SL} = 4000 ns.

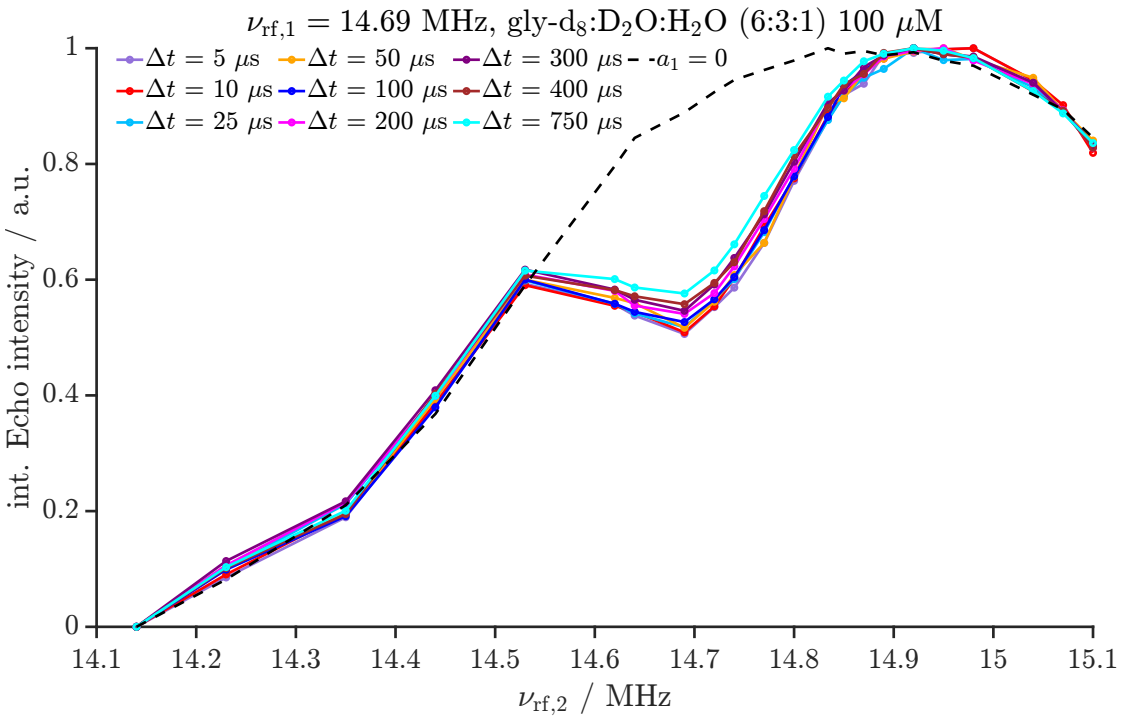

Figure S102: Hole burning spectra for delays Δt between the two Gauss pulses varying from 5 to 750 μs. The hole was burned at $\nu_{rf,1}$ = 14.69 MHz. The black dashed line is obtained by using the data points in Fig. S101 with a_1 = 0. The spectra with a hole burned are obtained by using the data points along the dashed line in Fig. S101. The sample is 100 μM trityl in gly-d$_8$:D$_2$O:H$_2$O (6:3:1). 22 shots were used for each individual data point, t_{del} = 800 μs and t_{SL} = 4000 ns.

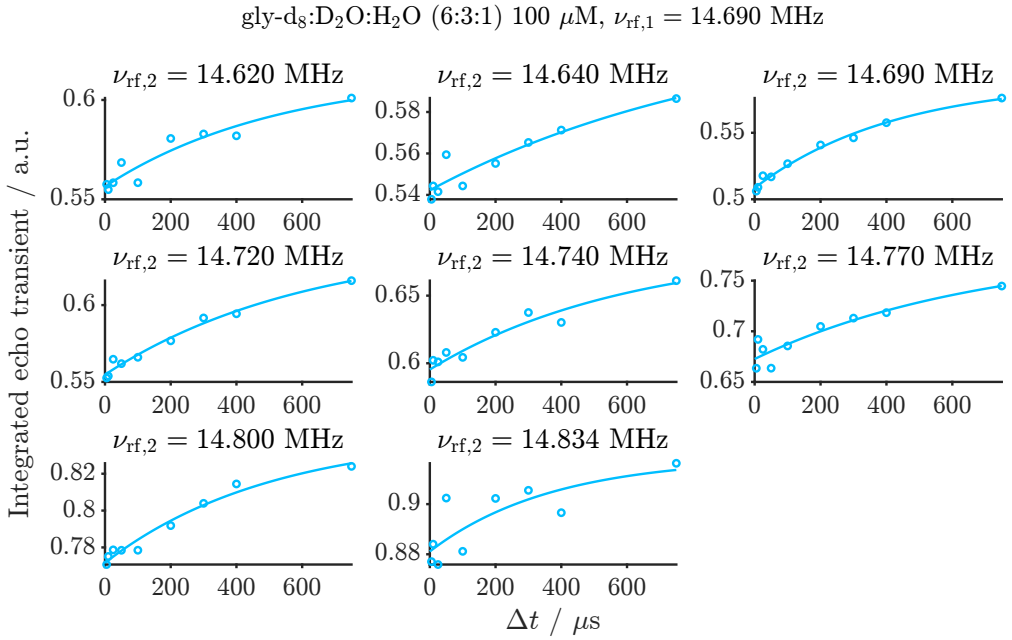

Figure S103: Diffusion traces for the hole burned at $\nu_{rf,1} = 14.69$ MHz using $t_{del} = 800$ μs and $t_{SL} = 4000$ ns. The individual data points are obtained from Fig. S102 for the corresponding frequency $\nu_{rf,2}$. The sample is 100 μM trityl in gly-d_8:D_2O:H_2O (6:3:1) and 22 shots were used for each individual data point. The data points are fitted to the function Eq. S.5 and the corresponding fitting parameters are given in Tab. S39.

$\nu_{rf,2}$ / MHz	ΔI / a.u.	τ / μs	I_0 / a.u.
14.620	0.057	529.374	0.556
14.640	0.082	953.057	0.542
14.690	0.081	426.585	0.509
14.720	0.087	613.878	0.555
14.740	0.090	600.476	0.595
14.770	0.110	699.535	0.673
14.800	0.070	504.083	0.772
14.834	0.037	371.377	0.881

Table S39: Extracted fit parameters from a mono-exponential build up as given in Eq. S.5 and shown in Fig. S103 for the hole burning at spectral position $\nu_{rf,1} = 14.69$ MHz. The sample is 100 μM trityl in gly-d_8:D_2O:H_2O (6:3:1).

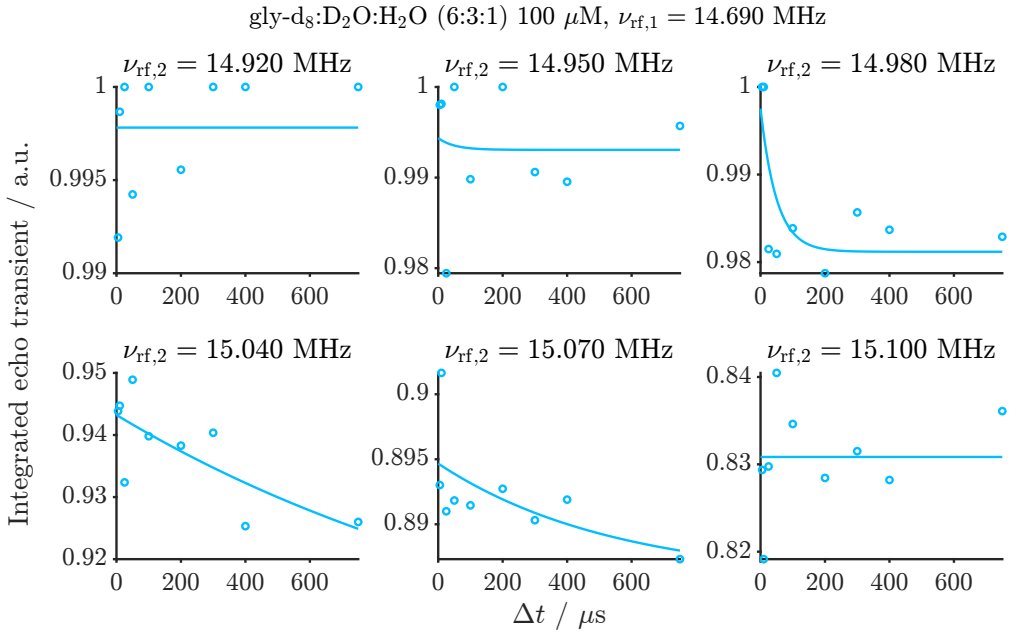

Figure S104: Diffusion traces for the hole burned at $\nu_{rf,1} = 14.69$ MHz using $t_{del} = 800$ μs and $t_{SL} = 4000$ ns. The individual data points are obtained from Fig. S102 for the corresponding frequency $\nu_{rf,2}$. The sample is 100 μM trityl in gly-d_8:D_2O:H_2O (6:3:1) and 22 shots were used for each individual data point. The data points are fitted to the function Eq. S.6 and the corresponding fitting parameters are given in Tab. S40.

$\nu_{rf,2}$ / MHz	ΔI / a.u.	τ / μs	I_∞ / a.u.
14.920	0.000	100.000	0.998
14.950	0.001	50.000	0.993
14.980	0.016	50.000	0.981
15.040	0.045	1447.332	0.898
15.070	0.009	543.891	0.886
15.100	0.000	100.000	0.831

Table S40: Extracted fit parameters from a mono-exponential decay as given in Eq. S.6 and shown in Fig. S104 for the hole burning at spectral position $\nu_{rf,1} = 14.69$ MHz. The sample is 100 μM trityl in gly-d_8:D_2O:H_2O (6:3:1).

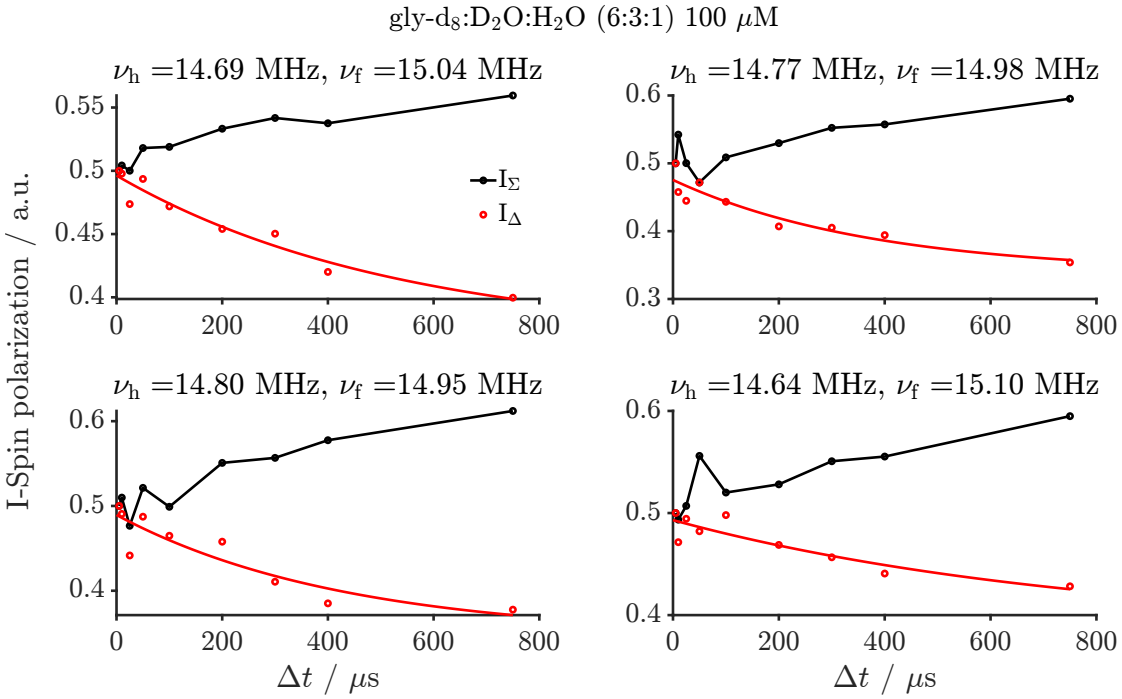

Figure S105: Sum and difference magnetization according to Eqs. (2)-(3) in the main text for different combinations of ν_h and ν_f. The hole is burned at $\nu_{rf,1}$ = 14.69 MHz. The sample is 100 μM trityl in gly-d$_8$:D$_2$O:H$_2$O (6:3:1).

ν_h / MHz	ν_f / MHz	ΔI / a.u.	τ / μs	I_∞ / a.u.
14.69	15.04	0.129	530.830	0.367
14.77	14.98	0.137	376.367	0.339
14.80	14.95	0.143	428.640	0.346
14.64	15.10	0.109	773.833	0.384

Table S41: Extracted fit parameters from a mono-exponential decay as given in Eq. S.6 and shown in Fig. S105 for difference magnetization I_Δ as given in Eq. (3) in the main text. The hole is burned at $\nu_{rf,1}$ = 14.69 MHz. The sample is 100 μM trityl in gly-d$_8$:D$_2$O:H$_2$O (6:3:1).

$\nu_{rf,1}$ **= 14.89 MHz**

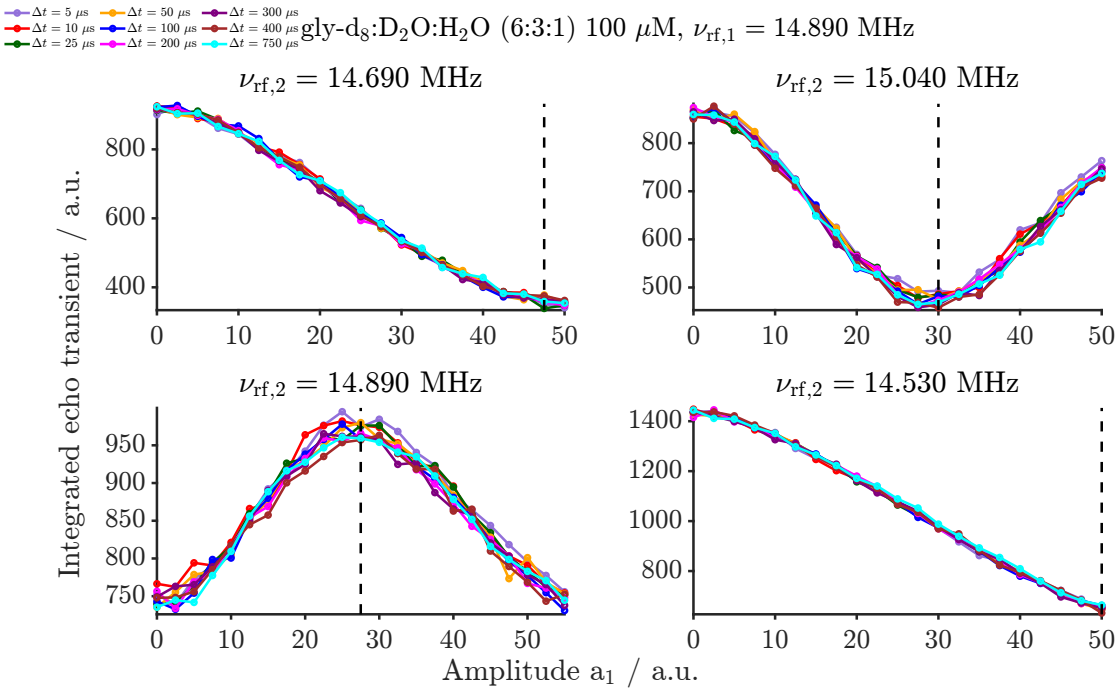

Figure S106: Amplitude traces recorded by sweeping the amplitude a_1 of the first Gauss pulse in steps of 2.5 for $\nu_{rf,1}$ = 14.89 MHz. An amplitude a_1 of 30 corresponds to a Rabi frequency of 100 kHz. The delay Δt between the first and second Gauss pulse was varied from 5 to 750 μs and is indicated in the legend of the figure. Here four different frequencies as examples are shown for the second Gauss pulse $\nu_{rf,2}$ = 14.53, 14.69, 14.89 and 15.04 MHz for the matrix gly-d_8:D_2O:H_2O (6:3:1) and a trityl concentration of 100 μM. 22 shots were used for each individual data point, t_{del} = 800 μs and t_{SL} = 4000 ns.

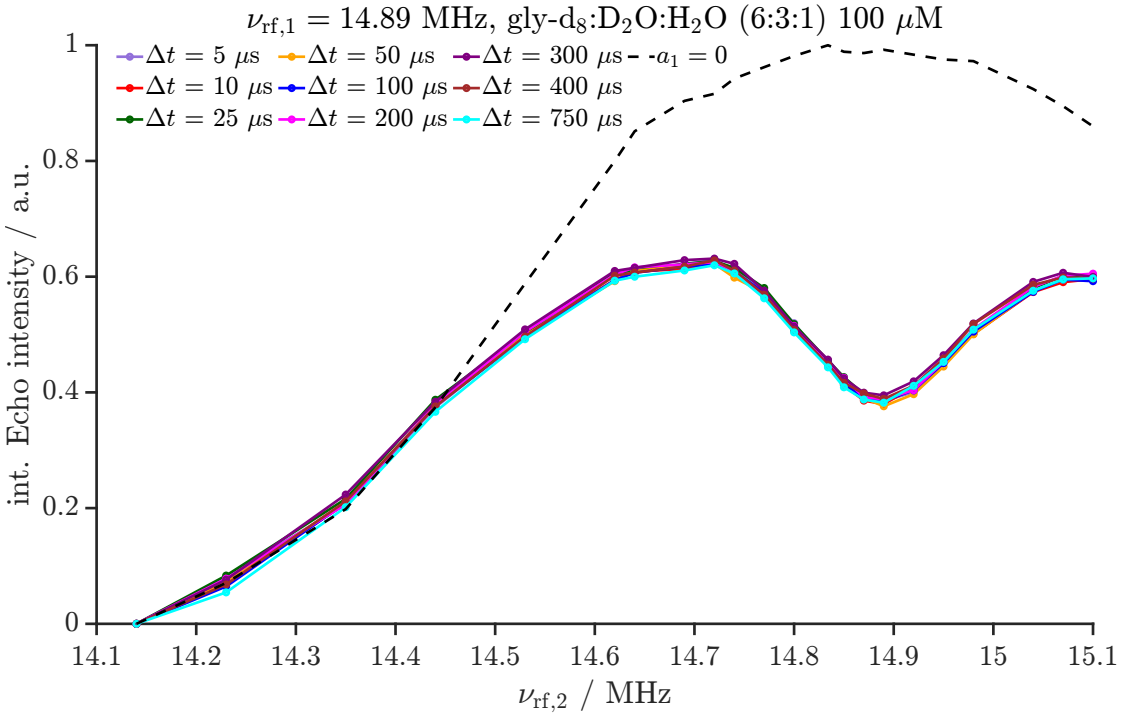

Figure S107: Hole burning spectra for delays Δt between the two Gauss pulses varying from 5 to 750 μs. The hole was burned at $\nu_{rf,1}$ = 14.89 MHz. The black dashed line is obtained by using the data points in Fig. S106 with a_1 = 0. The spectra with a hole burned are obtained by using the data points along the dashed line in Fig. S106. The sample is 100 μM trityl in gly-d$_8$:D$_2$O:H$_2$O (6:3:1). 22 shots were used for each individual data point, t_{del} = 800 μs and t_{SL} = 4000 ns.

$\nu_{rf,1}$ = **15.04 MHz**

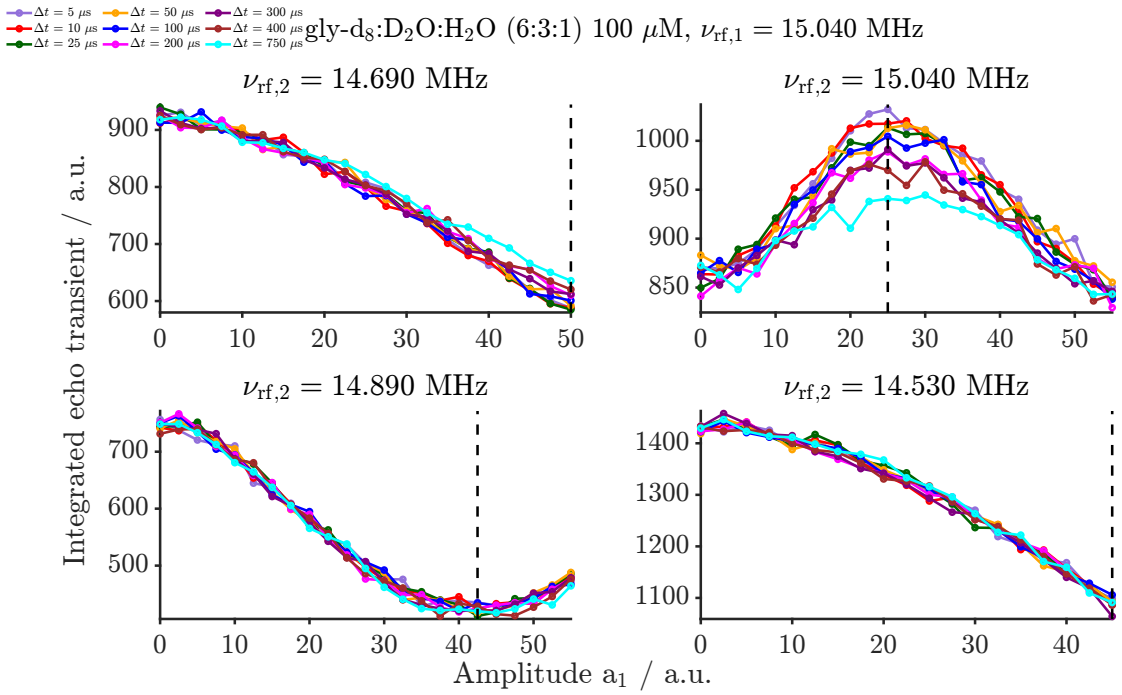

Figure S108: Amplitude traces recorded by sweeping the amplitude a_1 of the first Gauss pulse in steps of 2.5 for $\nu_{rf,1}$ = 15.04 MHz. An amplitude a_1 of 30 corresponds to a Rabi frequency of 100 kHz. The delay Δt between the first and second Gauss pulse was varied from 5 to 750 μs and is indicated in the legend of the figure. Here four different frequencies as examples are shown for the second Gauss pulse $\nu_{rf,2}$ = 14.53, 14.69, 14.89 and 15.04 MHz for the matrix gly-d_8:D_2O:H_2O (6:3:1) and a trityl concentration of 100 μM. 22 shots were used for each individual data point, t_{del} = 800 μs and t_{SL} = 4000 ns.

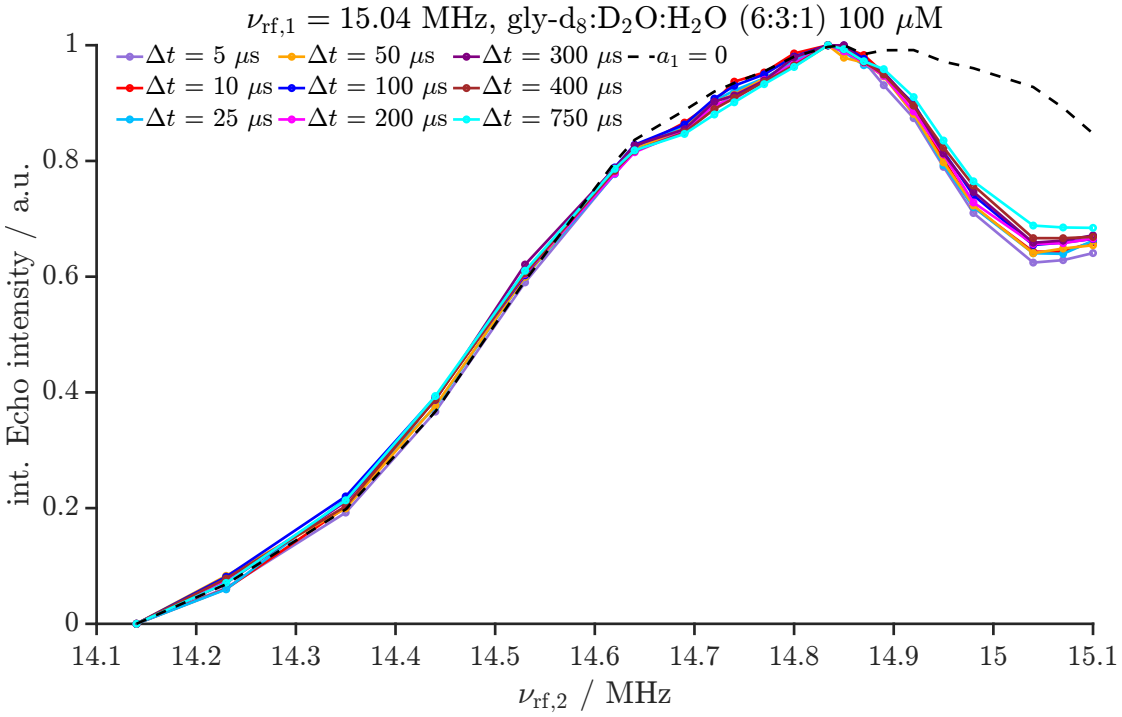

Figure S109: Hole burning spectra for delays Δt between the two Gauss pulses varying from 5 to 750 μs. The hole was burned at $\nu_{rf,1}$ = 15.04 MHz. The black dashed line is obtained by using the data points in Fig. S108 with a_1 = 0. The spectra with a hole burned are obtained by using the data points along the dashed line in Fig. S108. The sample is 100 μM trityl in gly-d$_8$:D$_2$O:H$_2$O (6:3:1). 22 shots were used for each individual data point, t_{del} = 800 μs and t_{SL} = 4000 ns.

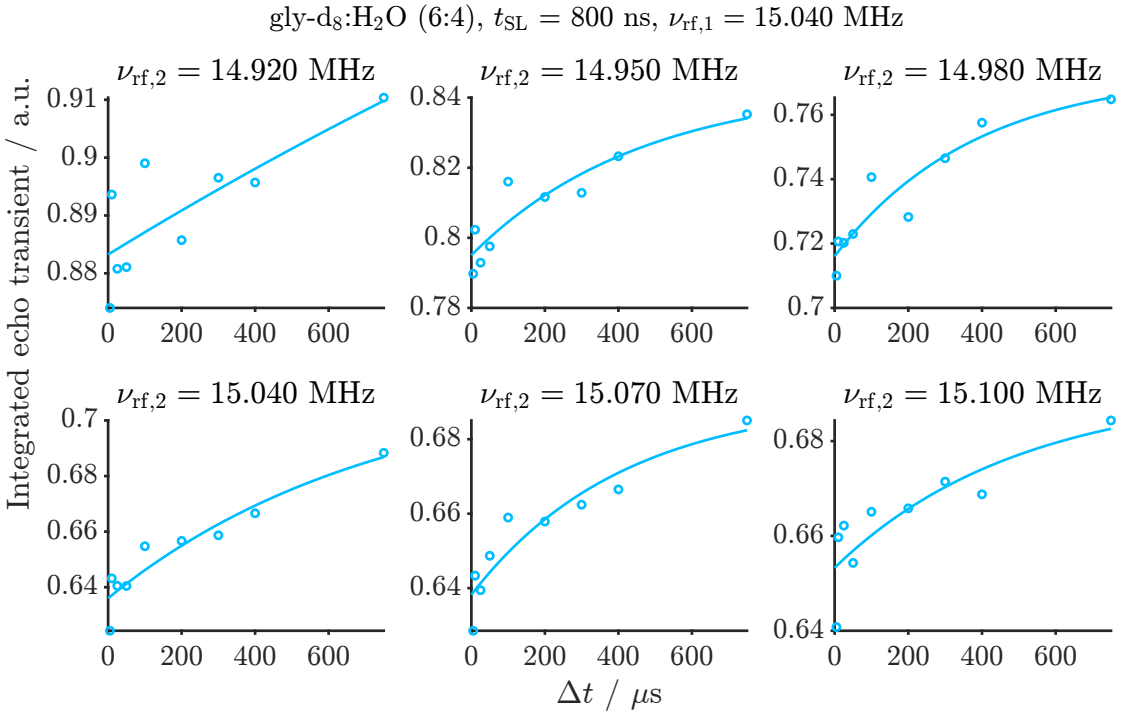

Figure S110: Diffusion traces for the hole burned at $\nu_{rf,1} = 15.04$ MHz using $t_{del} = 800$ μs and $t_{SL} = 4000$ ns. The individual data points are obtained from Fig. S109 for the corresponding frequency $\nu_{rf,2}$. The sample is 100 μM trityl in gly-d_8:D_2O:H_2O (6:3:1) and 22 shots were used for each individual data point. The data points are fitted to the function Eq. S.5 and the corresponding fitting parameters are given in Tab. S42.

$\nu_{rf,2}$ / MHz	ΔI / a.u.	τ / μs	I_0 / a.u.
14.920	0.148	3796.769	0.883
14.950	0.049	461.879	0.795
14.980	0.057	381.585	0.716
15.040	0.079	735.275	0.636
15.070	0.053	412.286	0.638
15.100	0.038	500.727	0.653

Table S42: Extracted fit parameters from a mono-exponential build up as given in Eq. S.5 and shown in Fig. S110 for the hole burning at spectral position $\nu_{rf,1} = 15.04$ MHz. The sample is 100 μM trityl in gly-d_8:D_2O:H_2O (6:3:1).

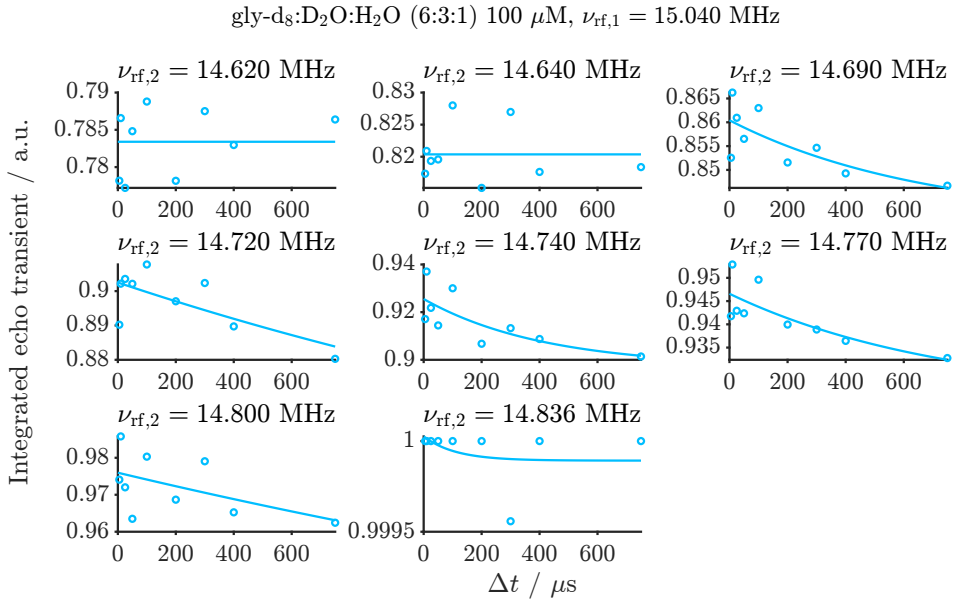

Figure S111: Diffusion traces for the hole burned at $\nu_{rf,1} = 15.04$ MHz using $t_{del} = 800$ μs and $t_{SL} = 4000$ ns. The individual data points are obtained from Fig. S109 for the corresponding frequency $\nu_{rf,2}$. The sample is 100 μM trityl in gly-d_8:D_2O:H_2O (6:3:1) and 22 shots were used for each individual data point. The data points are fitted to the function Eq. S.6 and the corresponding fitting parameters are given in Tab. S43.

$\nu_{rf,2}$ / MHz	ΔI / a.u.	τ / μs	I_∞ / a.u.
14.620	0.000	100.000	0.783
14.640	0.000	100.000	0.820
14.690	0.021	671.489	0.839
14.720	0.080	2828.329	0.822
14.740	0.028	412.614	0.897
14.770	0.022	746.383	0.924
14.800	0.080	4291.694	0.896
14.836	0.000	109.761	1.000

Table S43: Extracted fit parameters from a mono-exponential decay as given in Eq. S.6 and shown in Fig. S111 for the hole burning at spectral position $\nu_{rf,1} = 15.04$ MHz. The sample is 100 μM trityl in gly-d_8:D_2O:H_2O (6:3:1).

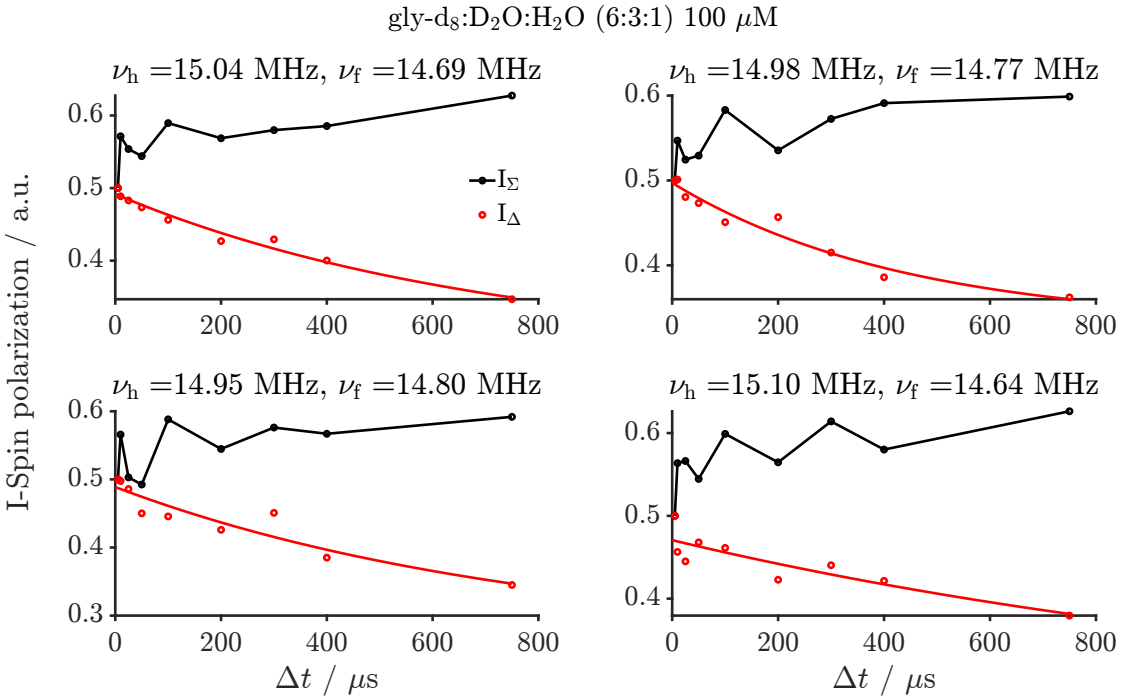

Figure S112: Sum and difference magnetization according to Eqs. (2)-(3) in the main text for different combinations of ν_h and ν_f. The hole is burned at $\nu_{rf,1}$ = 15.04 MHz. The sample is 100 μM trityl in gly-d$_8$:D$_2$O:H$_2$O (6:3:1).

ν_h / MHz	ν_f / MHz	ΔI / a.u.	τ / μs	I_∞ / a.u.
15.04	14.69	0.219	715.972	0.272
14.98	14.77	0.167	438.409	0.330
14.95	14.80	0.230	781.659	0.259
15.10	14.64	0.216	1408.415	0.255

Table S44: Extracted fit parameters from a mono-exponential decay as given in Eq. S.6 and shown in Fig. S112 for difference magnetization I_Δ as given in Eq. (3) in the main text. The hole is burned at $\nu_{rf,1}$ = 15.04 MHz. The sample is 100 μM trityl in gly-d$_8$:D$_2$O:H$_2$O (6:3:1).

F. Reproducibility of the measurements of electron-detected proton spectra

In this section we show the good reproducibility of the measurements by comparing electron-detected proton spectra measured within the same measurement session (Fig. S113) and across two measurement sessions (Fig. S114). The experimental data show very good reproducibility, confirming the robustness of the measurement of the electron-detected proton spectra.

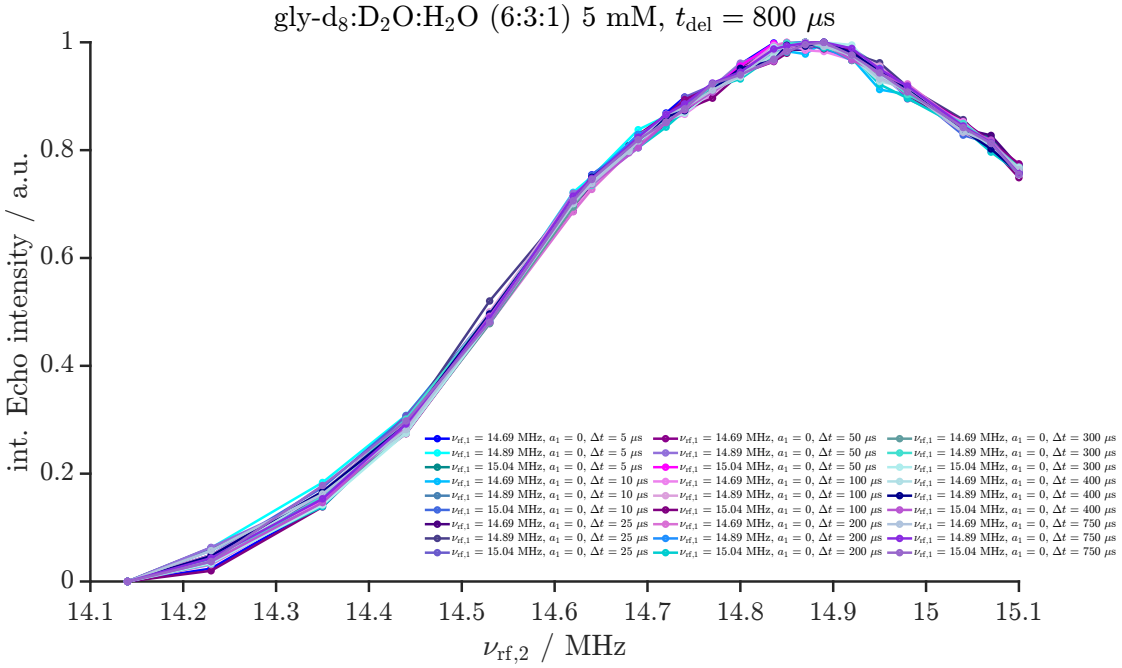

Figure S113: Comparison of electron-detected proton spectrum of the sample 5 mM trityl in gly-d_8:D_2O:H_2O (6:3:1) by volume for t_{SL} = 4000 ns for a delay t_{del} = 800 μs measured within the same measurement sessions. The nutation pulse was was placed at the end of t_{del}.

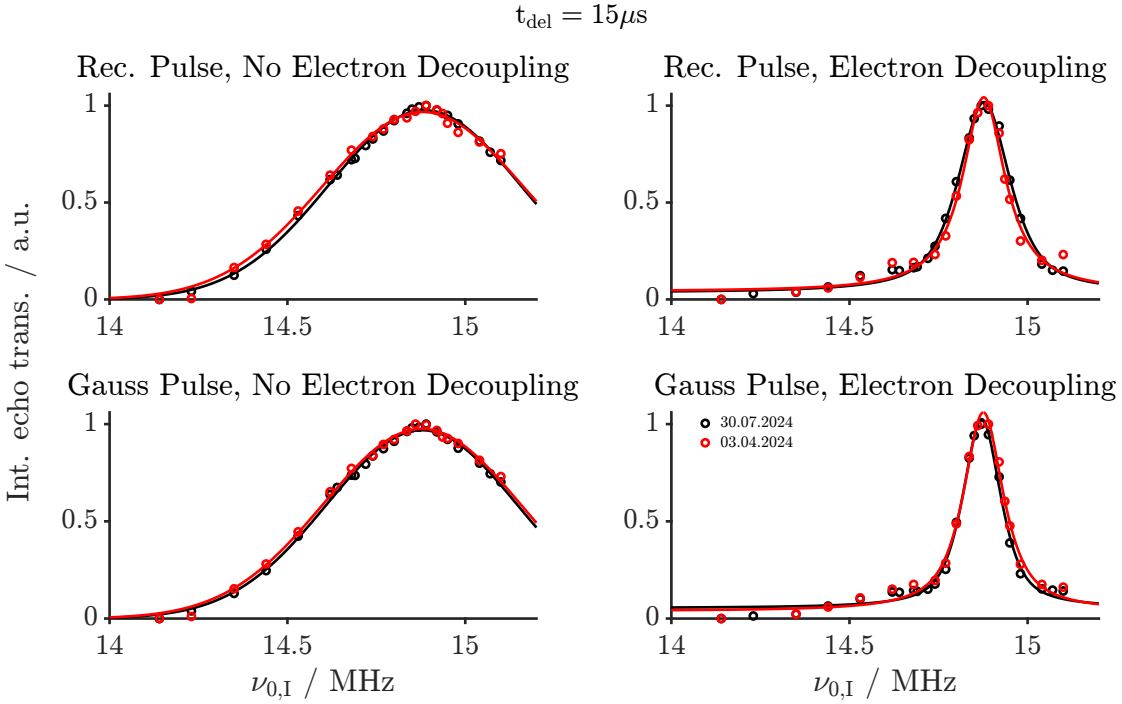

Figure S114: Comparison of electron-detected proton spectrum of the sample 5 mM trityl in gly-d_8:D_2O:H_2O (6:3:1) by volume for t_{SL} = 4000 ns for a delay t_{del} = 15 μs measured across different measurement sessions as indicated in the legend. The data show very good reproducibility, confirming the robustness of the measurements.